IMPACTS OF LANDUSE CHANGE ON RAINFALL-RUNOFF PROCESS AT HUMID TROPICAL HILLSLOPES IN INDONESIA

EILIF KURNIA DEDA DJAMRES

2024

IMPACTS OF LANDUSE CHANGE ON RAINFALL-RUNOFF PROCESS AT HUMID TROPICAL HILLSLOPES IN INDONESIA

(インドネシアの熱帯湿潤域における土地利用変化が山腹斜面の降雨流出過程に及ぼす影響)

by

EILIF KURNIA DEDA DJAMRES

A dissertation

Submitted in partial fulfillment of the requirements for the

Degree of Doctor of Engineering

Department of Civil and Earth Resources Engineering

Graduate School of Engineering

Kyoto University, Japan

March 2024

Acknowledgements

Alhamdulillah, I am deeply grateful to Allah, my merciful and gracious God, for bestowing upon me the blessings, strength, and opportunity to successfully complete my studies. The completion of the dissertation entitled “Impact of Landuse Change on Rainfall-Runoff Process at Humid Tropical Hillslopes in Indonesia” was carried out in Innovative Disaster Prevention Technology and Policy Research Laboratory, Disaster Prevention Research Institute (DPRI), Kyoto University. This accomplishment was possible due to the helps and thoughts of many people.

I express my heartfelt appreciation to Professor Takahiro Sayama for his invaluable supervision, guidance, and motivational encouragement, which played a crucial role in the steady progress and timely completion of this study. Professor Sayama's dedication to research consistently reignited my motivation to keep focus in my academic pursuits. His commitment extended beyond academic matters, he generously allocated time to discuss research outcomes and address challenges, demonstrating a genuine concern for both academic and life matters. Additionally, Professor Sayama facilitated numerous opportunities and connections for research, fostering a collaborative environment not only within Japan but also on an international scale.

I also extend my gratitude to Professor Yasuto Tachikawa and Professor Kenji

Tanaka for their valuable suggestions and motivations as my sub–supervisors in Department of Civil and Earth Resources Engineering, Kyoto University.

I also wish to thank Jr. Assoc. Prof. Florence Lahournat for her valuable insights and advises especially on how to make a good research presentation. Furthermore, I wish also to thank the work of Sayama laboratory staff members: Ms. Sono Inoue and Ms. Kaori Saidera for their continuous support in paper works and administrative tasks during my study at Kyoto University.

Furthermore, I extend my sincere gratitude to Dr. Eva Mia Siska Yamamoto and Dr. Kodai Yamamoto for their tremendous support in my research and daily life. Their help has played a crucial role in guiding my academic journey.

I also extend my gratitude for Indonesian counterparts, Research Center for Limnology BRIN, Bogor–Indonesia. I wish to extend my deep appreciation for Dr. Apip for his continues support in providing both data and information, field experience and technical knowledge.

I express my acknowledgment to all former laboratory members: Dr. Netrananda Sahu, Ms. Ryoko Araki, Dr. Try Sophal, Dr. Sohaib Baig, Dr. Steven Ly, Dr. Masafumi Yamada, Mr. Wang Shuangtao; and all my laboratory colleagues: Dr. Yoshito Sugawara, Mr. Ayato Yamakita, Mr. Chen Jiachao, Mr. Syouta Tanioka, and Mr. Yuma Yamauchi, Ms. Aurelene Arcenal, Mr. Tang Zeming, Mr. Tsuyoshi Ohno, and Ms. Peng Jiaqi.

I am deeply grateful to Prof. John Steven Selker for his invaluable advice and guidance during his visit to Kyoto University. His expertise and insights greatly enriched my understanding about Hydrology field.

I am deeply grateful to the the Indonesia Endowment Fund for Education (LPDP - Lembaga Pengelola Dana Pendidikan) for financially supporting my study at Kyoto University for the past four years. My study in Japan would not be possible without their support.

Lastly, words fall short in capturing the depth of my gratitude for my family: my late mother, my late father, my sister, my brother–in–law, my beloved wife, and my children (Ammar, Keyaan, and Farezel) who have consistently support me. Especially, I would like to express my gratitude again to my wife who always standing by me and supporting me on hardship.

Kyoto, March 2024

Abstract

Comprehending the spatiotemporal trends in groundwater (GW) is essential to understand hydrological mechanisms at the hillslope scale. Many researchers have investigated the dynamics of GW and soil moisture along hillslopes. Some previous studies have highlighted that soil characteristics in the humid tropic region allow for a high vertical infiltration rate and the generation of transient saturated subsurface runoff. However, the role of hillslope and bedrock topography, such as length, gradient and land cover factors, have not been fully understood. This study investigates the impacts of landuse change (LUC) on different hydrologic variables using field observation data and hydrologic models. The primary goals of this research are as follows.

1. To investigate whether the high GW responses can be observed and generalized in humid tropical hillslopes in Sumatra, Indonesia;
2. To identify major contributing factors to the high GW responses based on field observations and numerical simulations;
3. To understand the influence of LUC on rainfall partitioning, including evapotranspiration and canopy interception;
4. To clarify the effects of LUC on pattern and water balance;
5. To clarify the impacts of different rainfall and evapotranspiration input (gross rainfall, net rainfall, potential evapotranspiration, and actual evapotranspiration) for the LUC assessment.

To achieve these objectives, GW dynamics and suction head were observed at two neighboring hillslopes characterized by different soil depths with varying land covers. The observed records showed significant difference between the two sites in terms of the temporal fluctuations of GW. In the jungle rubber forest site (hereafter JR), characterized by steeper topography and shallower soil layer, the GW at the foot of the hillslope exhibited a more responsive pattern to rainfall. This can be attributed to the subsurface flow from the uphill, whose soil layer is approximately 1.5 m underlain by weathered bedrock. On the other hand, at an oil palm site (hereafter OP) with comparatively gentle slope and deeper soil layer, the GW reacted more slowly to rainfall, despite having similar surface soil properties such as hydraulic conductivity and effective porosity. The finding suggests that different patterns of GW dynamics coexist even at the neighboring hillslopes, which shares the similar climatic conditions.

To explore the primary controlling factors, we employed a hydrologic model, specifically the Rainfall-Runoff-Inundation (RRI) model. The results indicated that slope topography and soil depth play crucial roles in the dynamic response of GW. The hydraulic conductivity and soil water retention curves were contributing factors to surface soil moisture. The model results emphasized the relevance of lateral saturated subsurface flow in soil layers, contributing to GW responses at the JR site. In contrast, these dynamic patterns were absent in the thicker soil layers with gentle gradient at the OP site. In general, the unique characteristics of the soil properties in the humid tropic region resulted in the high GW response. However, this phenomenon may not be applicable to hillslopes with gentle gradient and thick soil layer.

Furthermore, to investigate the impacts of LUC to rainfall partitioning, evapotranspiration and canopy interception, this study couples an interception model to the RRI model to quantify the interception rates of both land covers. As for the potential evapotranspiration (PET) estimated by the Penman-Monteith equation, the PET at the JR site was approximately 1420 mm, while it was approximately 1060 mm at the OP site. The JR sites showed higher potential evapotranspiration than at the OP site mainly due to higher canopy and surface roughness. The interception was estimated the Suzuki model incorporating reported parameters by previous studies in humid tropics. The results indicated a higher interception rate at the JR site (30%) than OP site (15%). Due to the smaller PET and interception, the OP site receives more net rainfall than at the JR site.

This study introduced two factors into the coupled model: “root zone” and “evapotranspiration threshold” to regulate plant water intake for more realistic estimations of actual evapotranspiration and GW dynamics. As a result, despite the higher potential evapotranspiration at the JR site in dry seasons, the model limits a relatively small actual evapotranspiration, which was necessary for a reasonable representation of the observed GW pattern during dry seasons at the JR site.

The estimated annual runoff at the JR and OP sites were 1740 mm at the JR site and 2060 mm at OP site, respectively. This means approximately 18% increase in annual runoff due to the LUC from JR to OP during the study period. The increase in annual runoff due to the deforestation has been reported in previous studies. However, on a monthly basis, the OP site exhibits lower runoff than the JR site during the dry season because of the different actual evapotranspiration patterns. The impact on runoff is further evident in the flow duration curve on a daily basis. The high flow (Q5) was higher and the low flow (Q90-Q95) was lower at the OP site compared to the JR site.

This study suggested that using net rainfall and actual evapotranspiration is essential for LUC assessment. The estimated 18% increase of annual runoff is modest compared to some other studies, some of which uses only PET and ignores the interception process, resulting in the estimated change more than 30 ~ 40%. Our findings showed that the reduction of net rainfall by the interception and the increase of actual evapotranspiration by LUC result in the comparatively modest impact of LUC on runoff.

Table of Contents

Acknowledgements.. i

Abstract……... iv

Table of Contents ix

List of Tables…………………………………………………………………xii

List of Figures... xiii

Chapter 1 General Introduction..1

1.1 Research Background...1

1.2 Objectives...4

1.3 Organization of the Dissertation...5

References...7

Chapter 2 Study Area..11

2.1 Two selected hillslopes in the Batanghari river basin 11

2.2 Climate...13

2.3 Geological settings and soil properties...13

References...15

Chapter 3 Groundwater Dynamics in Two Adjacent Hillslopes with Contrasting Soil Layer Depths: A Case Study in Sumatra,

Indonesia 17

3.1. Introduction 17

3.2. Methods 20

3.2.1. Field monitoring of hillslope GW and suction head 20

3.2.2 Hillslope hydrologic modeling 21

5.1 Results and Discussions 25

3.3.1 Seasonal GW patterns 25

3.3.2 Groundwater and tensiometric responses based on storm events analysis …………………………………………………………………..30

3.3.3 Model-based sensitivity analysis to understand the groundwater dynamics 34

3.3.4 Surface soil moisture dynamics from different scenarios 43

Conclusion 47

References 49

Chapter 4 Assessing Land Use Change Impacts on Water Balance and Groundwater Dynamics 57

4.1. Introduction 57

4.2. Methods 61

4.2.1 Field Monitoring of Rainfall and GW in Hillslope 61

4.2.2 Hourly Potential Evapotranspiration 61

4.2.3 Changing of Rainfall partitioning from Jungle rubber to Oil palm plantation.. 65

4.2.4 Hillslope hydrologic modeling 72

4.2.5 Model experiment settings.. 77

4.3. Results and Discussions 78

4.3.1 The changing of PET to land use changes...................................... 78

4.3.2 Attribution of changes in rainfall partitioning to land use change .. 79

4.3.3 Seasonal observed and modeling GW results of some different settings..81

4.3.4 Annual and monthly water budget.. 86

4.3.5 Impacts on runoff.. 89

4.3.6 Impacts of simulation conditions on the assessment 93

Conclusion 95

References..100

Chapter 5 Concluding Remarks 115

5.1 Conclusion..115

5.2 Assumptions 118

List of Tables

Table 3-1 Analysis of storm events..31

Table 3-2 Hydrologic modelling parameters 35

Table 3-3 Measured and calibrated soil properties 37

Table 4-1 Meteorological data required for P-M equation 62

Table 4-2 Trees parameters required for P-M equation...62

Table 4-3 Parameters for the P-M model and their calculation method 65

Table 4-4 Model simulation settings..77

Table 4-5 Throughfall and stemflow regression in OP..80

Table 4-6 Measured and calibrated parameters 82

List of Figures

Figure 2-1 (a) Sumatra island, (b) Location of the studied hillslopes, (c) Topography of the forest hillslope, (d) Cross–sectional view of the transect on forest hillslope, (e) Cross–sectional view of transect on oil palm hillslope, (f) Topography of the oil palm 12

Figure 3-1 Slope runoff diagram in the storage-discharge relationship of the rainfall-runoff-inundation model 22

Figure 3-2 Precipitation (a), observed groundwater of JR hillslope (b), and OP hillslope (c).. 28

Figure 3-3 Storm events analysis 33

Figure 3-4 Comparison of Observed, uncalibrated, and calibrated groundwater of (a) SK1, and (b) PR3. 39

Figure 3-5 Comparison of the simulated GW dynamics between (b) SK1 and (c) PR3 with the different conditions by switching hydraulic conductivity ("switch Ks"), soil water retention curve ("switch SWRC"), soil depth ("switch soil depths") and all the above conditions ("switch all"). Input hourly rainfall series is shown in (a). 40

Figure 3-6 Modified flashiness index (FI) of SK1 and PR3. 43

Figure 3-7 Volumetric water content at 30 cm depth of some scenarios in (a) SK1, and (b) PR3 45

Figure 3-8 Perceptual model of hillslope hydrology in the study site for: (a) JR

hillslope, and (b) OP hillslope.. 46
Figure 4-1 Interception calculative model (Suzuki et al., 1979)........................... 67
Figure 4-2 Diagram of evapotranspiration in the Suzuki model........................... 68
Figure 4-3 Oil palm configuration of this research and Bejo et al., (2015)'s research 71
Figure 4-4 RRI–GW conceptual model (adopted from Sayama et al., 2015)....... 72
Figure 4-5 Evapotranspiration from the soil (AET2).. 76
Figure 4-6 Comparison of the observed and simulated GWL from various simulation settings.. 83
Figure 4-7 Change of PET, AET, and Discharge from JR to OP 88
Figure 4-8 Flow Duration Curve (FDC) of daily discharge of JR and OP 91
Figure 4-9 Water balance of model simulations 92

Chapter 1 General Introduction

1.1 Research Background

Hydrological processes in humid tropical region are distinct from global locations. Understanding the main cause of the differences in the hydrological processes between humid tropics and other climates is important, particularly in hydrological modelling which are mostly developed for temperate regions. There are two main factors which creates distinct characteristics between humid tropical and temperate regions – constant high temperature and rainfall. Adapting to these distinct conditions, the soil and plants in the humid tropics can be very different to those in the typical temperate region. This study focuses on how these factors influencing the hydrological process in the region, in particular dynamic ground water response, rainfall partitioning and actual evapotranspiration.

The first part of this study is focusing on the GW dynamics in the humid tropical region which are highly responsive to rain. Even though the soils in this region are characterized by higher clay content, deep weathered, and has several meters of depth (Verheye, 2009), however, previous studies on sub–surface flow in humid tropical hillslopes have highlighted the unique soil characteristics in this region, including high hydraulic conductivity (*Ks*) and water retention capacity, which could enable rapid and profound infiltration (e.g., Dykes and Thornes, 2000; Muñoz-Villers and McDonnell, 2012; Sayama et al., 2021). This is counter-intuitive since the clayey soils in temperate regions are typically have lower permeability, hindering the infiltration of rainwater into deeper soil layers. several studies from temperate regions have also confirmed the substantial impact of weathered bedrock on hydrological processes. These studies indicated that the transient saturation at the soil–bedrock interface is linked to fluctuations of GW levels (Katsuyama et al., 2005; Kosugi et al., 2008; and Onda et al., 2001).

Most of the published works on GW dynamics were concentrated on investigating one hillslope and concentrated on documenting the features of a hillslope environment, rather than conducting a systematic exploration of the primary factors influencing the hillslope hydrology in these unique environments. Although those researches intensively produced numerous valuable insights, it is challenging to understand how the factors controls the GW behavior only by studying a single hillslope (Uchida et al., 2006; Kirchner, 2003; Weiler and McDonnell, 2004). Therefore, a study that compares two hillslopes with distinct GW response is necessary to clarify the role of each parameters to the subsurface flow dynamics on the hillslope.

The first part of the study expands on our earlier research, where we investigated the GW dynamics on a steep hillslope characterized by a thick soil layer in the humid tropical forest of Sumatra Island, Indonesia. The study highlighted that soil allows high vertical infiltration and create transient saturation contributing to storm runoff (Sayama et al. 2021) creating a high GW response to rainfall, particularly at the foothill of the hillslope. An adjacent hillslope that is seemingly similar was monitored to understand the influence of surface hillslope and bedrock topography, including factors like length and gradient through this study, it was clarified that the high GW responses are not consistent across various hillslopes in the same region, hindering the generalization of runoff processes in Sumatra, Indonesia.

The second part of the study is focusing on impact of the LUC to the GW and the water balance. This part contributes to improve the RRI model for understanding the LUC in the humid tropical region. The transformation of forested regions into oil palm plantations, a widespread phenomenon in humid tropical regions, has been extensively documented (Hansen et al., 2013; Gibbs et al., 2010; Margono et al., 2014). In Southeast Asia, vast forested regions have been transformed into monoculture plantations such as oil palm over recent decades, leading to significant ecological and hydrological consequences (Hansen et al., 2013; Margono et al., 2014; Clough et al., 2016).

This substantial LUC has been linked to the degradation of ecohydrological functions (Bruijnzeel, 2004; Bradshaw et al., 2007; Ellison et al., 2017) and poses a substantial threat to water reservoirs and watershed management (Woldemichael et al., 2012; Yigzaw & Hossain, 2016). Therefore, it is important to analyze the effect of LUC in this environment.

In order to encompass the complicated impacts of LUC in a hillslope scale, this study integrated some hydrological modeling techniques to quantify PET variations, rainfall partitioning between JR and OP that two dominant LUC in the area, and RRI model to estimate the GW dynamics and water balance changing.

It is common for LUC studies to use variables in different state such as "gross rainfall (P_G)" instead of "net rainfall (P_n)" or "potential evapotranspiration" instead of "actual evapotranspiration (AET)". In humid tropical region, subsurface flow is dominant therefore the simulation results of a hydrological model are strongly influenced by cumulative antecedent storm events. Accordingly, using different states of same variables of rainfall and evapotranspiration may results in different hydrological impacts.

To get sufficient AET, we improved the RRI model by applying the application root zone and "Evapotranspiration threshold" to regulate plant water intake due to evapotranspiration, particularly during dry season. Then, to understand the impact of using different variables of rainfall and evapotranspiration input to the RRI model, we demonstrated three different state of variables (P_G and PET, P_n and PET, and P_n and AET) in the LUC simulations.

1.2 Objectives

The general objectives of this study are to comprehend the characteristics of GW and identify the primary controlling factors of dynamically GW in humid tropical hillslopes related to its soil characteristics, hillslope features, and lad cover. In order to achieve these objectives, we constructed the following specific objectives:

1) To investigate whether the high GW responses can be observed and generalized in humid tropical hillslopes in Sumatra, Indonesia;
2) To identify major contributing factors to the high GW responses based on field observations and numerical simulations;
3) To observe the influence of LUC on rainfall interception and evapotranspiration;
4) To understand the influence of LUC on groundwater dynamics and water balance;
5) To clarify the impacts of different rainfall and evapotranspiration input (gross rainfall, net rainfall, potential evapotranspiration, and actual evapotranspiration) for the LUC assessment.

1.3 Organization of the Dissertation

This dissertation consists of four chapters which are briefly explained as follows:

Chapter 1 introduces the general knowledge of hydrological processes in humid tropical hillslope. The main purpose, specific objectives, and key contents of this dissertation are also described in this chapter.

Chapter 2 describes key information of the studied hillslopes such as the hillslope topography, climate, geological features, etc.

Chapter 3 presents the observational and modelling results of groundwater and surface soil moistures of two adjacent hillslopes with some scenarios. The chapter mainly discussed the predominant control factors of GW dynamics and the importance of lateral subsurface flow in soil layers that can leads rapid responses of GW in the humid tropics in Sumatra island.

Chapter 4 analyzes the hydrological consequences of LUC in a hillslope scale. This chapter showed that by incorporating some hydrological modeling techniques to quantify the effect of LUC will give more reliable result. This part also demonstrated how the use of different state of rainfall and evapotranspiration giving different LUC simulation results.

Chapter 5 summarizes the findings and gives the overall conclusion to this dissertation.

References

Bradshaw, C. J. A., N. S. Sodhi, K. S.-H. Peh, and B. W. Brook. (2007). Global evidence that deforestation amplifies flood risk and severity in the developing world. Global Change Biology 13 (11):2379-2395. https://doi.org/10.1111/j.1365-2486.2007.01446.x

Bruijnzeel, L. A. (2004). Hydrological functions of tropical forests: not seeing the soil for the trees? Agriculture, Ecosystems and Environment 104(1):185-228. https://doi.org/10.1016/j.agee.2004.01.015

Dykes A.P., Thornes J.B. (2000). Hillslope hydrology in tropical rainforest steep lands in Brunei. Hydrol Proc 14:215-235. doi:10.1002/(SICI)1099-1085(20000215)14:2

Ellison, D., C. E. Morris, B. Locatelli, D. Sheil, J. Cohen, D. Murdiyarso, V. Gutierrez, M. van Noordwijk, I. F. Creed, J. Pokorny, D. Gaveau, D. V. Spracklen, A. B. Tobella, U. Ilstedt, A. J. Teuling, S. G. Gebrehiwot, D. C. Sands, B. Muys, B. Verbist, E. Springgay, Y. Sugandi, and C. A. Sullivan. (2017). Trees, forests and water: cool insights for a hot world. Global Environmental Change 43(51):51-61. https://doi.org/10.1016/j.gloenvcha.2017.01.002

Gibbs, H. K., Ruesch, A. S., Achard, F., Clayton, M. K., Holmgren, P., Ramankutty, N., and Foley, J. A. (2010). Tropical forests were the primary sources of new agricultural land in the 1980s and 1990s, P. Natl. Acad. Sci. USA, 107, 16732–16737

Hansen, M. C., Potapov, P. V., Moore, R., Hancher, M., Turubanova, S. A., Tyukavina, A., Thau, D., Stehman, S. V., Goetz, S. J., Loveland, T. R., Kommareddy, A., Egorov, A., Chini, L., Justice, C. O., and Townshend, J. R. G. (2013). High-Resolution Global Maps of 21st-Century Forest Cover Change, Science, 342, 850–853, https://doi.org/10.1126/science.1244693

Katsuyama M, Ohte N, Kabeya N. (2005). Effects of bedrock permeability on hillslope and riparian groundwater dynamics in a weathered granite catchment. Water Resour Res 41:W01010

Kirchner, J. W. (2003). A double paradox in catchment hydrology and geochemistry. Hydrol Proc 17:871-874. doi: 10.1002/hyp.5108

Kosugi, K.I., Katsura, S.Y., Mizuyama, T., Okunaka, S., 530 & Mizutani, T. (2008). Anomalous behavior of soil mantle groundwater demonstrates the major effects of bedrock groundwater on surface hydrological processes. Water Resour Res 44:W01407

Margono, B. A., P. V. Potapov, S. Turubanova, F. Stolle, and M. C. Hansen. (2014). Primary forest cover loss in Indonesia over 2000-2012. Nature Climate Change 4:730-735. https://doi.org/10.1038/nclimate2277

Muñoz-Villers, L. E., and McDonnell, J. J. (2012). Runoff generation in a steep, tropical montane cloud forest catchment on permeable volcanic substrate, Water Resour. Res., 48, W09528, doi:10.1029/2011WR011316

Onda, Y., Komatsu, Y., Tsujimura, M., & Fujihara, J.553 I. (2001). The role of subsurface runoff through bedrock on storm flow generation. Hydrol Process 15:1693-1706

Sayama, T., Araki, R., Yamamoto, K., & Apip. (2021). Characteristics of soil and hillslope responses in humid tropical forests in Sumatra, Indonesia. Hydrol Res Lett 15:23-30

Sayama, T., Ozawa, G., Kawakami, T., Nabesaka, S., & Fukami, K. (2012). Rainfall–Runoff–Inundation Analysis of the 2010 Pakistan Flood in the Kabul River Basin. Hydrol Sci J., 57(2), 298–312. https://doi.org/10.1080/02626667.2011.644245

Sayama, T., Tatebe, Y., Iwami, Y., & Tanaka, S. (2015). Hydrologic Sensitivity of Flood Runoff and Inundation: 2011 Thailand Floods in the Chao Phraya River Basin. Natural Hazards and Earth System Sciences, 15(7), 1617–1630. https://doi.org/10.5194/NHESS-15-1617-2015

Uchida T, McDonnell JJ, Asano Y. (2006). Functional intercomparison of hillslopes and small catchments by examining water source, flow path and mean residence time. J Hydrol 327, 627-642

Verheye W. (2009). Soils of the humid and sub-humid tropics. Land Use, Land Cover and Soil Sciences-Volume VII: Soils and Soil Sciences-2, UNESCO-EOLSS Publication, ISBN: 9781848262379

Weiler, M., McDonnell, J., (2004). Virtual experiments: a new approach for improving process conceptualization in hillslope hydrology. J. Hydrol. 285 (1–4), 3–18

Yigzaw, W. & Hossain F., (2016). Land Use and Land Cover Impact on Probable Maximum Flood and Sedimentation for Artificial Reservoirs: Case Study in the Western United States. J. Hydrol. Eng. 21:501-502. doi: 10.1061/(ASCE)HE.1943-5584.0001287

Woldemichael, A. T., Hossain, F., Pielke, R., and Beltrán-Przekurat, A. (2012). Understanding the impact of dam-triggered land use/land cover change on the modification of extreme precipitation, Water Resour. Res., 48, W09547. doi:10.1029/2011WR011684

Chapter 2 Study Area

2.1 Two selected hillslopes in the Batanghari river basin

The Batanghari River basin is located on the island of Sumatra, Indonesia. The Batanghari River is the longest river on the island, originating from the Barisan Mountains and flowing eastward towards the coast. As it progresses, it merges with the Tembesi River and later splits into the Kumpeh River before rejoining in the downstream.

The basin's topography varies, featuring mountains in the western section and low–lying flat areas with wetlands. The mountainous region is source of some rivers, with elevations expand from 1,000 m to 3,700 m. Approximately 60% of the basin area is characterized by rolling terrain, with elevations between 10 to 100 m above sea level (Ministry of Public Works, 2003). In the middle part of the basin, close to the Muara Tembesi station, the Batanghari River merges with the Tembesi River, flowing eastward through flat swampy terrain up to 200 km from the coast (NASA and METI (National Aeronautics and Space Administration and Ministry of Economy Trade and Industry of Japan), 2017). Along the eastern province's coastline, there are extensive peatland areas covering approximately 700,000 hectares (Wahyunto and Subagjo, 2003).

The selected hillslopes are located in the Batanghari river basin, Sumatra, Indonesia (**Figure 2–1(a)**), consist of a forested hillslope in Sekancing township

(JR), and a hillslope with15-year-old palm plantation in Pulau Raman township (OP). Both hillslopes have identical climatic conditions, as they are only 900m apart from each other.

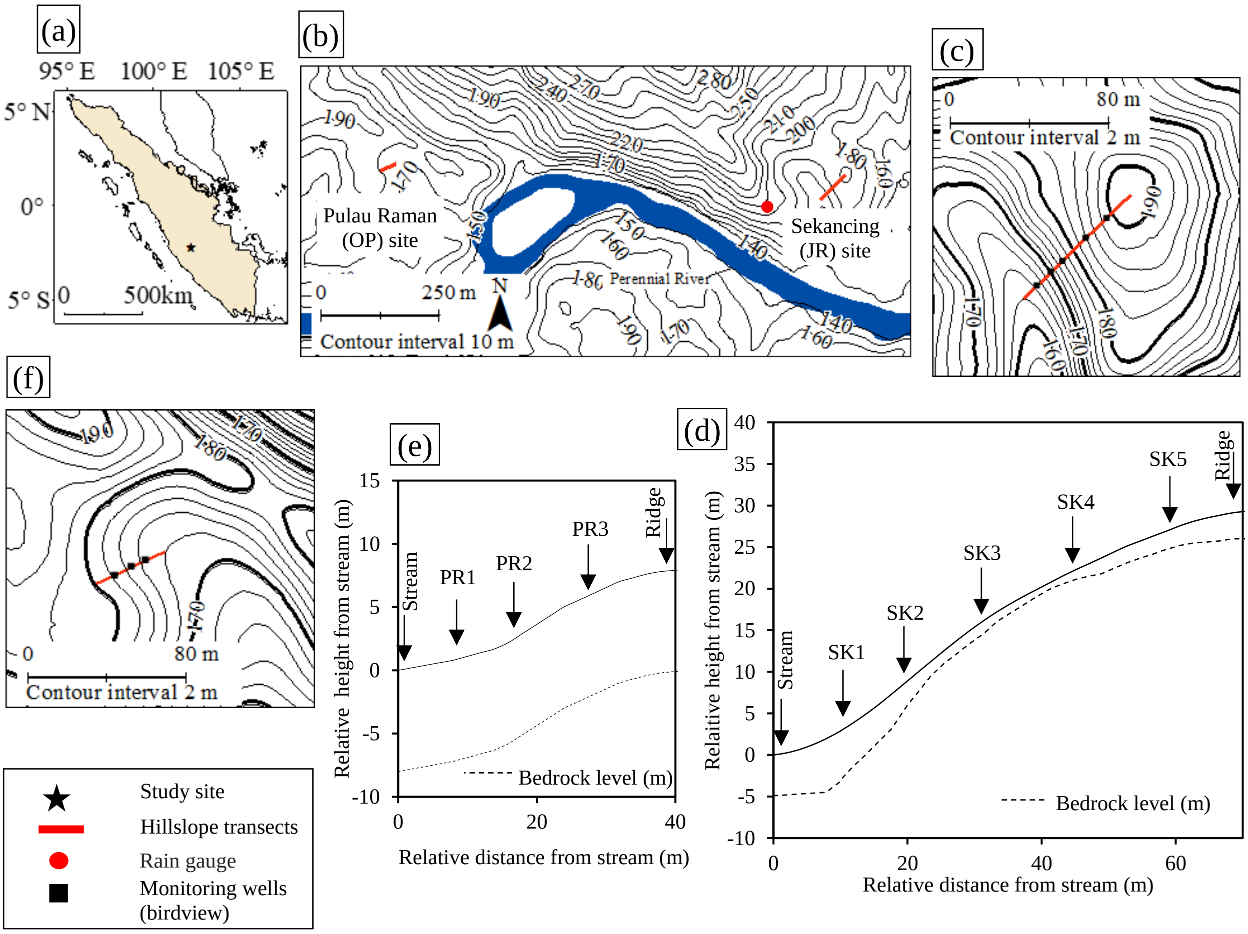

Figure 2-1 (a) Sumatra island, (b) Location of the studied hillslopes, (c) Topography of the forest hillslope, (d) Cross–sectional view of the transect on forest hillslope, (e) Cross–sectional view of transect on oil palm hillslope, (f) Topography of the oil palm

The JR hillslope is covered by a secondary forest or we know as the “jungle rubber agroforest” (Joshi et al., 2002), where rubber trees are cultivated without using of slash–and–burn methods. Alternatively, the OP hillslope is covered by 15–year–old palm trees and sparse grass. Both hillslopes have streams at the bottom of the slopes, where that at JR persists year-round, while the stream at OP is only seen during the wet season. The JR hillslope is nearly twice longer and steeper than OP hillslope.

2.2 Climate

The climate in Jambi is humid tropical characterized by monthly rainfall exceeding 100 mm, as documented by Chang and Lau (1993). Climate stations maintained by the Indonesian Agency for Meteorological, Climatological, and Geophysics (BMKG) between 2001 and 2013 indicate an average air temperature ranging from 22.2±0.2°C (upstream) to 26.8±0.2°C (downstream) (Eva et al., 2020). Despite the high monthly rainfall, the area exhibits distinct wet and dry seasons, driven by two monsoons.

According to Aldrian and Susanto (2003), the wet northwest monsoon, originating in the northern hemisphere, affects the basin from November to March, while the dry southeast monsoon, originating in the southern hemisphere, prevails from May to September. The wet monsoon exhibits two distinct peaks, occurring in December and April, leading to bimodal rainfall patterns.

2.3 Geological settings and soil properties

Soil depths were measured at five points along the JR slope (SK1-SK5), and three points at the OP slope (PR1-PR3) using a portable dynamic cone penetrometer, with a weight of 5 kg and falling distance of 50 cm. The 20 hits for penetrating 10 cm (i.e. $N_c > 20$) can be regarded as a guide of the interface of soil and bedrock (Dykes et al, 2000; Hosoda et al, 2016). The bedrock level was approximately 450 cm below the soil surface at SK1, 415 cm below at SK2, approximately 150 cm below at SK3, 90 cm, and 220 cm below for SK4 and SK5, respectively. The N_c values of PR2 and PR3 were less than 20 even at a penetration depth of 5 m. Due to the limitation of the used cone penetration stick, the depth of bedrock in PR2 and PR3 could not be ascertained. However, the depth soil layer was estimated by well drilling at PR2 and PR3, located approximately 800 cm below the soil surface for the two points.

Soil particle analyses were conducted on 3 soil samples in JR and 1 soil sample in OP. The samples were taken from depths of 60 cm to determine the soil textures at two sites. According to the sieve and hydrometer methods and USDA definitions, the soil textures were classified as clay at JR and silty clay at OP. Five undisturbed soil samples on rings were collected from depth of 5, 30, 60, and 90 cm nearby boreholes and analyzed it to the laboratory to get its characteristics. The average hydraulic conductivity in JR hillslope is 1.7 times higher with wider variation than OP hillslope. The K_s value is higher near the soil surface and become smaller with depth. The porosity at both sites ranged from 57.5 to 65.6%. Volumetric water contents at pF1, pF2, pF2.54 and pF 4.2 were analyzed using the undisturbed soil samples to get the pF curves.

References

Aldrian E., Susanto D. (2003) Identification of three dominant rainfall regions within Indonesia and their relationship to sea surface temperature. International Journal of Climatology 23: 1435–1452. DOI: 10.1002/joc.950.

Chang J.H., Lau L.S. (1993) A definition of the humid tropics. In Hydrology and Water Management in the Humid Tropics: Hydrological research issues and strategies for water management, Bonell M, Hufschmidt MM, Gladwell JS (eds). UNESCO, Cambridge: Cambridge University Press; 571–574.

Dykes A.P., & Thornes J.B. (2000) Hillslope hydrology in tropical rainforest steeplands in Brunei. Hydrol Proc 14:215-235. doi:10.1002/(SICI)1099-1085(20000215)14:2

Hosoda I., Tani M. (2016) Influence of moisture fluctuation in thick, weathered bedrock layer on rainfall–runoff response in a small, forested catchment underline by Paleozoic sedimentary rocks in Japan (in Japanese with English abstract). Trans Jap Geomorph Union 37:465-492

Joshi, L, Wibawa, G., Vincent, G., Boutin, D., Akiefnawati, R., Manurung, G., Van Noordwijk, M., Williams, S. (2002) Jungle rubber: A traditional agroforestry system under pressure. International Centre for Research in Agroforestry. ICRAF, Indonesia.

Ministry of Public Works. (2003) Direction of Regional Spatial Planning in Batanghari River Basin. Ministry of Public Works, Indonesia

NASA and METI (National Aeronautics and Space Administration, Ministry of Economy Trade and Industry of Japan) (2017) ASTER GDEM 2.

Wahyunto, Ritung S, Subagjo H. (2003) Maps of area of peatland distribution and carbon content in Sumatra, 1990–2002. Wetlands International–Indonesia Programme & Wildlife Habitat Canada (WHC), Bogor.

Yamamoto EvaMiaSiska, Sayama T, Yamamoto K, Apip (2020) Comparison of runoff generation methods for land use impact assessment using the SWAT model in humid tropics. Hydrological Research Letters 14(2): 81–88. DOI: 10.3178/hrl.14.81

Chapter 3 Groundwater Dynamics in Two Adjacent Hillslopes with Contrasting Soil Layer Depths: A Case Study in Sumatra, Indonesia

3.1. Introduction

The spatiotemporal pattern of groundwater (GW) is important for understanding environmental, agricultural, and bio–geochemical processes at the hillslope scale (Gish et al. 2011; Lin et al. 2006). Accordingly, GW and soil moisture pattern of hillslopes and its main influenced parameters have been widely studied (Penna et al. 2013; Qiu et al. 2001; Sela et al. 2012). The GW fluctuation and soil moisture variations and their responses according to rainfall events typically vary by the landscape. Wilson and Dietrich (1987) assessed a zero–order basin in California and found the significant influence of weathered bedrock on hydrological processes. Kosugi et al (2008), Katsuyama et al (2005) and Onda et al (2001) has confirmed the significance of bedrock groundwater in granitic catchments in Japan. This suggests that the temporary saturation at the soil–bedrock interface is linked to the fluctuation of bedrock groundwater levels.

Many of those findings are coming from humid temperate regions (Burt & McDonnell 2015). The previous works in that area had showed the primary controls on redistribution of water across landscapes (Montgomery & Dietrich (1988);

Jencso et al (2009); Detty & McGuire (2010); Jencso & McGlynn (2011)). Sidle et al. (2000), Buttle & McDonald (2002), Gannon et al., (2014) have shown the importance of soil properties on hydrological processes, and Du et al. (2016); Elsenbeer (2001); Meerveld & McDonnell (2006) have shown the importance of the contrasting hydraulic conductivities.

In recent years, attentions have been also given to humid tropical regions. Similar to the temperate regions, many of runoff process studies highlight subsurface flow and the primary contribution of the pre-event water in storm runoff (Barthold & Woods 2015; Birch et al. 2021; Saito et al. 2023). Furthermore, Dykes & Thornes (2000) and Negishi et al. (2007) reported the rapid responses of subsurface flow even in comparatively thick soil layers due to macropore structures. Vertical preferential flow has been also observed in tropical regions by Birch et al. 2021, Cheng et al. 2018, Gardner et al. 2017, Kinner & Stallard 2004 and Ogden et al. 2013. These macropore networks are primarily formed through root decay and the tunneling activities of soil fauna, which are commonly found in humid tropical forest (Dykes & Thornes 2000; Crespo et al. 2011). Other explanations of the dynamic response of GW in humid tropics are associated to the unique soil properties with high hydraulic conductivity and large water retention capacity, which could facilitate fast and deep percolation (e.g., Cheng et al. 2023; Ghimire et al. 2014; Noguchi et al. 1997a, b; Sayama et al. 2021).

This study builds upon our previous work, which examined the dynamics of

GW on a steep hillslope with thick soil layer in a humid tropical forest of Sumatra Island, Indonesia (Sayama et al. 2021). Our previous study was in line with other previous studies in Southeast Asia in terms of the rapid GW responses during storm events (Dykes & Thornes (2000) in Brunei and Noguchi et al. (1997b) in Malaysia). Our previous study highlighted that soil allows high vertical infiltration rate and create transient saturation contributing to storm runoff (Sayama et al. 2021). However, the role of hillslope and bedrock topography such as length, gradient and other factors have not been clarified. Moreover, we have not clarified if such high GW responses appear in any hillslope in the same region to generalize the runoff processes in Sumatra, Indonesia.

To address the question, we conducted GW monitoring at another adjacent hillslope, which has different landcover conditions with even thicker soil layer. Unlike our previous study conducted in secondary growth jungle rubber forest, the new adjacent hillslope is covered by oil palms, which is another typical land cover condition in the region. These hillslopes share the similar climatic conditions as the two monitoring sites are only 900m apart from each other. For both slopes, we measured GW at three positions along the hillslopes together with soil characteristics and depths. Based on the GW monitoring results, we applied a physically based hydrological model, the RRI model representing the local soil characteristics, so that we can conduct a numerical experiment by switching the properties. The main objectives of this study are 1) investigating if the high GW responses can be observed and generalized in humid tropical hillslopes in Sumatra, Indonesia and 2) identifying the major contributing factors of such high GW response based on field observations and numerical simulation results.

3.2. Methods

3.2.1. Field monitoring of hillslope GW and suction head

The monitoring period was from August 2017 to December 2020 in JR, and from November 2018 to December 2020 in OP. Ten–minute rainfall data were gauged with a tipping bucket (CPK-RAIN-1, Climatec; Phoenix, AZ, USA). The tipping bucket was set in an open area with 2m above the ground (on top of the local house rooftop) that can protect from any obstruction and located within 100m from JR hillslope and 800m from OP hillslope. Pressure sensors (DIK-615A-B1, Daiki; Tokyo, Japan) were used to gauge GW levels in boreholes. The sensors determined the height of a water column by gauging water pressure through the integrated pressure sensor. We measured the GW level from three observation boreholes installed along each hillslope (SK1–SK3 and PR1–PR3) (**Figure 1(d, e)**). Temperature and atmospheric pressure were also recorded by a barometer (TD-Diver DI800, Van Essen; Delft, Netherlands). The atmospheric pressure data collected by the barometer was used to compensate the variations of measured pressure of the pressure data (DIK-615A-B1, Daiki; Tokyo, Japan).

To get a soil water suction in the soil surface or shallow soil layer, dielectric soil-moisture meters (UIZ-SM150T, Uizin; Tokyo, Japan.) were installed near each borehole at certain depths. These soil suction dynamics data were used to analyze the soil surface response to storm events and as a supporting data to the groundwater response during such events. Accordingly, we divided precipitation, soil surface suction, and groundwater records into multiple events. In addition, storm events were recorded by adopting the storm separation method from Itokazu et al. (2013), in which an individual event was identified only if there had been no rainfall for ≥ 12 hr after the last precipitation.

3.2.2 Hillslope hydrologic modeling

The rainfall–runoff–inundation (RRI) was employed in this study. Sugawara and Sayama (2021) developed an unsaturated flow component for the RRI model based on measured water retention curve parameters determined by experimental and observational data. This model assumed an equilibrium water distribution along vertical infiltration throughout the hillslope, and the bedrock conductivity was impermeable. The model's slope runoff diagram is shown in **Figure 2** (Yamamoto et al. (2022)), where *x* is the coordinate along the bedrock, and *z* is the vertical coordinate to the bedrock. Water storage S and lateral discharge q were defined according to Eqs. (1,2):

$$S = \int_0^L \theta dz \,, \tag{1}$$

$$q = \sin\phi \int_0^L K dz \,. \tag{2}$$

where θ is volumetric water content, K is hydraulic conductivity, L is soil depth, ϕ

is slope angle. Eq. 2 is explained that the model assumed the hydraulic gradient was equivalent to the surface topography.

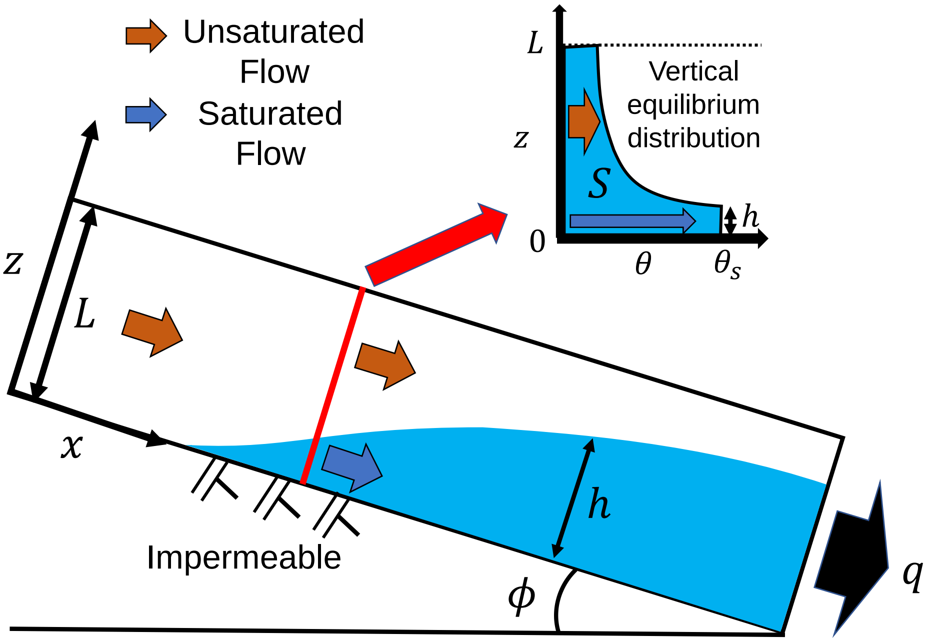

Figure 3-1 Slope runoff diagram in the storage-discharge relationship of the rainfall-runoff-inundation model

This model used the Brooks-Corey and Mualem model for estimating water retention curves and unsaturated hydraulic conductivities according to Eqs. (3,4):

$$S_e = \frac{\theta - \theta_r}{\theta_s - \theta_r} = \begin{cases} \left(\frac{\psi_e}{\psi}\right)^{\lambda} & (\psi < \psi_e) \\ 1 & (\psi \geq \psi_e) \end{cases}, \tag{3}$$

$$K = K_s \cdot S_e^n , \qquad \left(n = 2.5 + \frac{\lambda}{2}\right), \tag{4}$$

where S_e is effective saturation; K_s is the hydraulic conductivity at saturation; θ_s

and θ_r are the soil saturated and residual volumetric water contents, respectively; ψ is the matric potential, ψ_e is the water entry pressure; and λ is the pore size distribution index. The model presumed immediate equilibrium conditions for the vertical water distribution within the soil profile.

$$\frac{\partial\psi}{\partial z} = -\cos\phi \ . \tag{5}$$

According to Eqs. (1-5), the storage and discharge were determined using Eqs. (6-10):

$$S \leq \theta_r L : \text{No flow}$$

$$\forall S \quad q = 0\,, \tag{6}$$

$$\theta_r L < S \leq S_{thre} : \text{Unsaturated lateral flow}$$

$$S = \theta_r L + \frac{(\theta_s - \theta_r)\psi_e}{(1-\lambda)\cos\phi}\left(\left(\frac{\psi_b}{\psi_e}\right)^{1-\lambda} - \left(\frac{\psi_b - L\cos\phi}{\psi_e}\right)^{1-\lambda}\right), \tag{7}$$

$$q = \frac{K_s\psi_e\sin\phi}{(1-n\lambda)\cos\phi}\left(\left(\frac{\psi_b}{\psi_e}\right)^{1-n\lambda} - \left(\frac{\psi_b - L\cos\phi}{\psi_e}\right)^{1-n\lambda}\right), \tag{8}$$

$$S_{thre} < S \leq \theta_s L : \text{Saturated + unsaturated lateral flow}$$

$$S = \theta_s h + \theta_r(L-h) + \frac{(\theta_s - \theta_r)\psi_e}{(1-\lambda)\cos\phi}\left(1 - \left(\frac{(h-L)\,cos\,\phi + \psi_e}{\psi_e}\right)^{1-\lambda}\right), \tag{9}$$

$$q = k_s h \sin\phi + \frac{K_s\psi_e\sin\phi}{(1-n\lambda)\cos\phi}\left(1 - \left(\frac{(h-L)\,cos\,\phi + \psi_e}{\psi_e}\right)^{1-n\lambda}\right), \tag{10}$$

where ψ_b is the pressure head at the bedrock boundary, h is the water level, and $S_{thre} = S(h = 0)$ represents the storage at which saturated flow occurs. When the soil layer was completely saturated, lateral discharge was calculated by the sum of Darcy and Manning flows (Eqs. (11-12)):

$$\theta_s L < S \text{ : Surface flow}$$

$$S = \theta_s L + h - L \,, \tag{11}$$

$$q = K_s L \sin\phi + \frac{\sqrt{\sin\phi}}{n_s}(h - L)^{\frac{5}{3}} + \frac{K_s n\, sin\,\phi}{\theta_s - \theta_r}(h - L)\,, \tag{12}$$

where n_s is Manning's roughness, and the third term on the right side of Eq. (12) is the correction term. The slope runoff was calculated according to the above storage–discharge relationship, and the next continuous equation (Eq. (13)):

$$\frac{\partial S}{\partial t} + \frac{\partial q}{\partial x} = r \,, \tag{13}$$

where t is time. and r is rainfall intensity. In the RRI model, the discharge was simulated by extending it to two dimensions and assuming $\cos\phi \approx 1$ and $\sin\phi$ is equal to the hydraulic gradient.

The observed soil parameter data, such as K_s and soil water retention characteristics (SWRCs) were used as initial parameters values to run the model. Then, if the simulation was not satisfactory, the parameter value and/or boundary conditions were adjusted within reasonable ranges until the simulated model results closely matched the observed data. For measuring the rate of satisfaction, the model results were measured by the Nash–Sutcliffe efficiency (NSE) index (Nash & Sutcliffe 1970).

The calibrated model was then used to investigate the effects of varied parameter values between the two sites. To better quantify the magnitude of GW fluctuation for each scenario, an index modified from a flashiness index (*FI*; Baker et al. 2004) was introduced to indicate the average change of GW from the previous hour, where higher *FI* values indicated more rapid GW fluctuation (Eq. (14)):

$$FI = \frac{\sum_{i=1}^{N} |q_i - q_{i-1}|}{N} \tag{14}$$

where N is the number of data (simulation period), q_i is the GW level in an hour, and q_{i-1} is the GW of the previous hour.

5.1 Results and Discussions

3.3.1 Seasonal GW patterns

Figure 3–2 shows how the observed GW patterns at JR and OP hillslopes significantly differs – the former fluctuated more greatly while the latter was smoother. The GW table at the foot of the JR hillslope (SK1) indicated the persistent existence of GW in the soil layer. The GW table was stabled at depths of 100–300 cm below the soil surface (150–350 cm above the bedrock, given ~450 cm soil layer at SK1) even in the middle of the dry season (September 2018, 2019, and 2020). The high water retention capacity could be a reason the existence of extremely rapid saturation within the soil profile during wet season storms. This situation could be elucidated by the transition of the “capillary fringe” into a fully saturated state. (Anderson & Burt 1990), Although the basic flow of water through macropores from the soil surface downward might be quick enough to create groundwater dynamics, similar to findings from earlier studies in this region (eg. Crespo et al 2011; Dykes & Thornes 2000; Negishi et al 2007). Likewise, the GW table remained at a depth of ~300 cm from the soil surface at SK2 in the early dry season (June), and decreased to 415 cm during the driest period (August–September), even reaching nearly 500 cm in 2019.

Alternatively, such a dynamic GW table was not observed at SK3 which located in the ridge. The persistent GW was observed at depths of approximately 150 cm from the surface. Compared to the cone penetration test, the GW table exists at nearly the same level as the interface between the soil and bedrock at SK3. The GW level increased during storm events but returned to the previous level quickly. In a few instances, the GW level decreased from the persistent level during long dry spells.

Even though we did not take a soil sample from the bedrock layer, however, based on the GW result in SK3 we expected that the bedrock layer was impermeable. On this condition, the bedrock could be an important impeding layer for water to infiltrated to the deeper soil horizons (Zimmer & McGlynn 2017; Meerveld & McDonnell 2006; Verseveld et al. 2008, and Graham et al. 2010). Moreover, this mechanism has been steering the lateral subsurface flow paths at the soil–bedrock interface, thereby serving as an additional factor intensifying groundwater dynamics in the lower area (Hardie et al. 2012; Ameli et al. 2015). More special in the area which the soil was always nearly saturated as uniqueness of the soil in forest humid tropic, when this condition was followed by intense rainfall, Various layers in the soil profile potentially contribute to the lateral subsurface flow (Crespo et al. 2011).

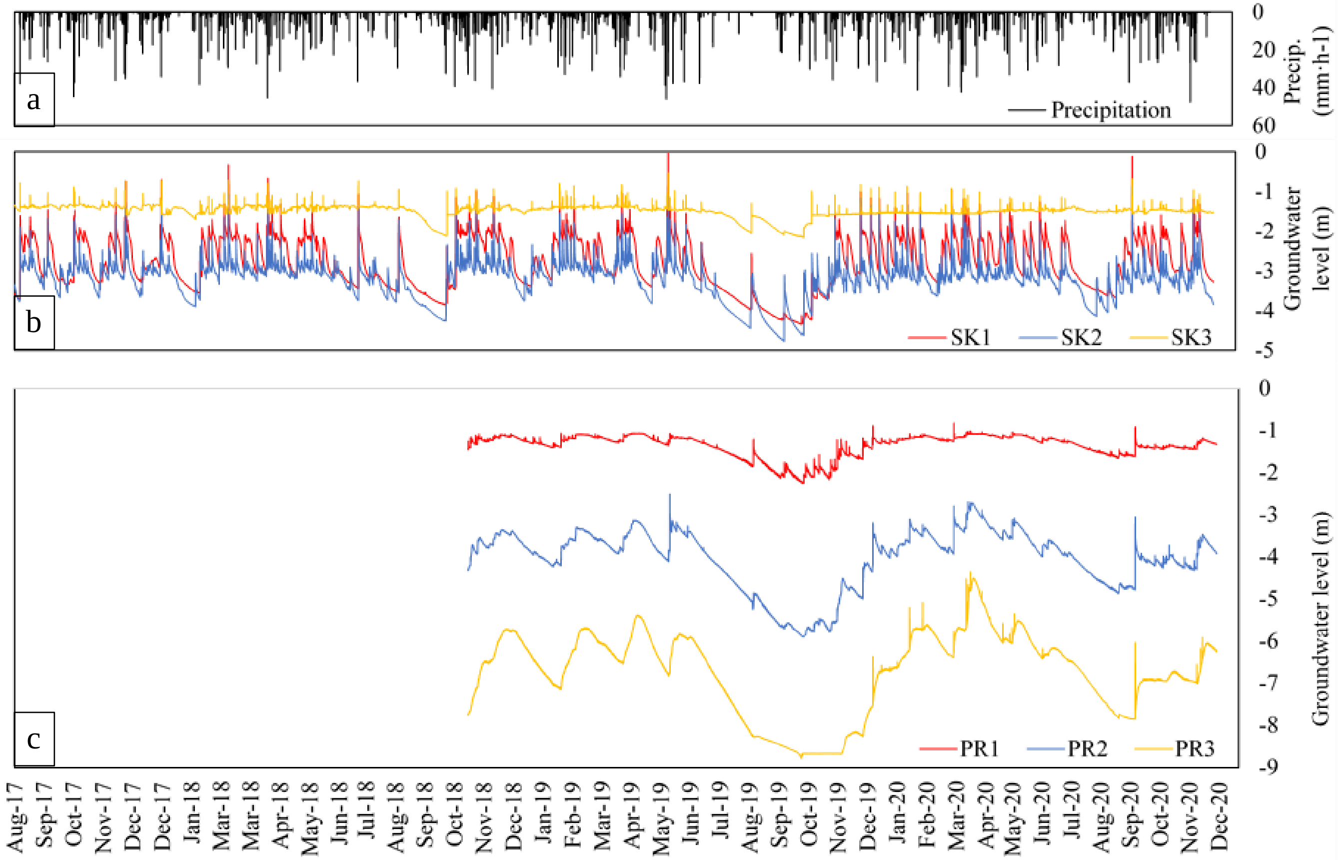

Figure 3-2 Precipitation (a), observed groundwater of JR hillslope (b), and OP hillslope (c)

The OP hillslope maintains a comparatively deeper soil depth (800 cm), particularly for PR3 located near the top of the hill, where the borehole recorded 550–600 cm depths in the early dry season (June), and then continuously decreased until ~800 cm below the soil surface (September 2020), reaching its absolute lowest level at 878 cm below the surface in October 2019. Similarly, the GW in PR2 showed a steadier pattern at depths between 300–500 cm, with much smoother temporal transitions compared to the JR hillslope, whereas the GW in PR1 showed the least variation in depth (at ~50–150 cm), likely influenced by the short distance of PR1 to the stream.

These observation result show that GW response in adjacent hillslopes in humid tropics can be very different. While the high GW response in JR hillslope is similar to earlier studies, the GW response in OP hillslope shows slower response. Based on this result, we cannot generalize high GW response in humid tropical hillslopes. Even though the slope surface of OP was steep (21°), however, the spatial changed gradient of the bedrock depth was less than JR which ranging from 1.5 to 4m, from top to foot hill. With bedrock depth of 8m from PR2 to PR3, it indicated that the bedrock slope angle in OP was gentler than JR and not identic with the surface topography. Similar hillslope characteristic was reported before by Clair et al (2015), the topography of bedrock can significantly differ from surface topography, especially in landscapes with deep soils, such as in the OP hillslope.

3.3.2 Groundwater and tensiometric responses based on storm events analysis

Table 3–1 shows the GW responses of the 10 selected storm events at JR and OP. Events #1 and #2 are the small rainfall events (< 10 mm), events #3–8 are the moderate events (40–80 mm) and events #9 and #10 are the large rainfall events (> 100 mm). Notably, no response was found during the small rainfall events at both JR and OP. **Figure 3–4** shows the observed GW and tensiometric records for the moderate and large events. Events #5 (total rainfall: 46.6 mm) and #6 (47.2 mm) occurred in dry and wet seasons, respectively. In Event #6, the GW in all boreholes responded to the rainfall. All tensiometers across all layers of JR and OP recorded the variations of the suction head, which even reached positive values. This indicates that the rainfall can easily infiltrate up to 90 cm at both sites and causes temporary saturation in the wet season. Alternatively, during event #5, the GW in JR responded to the rainfall quickly; whereas the GW in OP did not respond at all. Notably, the suction head before the two rainfall events were different, for example, -60 cm at PR2 (30 cm depth) for event #5 and -20 cm for event #6.

Table 3-1 Analysis of storm events

Event No.	**Month**	**Duration (h)**	**Total prec. (mm)**	**Hourly max prec. (mm·h^{-1})**	**Max change of groundwater depth (cm)**						**Time to reach a peak (h)**					
					SK1	*SK2*	*SK3*	*PR1*	*PR2*	*PR3*	*SK1*	*SK2*	*SK3*	*PR1*	*PR2*	*PR3*
1	Jul.	14	10.0	3.2	0*	0*	0*	0*	0*	0*	0	0	0	0	0	0
2	Feb.	21	9.0	4.4	0*	0*	0*	0*	0*	0*	0	0	0	0	0	0
3	Jun.	15	43.8	15.6	118.5	98.8	35.5	0*	0*	0*	8.0	2.8	0.2	0	0	0
4	Aug.	20	46.2	15.2	12.5	119.8	0.0	10.8	0*	0*	0.8	19.0	0.0	1.3	0	0
5	Jul.	37	46.6	28.2	127.6	95.3	52.3	0.0	0*	0*	6.3	3.2	1.0	0	0	0
6	Dec.	14	47.2	27.8	92.3	160.3	65.8	63.9	112.1	170.9	2.2	2.3	1.3	1.5	1.3	1.0
7	Dec.	22	65.8	29.4	208.8	236.6	84.7	55.1	82.3	0*	2.5	2.2	1.0	1.7	1.3	0
8	Feb.	20	73.2	26.8	143.2	183.4	82.5	14.5	56.8	152.5	1.9	2.9	0.1	3.5	3.8	0.3
9	Sep.	45	130.0	37.0	276.7	270.9	94.5	77.9	190.4	256.9	1.5	2.7	0.7	3.2	3.0	1.8
10	Apr.	72	142.2	42.4	100.0	174.0	72.4	15.3	64.7	191.0	1.8	1.7	0.2	1.5	1.3	0.7

*Indicates no change in groundwater level, or changed by < 10 cm

The largest events #9 (130 mm) and #10 (142.2 mm) occurred in the dry and wet seasons, respectively. During event #9, the boreholes in SK1 and PR1 recorded a substantial increase and the GW levels reached nearly the soil surface, especially at SK1 (9 cm below the surface). The phenomenon can be confirmed by the positive suction head in all layers of SK1. Event #10 is caused by three consecutive rain days. During this event, the response time between the peak rainfall to peak GW varied between the two sites, being generally faster in JR (0.7-2.7 hr for event #9, 0.2–1.8 hr for event #10) than OP (0.7–1.5 hr for event #10, 1.8–3.2 hr for event #9).

From GW and tensiometric responded above could be a proof that GW and soil moisture responses were depended strongly on the antecedent soil wetness. In all events, soil suctions of JR were higher than OP (**Figure 3–3**) then it made the GW and tensiometrics in JR were more sensitive to a storm events, even for the rainfall about 40mm (**Table 3–1**). This result was agreed with other published research such as, Crespo et al (2011), Dahlke et al (2012), Dusek & Vogel (2016), Noguchi et al (1997), and Tetzlaff et al (2014).

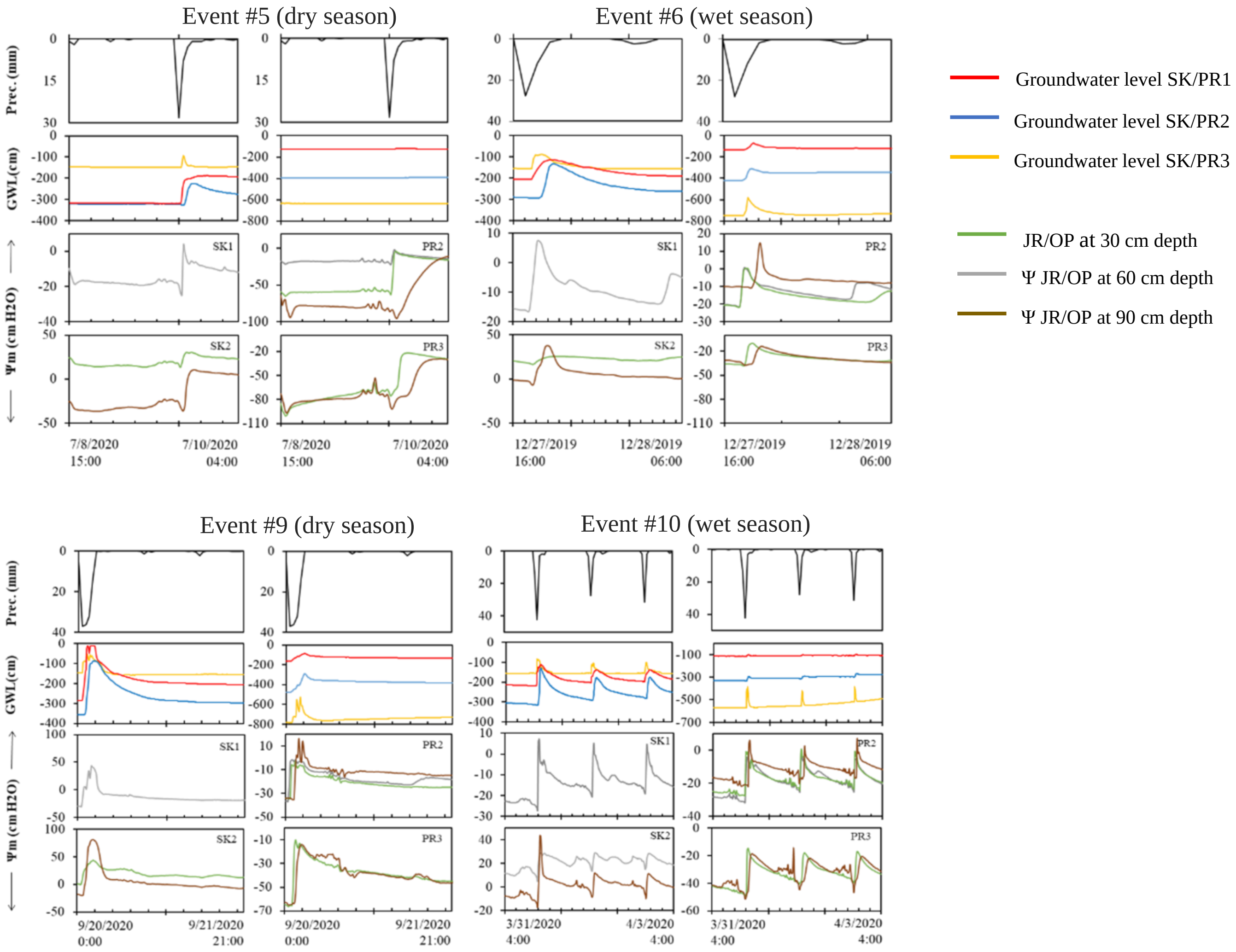

Figure 3-3 Storm events analysis

By observing the GW and suction head dynamics at the two hillslopes in Sumatra, this research presents evidence to support that tropical hillslopes with fine particle soils (classified as silty-clay to clay), and high soil permeability (Ks ≤ 12.41 cm·h-1) cause rapid vertical infiltration to unconfined GW (Dykes & Thornes 2000; Noguchi et al, 1997a, b; Sayama et al, 2021). The finding aligns with the tensiometer network observations made in Brunei (Dykes & Thornes 2000) and

Malaysia (Noguchi et al, 1997a, b), where deep percolation led to the saturation of thick soil layers, and substantial responses of streamflow discharge.

3.3.3 Model-based sensitivity analysis to understand the groundwater dynamics

To clarify major controlling factors affecting GW dynamics at the two adjacent hillslopes, a numerical experiment was conducted using the RRI model with the parameters as presented in **Table 3–2**. The model was employed for simulating the GW level from the following five scenarios. These were "Control" which used the original parameters as a reference, and "Switching K_s", "Switching *SWRC*", "Switching Soil Depth", and "Switching All" parameters between the two sites. Through analyzing the results of these scenarios, We investigated the differences and dominant factors that influenced the GW dynamics. We used Flashiness Index (*FI*) to analyze the simulation results as shown in **Figure 3–6**. To more easily interpret the results, we focused on one year (December 2019 to December 2020).

Table 3-2 Hydrologic modelling parameters

Parameters		Control		Switch K_s		Switch *SWRC*		Switch Soil depth		Switch All	
		JR	OP	JR	OP	JR	OP	JR	OP	JR	OP
SWRC	θs	0.6017	0.5532	0.6017	0.5532	0.5532	0.6017	0.6017	0.5532	0.5532	0.6017
	θr	0.0525	0.0753	0.0525	0.0753	0.0753	0.0525	0.0525	0.0753	0.0753	0.0525
	λ	0.06	0.13	0.06	0.1105	0.13	0.06	0.06	0.13	0.13	0.06
	N	24.62	20.6	24.62	20.6	20.6	24.62	24.62	20.6	20.6	24.62
	ψ_e (mm)	-45	-160	-45	-160	-160	-45	-45	-160	-160	-45
K_s (mm·h^{-1})		30.6	14.4	14.4	30.6	30.6	14.4	30.6	14.4	14.4	30.6
Soil depth (m)		4.4	8.0	4.4	8.0	4.4	8.0	8.0	4.4	8.0	4.4

Moreover, SK1 and PR3 were selected as the target points for our simulation. As suggested by **Figure 3–2,** both slopes show high temporal fluctuations in the GW responses but in substantially different ways. The JR site shows the highest variation in the lower part of the slope including SK1 and SK2, while the OP site shows the highest variation in the upper part of the slope at PR3. For the upward point of JR (i.e. at SK3), the persistent GW level normally stays at the soil and bedrock interface. For the downward point of OP (i.e. PR1), the GW level variation is constrained by the adjacent stream water level. The model simulation in this research was primarily focused on the thick surface soil layer. For this reason, we chose to investigate the groundwater variations at SK1 and PR3, as these locations are known to exhibit significant fluctuations. By concentrating our efforts on these specific points, we can gain a deeper insight into the factors driving groundwater variability in the surface layer and potentially identify strategies for managing these fluctuations.

Figure 3–4 shows the comparison of observed and simulated groundwater (GW) depths at SK1 and PR3. The model parameters for saturated hydraulic conductivity (K_s), air-entry value (ψ_e), and pore size index (λ) were fine-tuned through manual calibration to improve the model's performance in reproducing GW depths. The adjustments made to the parameters and their relative differences are presented in **Table 3–3**. The model was successful in replicating the observed GW depths, with Nash-Sutcliffe efficiency (*NSE*) values of 0.70 for SK1 and 0.84 for PR3 during the validation periods (From August 3, 2017 to December 12, 2020 for

SK1; From November 9, 2018 to December 12, 2020 for PR3).

Table 3-3 Measured and calibrated soil properties

Soil Parameters	Measured		Calibrated	
	JR	OP	JR	OP
λ	0.0904	0.1105	0.06	0.13
ψ_e (mm)	-71.6	-172.5	-45.0	-160.0
K_s (mm·h^{-1})	42.42	25.08	30.60	14.40

The model results confirmed that the GW at SK1 (control) fluctuated rapidly with rainfall compared to GW at PR3 **(Figure 3–5)**; whereas **Figure 3–6** summarizes the *FI* values of the two sites across different simulation settings. The original *FI* value in PR3 (control) was 0.004. It was slightly more than half of that at SK1 (control) whose *FI* value was 0.009.

By replacing the K_s of SK1 and PR3, the GW at SK1 became shallower (**Figure 3–5**), while that at PR3 became deeper. Notably, the original K_s values differed substantially from each other, with those at SK1 bringing about double those at PR3. Accordingly, the fluctuation of the GW table at SK1 became even higher in SK1 control, primarily due to shallower GW depths at SK1, resulting in a more direct impact from rainfall and lateral flow from upstream. By investigating the connection among lateral saturated hydraulic conductivity and hydrological connectivity at the hillslope spatial scale, Pirastru et al (2022) summarized that the hydraulic conductivity increased sharply when the GW was close to the soil surface, where macropores in the forest were mostly present. Probably, having a GW table in the drained area was important to create hydraulic connections in the macropore system.

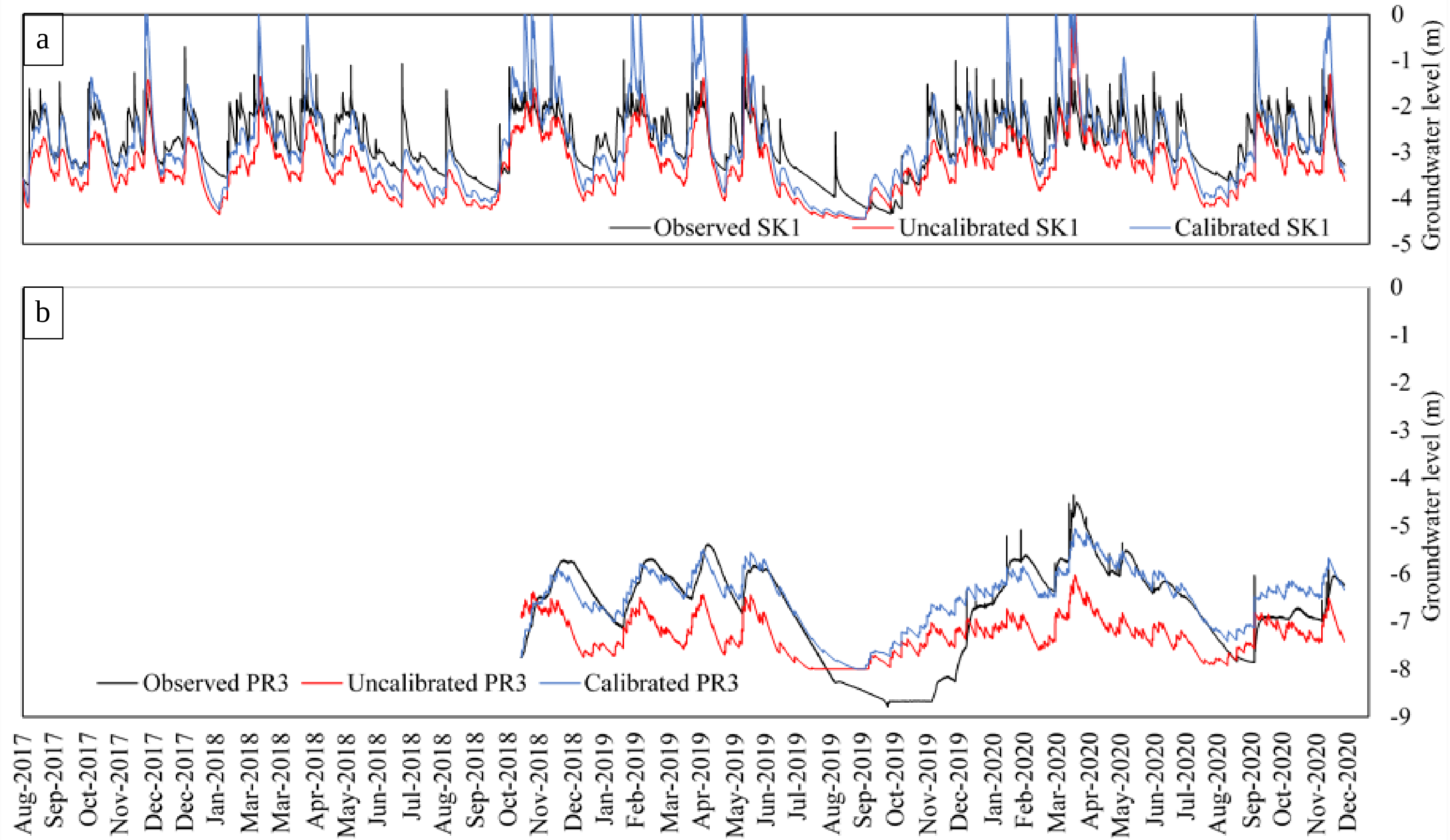

Figure 3-4 Comparison of Observed, uncalibrated, and calibrated groundwater of (a) SK1, and (b) PR3.

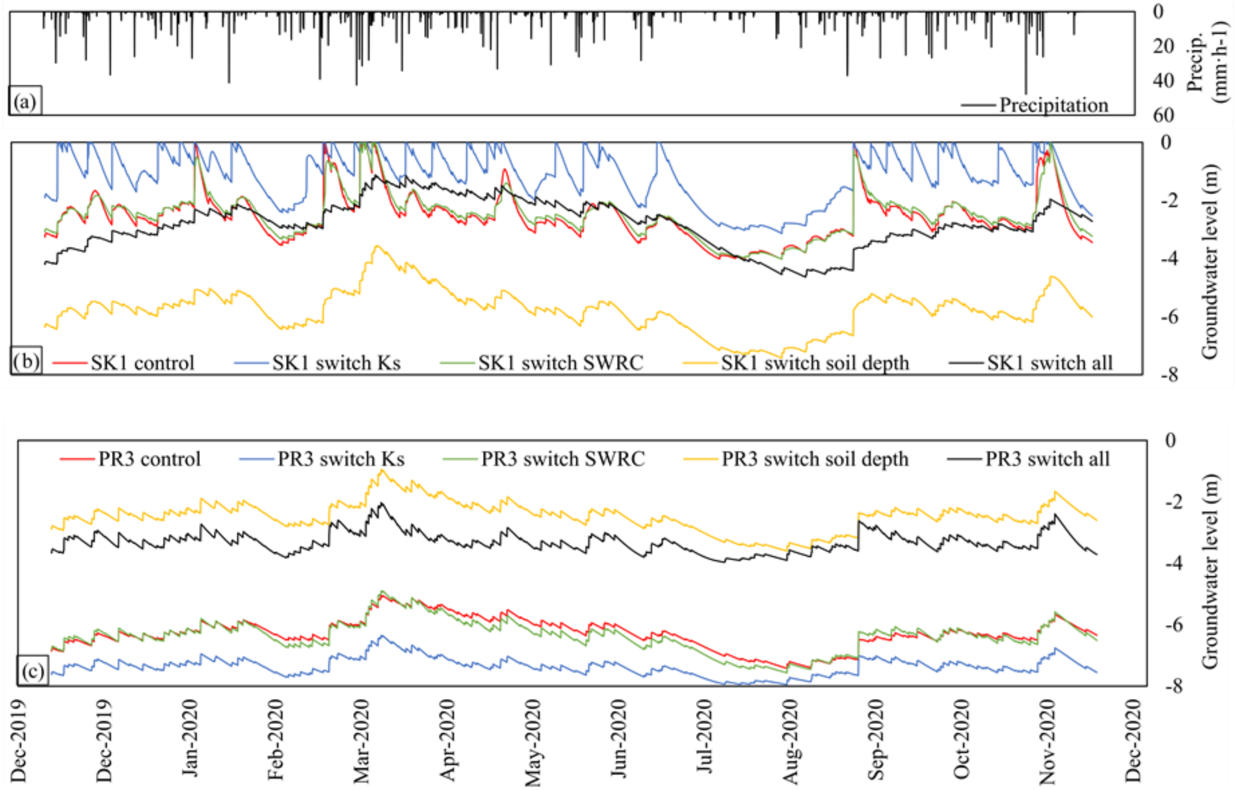

Figure 3-5 Comparison of the simulated GW dynamics between (b) SK1 and (c) PR3 with the different conditions by switching hydraulic conductivity ("switch Ks"), soil water retention curve ("switch SWRC"), soil depth ("switch soil depths") and all the above conditions ("switch all"). Input hourly rainfall series is shown in (a).

The position of SK1 was another trigger to made this high *FI*. As indicated by numerous researchers, factors like slope angle, topographic wetness index, and soil depths are commonly recognized as controlling elements for subsurface saturation development at the hillslope scale (Hopp & McDonnell 2009; Liang & Uchida 2014). However, this condition was not occurred at PR3. The *FI* at PR3 is still similar to control with 2 times *Ks* value. The higher *Ks* had been made the GW deeper and less of lateral effect from upstream.

When switching the *SWRC* between the two sites, the effects were unclear, likely a result of the marginal differences between the two locations. Although the results do not directly indicate that the effects of *SWRC* are negligible, they suggest it is not the dominant factor controlling the differences in GW dynamics between the two sites.

By adjusting the soil depth in SK1 to 8 m (as obtained from the OP site), the GW depths also gained depth (5–7 m), with much smaller magnitudes of fluctuation. Further, the *FI* became 43% that of the control case. Alternatively, by decreasing the soil depth at PR3, the range of GW also became shallower (**Figure 3–6**), and as a result, the *FI* increased by 28.2%. Nevertheless, the GW fluctuation pattern was markedly more dampened compared to that of SK1 Control.

Finally, all parameters in the model were switched between the two sites. As a result, PR3 showed a slightly higher *FI* value than SK1 (**Figure 3–6**); however, a perfect exchange from the original case was not observed, suggesting that factors other than soil depths also contribute to the higher fluctuation of GW at SK1, and lower fluctuation at PR3. Potential other controlling factors include the topography, such as slope lengths and gradients, as well as the position of SK1 and PR3.

As shown in **Figure 3–5** and **Figure 3–6**, most of simulation results in JR hillslopes show high GW response with *FI* more than 0.007, except after the soil layer is deepened. However, all simulation results in OP hillslope never show high GW response with *FI* less than 0.007, even with shallower soil layer. If we compare simulation with similar Ks and soil depth (JR-Switch Ks versus OP-switch depth), the result in JR shows typical high GW response but in OP the GW response remains slow. The results suggest that the higher fluctuation of GW at SK1 was associated with the soil depth distribution (i.e., shallower soil depths in the middle of the slope, and deeper at the foot), as well as the longer and steeper slope, resulting in more rapid GW fluctuations at the foot of the slope, even with the deeper soil layer.

Alternatively, smaller GW fluctuations at PR3 are associated with the deeper soil depth and gentler topography, resulting in less rapid changes, especially at the upper part of the slope. The numerical experiment shows that in humid tropical region, where soil characteristics can facilitate fast subsurface flow, high GW response will likely to occur particularly in hillslopes with thinner upstream soil layer and steeper slopes. However, the soil characteristics cannot facilitate such a fast flow in hillslopes with deep soil layer and gentler slope.

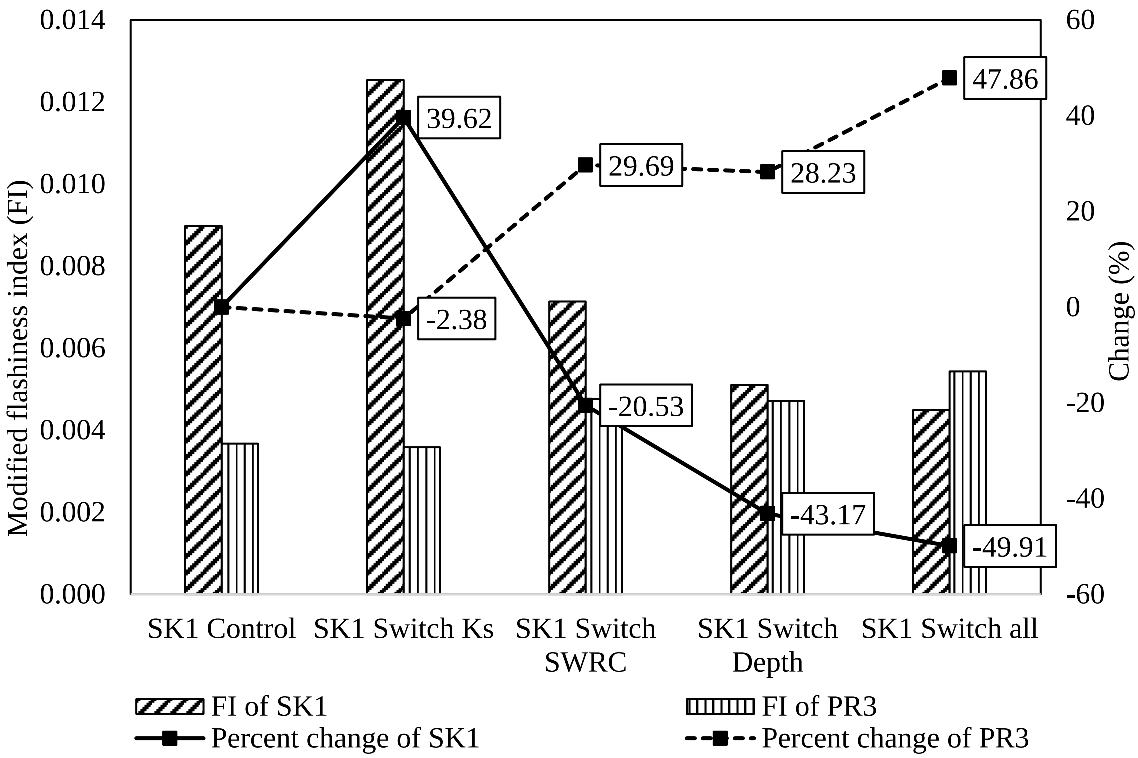

Figure 3-6 Modified flashiness index (FI) of SK1 and PR3.

The findings from the adjacent hillslopes here are summarized in **Figure 3–7**. Although the findings of the present study are limited in their spatial coverage, the results indicate that GW dynamics are strongly influenced by soil depths and formations. With the comparatively shallower soils, subsurface water contributed to the fairly sustainable GW table at the foot of the slope in JR; whereas with a deeper soil layer, the GW table was located fairly deep, and thus less responsive to rainfall at OP.

3.3.4 Surface soil moisture dynamics from different scenarios

In this study, soil moisture contents were estimated to be 30 cm below the soil surface at both SK1 and PR3 using identical experimental settings. Similar to the GW pattern in SK1, the surface soil moisture here also changed more dynamically compared to that at PR3 (**Figure 3–7**), sometimes reaching saturation (54%). The surface soil moisture at PR3 never reached saturation (= 56%), and the temporal variation was smaller as well.

Overall patterns generally corresponded to GW fluctuations, where higher GW changes corresponded to higher soil moisture fluctuations; however, when assessing surface soil moisture, the position of the GW table also plays an important role. For example, by switching K_s at SK1, the GW table began to fluctuate more greatly, and became shallower, leading to an increase in surface soil moisture. Furthermore, unlike the GW table, SWRC is more sensitive to soil moisture, as it determines the water–holding capacity.

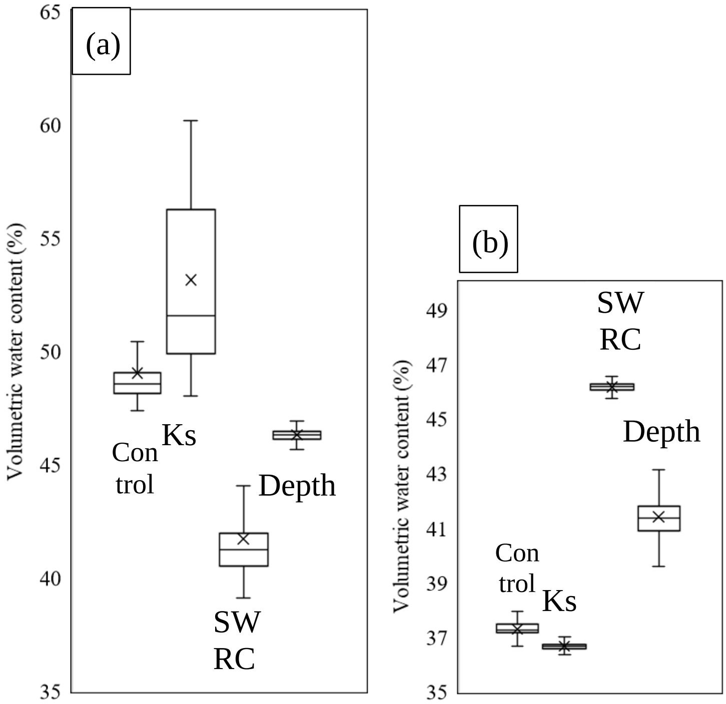

Figure 3-7 Volumetric water content at 30 cm depth of some scenarios in (a) SK1, and (b) PR3

(a)

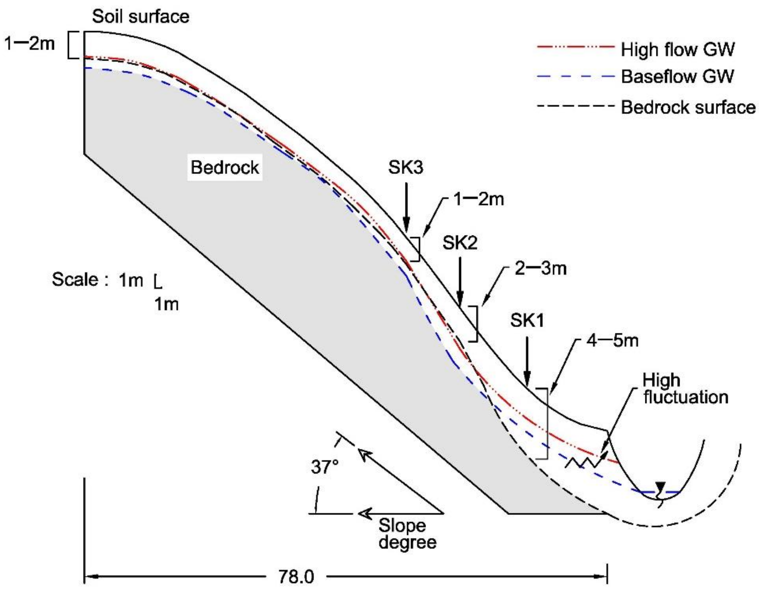

(b)

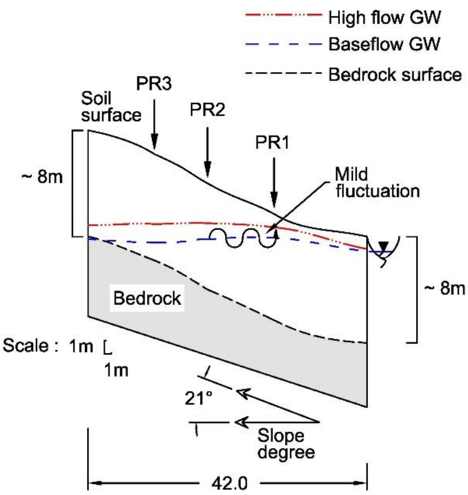

Figure 3-8 Perceptual model of hillslope hydrology in the study site for: (a) JR hillslope, and (b) OP hillslope

Conclusion

Field observations and numerical simulations were conducted at the two adjacent hillslopes in a forest and an oil palm plantation in Sumatra, Indonesia. One of the scientific questions was whether we can generalize the rapid GW responses observed in our previous study and many other studies in humid tropics. Our new monitoring site covered with oil palm plantation with even thicker soil depth (approximately 8 m) showed the rapid GW response cannot be generalized in this region. We found that the GW response was much smaller and slower during storm events. The pattern was very different from the rapid GW response observed in the foot of the forested hillslope. Even though the soil depth was as thick as 4.5 m at the foot of the forested hillslope, the soil depth in the mid-to-upper slope exhibits comparatively shallower soil layer with about 1.5 m. Below the soil layer, we found weathered bedrock layer, in which fairly steady GW exists throughout a year. Based on the GW and soil moisture observations, the rapid GW dynamics at the foot of the slope is affected from the direct infiltration and the subsurface water from the upper part of the slope.

The dynamic GW responses at the forested site have been more reported in steep mountainous tropical forest, while the smoother and slower response has been less reported, except for some gentle topographic regions (Cobb et al., 2017 and Pratama et al., 2019). The important finding of this study is that both distinct GW patterns coexist at the adjacent hillslopes. The other scientific question was what are the dominant controlling factors for the GW dynamics. By swapping the model parameters, including hydraulic conductivities, soil water retention curves and soil depths, our numerical experiment showed that the GW dynamic in the forested slope became slightly smaller than the one in the oil palm slope, i.e. opposite from the observed pattern. However, we confirmed that even if all the above parameters were swapped, the GW patterns were not be swapped completely. This means that not only soil depth and hydraulic conductivity, the topography and the position of the GW monitoring play important roles. At the foot of the long and steep hillslope, even if the soil depth in the uphill has thicker soil depth with smaller hydraulic conductivity than the actual case, the GW dynamics was still faster than the one observed in the oil palm site. On the other hand, even if the soil depth becomes comparatively shallower (with approximately 4.5m) with higher hydraulic conductivity, the GW dynamic was still slower than the one observed in the foot of the forested site.

Overall this study showed unique characteristics of GW patterns in mountainous areas in humid tropics in Sumatra, Indonesia. The different GW patterns exist at different positions, and therefore we cannot generalize the rapid GW response in these regions which have been more reported by previous studies. Future study is needed to estimate the spatial distribution of the soil depths in order to extend our understandings to larger scale. Additional observation data from other sites in the region are also needed to clarify the results. Further, the effects of land cover on subsurface flow processes could not be fully investigated as the data on evapotranspiration and interception was limited.

References

Ameli, A. A., J. J. McDonnell, & K. Bishop (2015) The exponential decline in saturated hydraulic conductivity with depth: A novel method for exploring its effect on water flow paths and transit time distribution, Hydrol. Processes, 30, 2438–2450, doi:10.1002/hyp.10777.

Anderson MG, Burt TP. (1990). Subsurface runo€ In Process Studies in Hillslope Hydrology, Anderson MG, Burt TP (eds); Wiley: Chichester; 365±400.

Baker, D.B., Richards, R.P., Loftus, T.T., Kramer, J.W. (2004) A new flashiness index: Characteristics and applications to midwestern rivers and streams. JAWRA J Am Water Resour Assoc 40:503-522.

Barthold, F. K., &R. A. Woods (2015) Stormflow generation: A meta-analysis of field evidence from small, forested catchments, Water Resour. Res., 51, 3730–3753, doi:10.1002/ 2014WR016221.

Birch, A. L., Stallard, R. F., & Barnard, H. R. (2021) Precipitation characteristics and land cover control wet season runoff source and rainfall partitioning in three humid tropical catchments in central Panama. Water Resources Research, 57(2), e2020WR028058. https://doi. org/10.1029/2020WR028058

Burt, T. P., & McDonnell, J. J. (2015) Whither field hydrology? The need for discovery science and outrageous hydrological hypotheses, Water Resour. Res., 51, 5919– 5928, doi:10.1002/2014WR016839.

Buttle, J. M., & McDonald, D. J. (2002) Coupled vertical and lateral preferential flow on a forested slope. Water Resources Research, 38(5), 18-11-18-16.

Cheng, Z., Yu, B., Fu, S., & Liu, G. (2018). Comparative evaluation of three infiltration models for runoff and erosion prediction in the Loess Plateau region of China. Hydrology Research, 49(5), 1484–1497. https://doi.org/10.2166/nh.2017.003

Cheng, Z., Zhang, J., Yu, B., Chappell, N. A., van Meerveld, H. J. (I.), & Bruijnzeel, L. A. (2023). Stormflow response and "effective" hydraulic conductivity of a degraded tropical Imperata grassland catchment as evaluated with two infiltration models. Water Resources Research, 59, e2022WR033625. https://doi.org/10.1029/2022WR033625

Cobb, A. R., Hoyt, A. M., Gandois, L., Eri, J., Dommain, R., Salim, K. A., et al. (2017). How temporal patterns in rainfall determine the geomorphology and carbon fluxes of tropical peatlands. *Proceedings of the National Academy of Sciences of the United States of America*, 114(26), E5187–E5196. https://doi.org/10.1073/pnas.1701090114

Crespo, P., J., Feyen, J., Buytaert, W., Bücker, A., Breuer, L., Frede, H-G., Ramírez, M. (2011) Identifying controls of the rainfall–runoff response of small catchments in the tropical Andes (Ecuador), J. Hydrol, 407: 164-174, https://doi.org/10.1016/j.jhydrol.2011.07.021.

Dahlke, H. E., Z. M. Easton, S. W. Lyon, M. T. Walter, G. Destouni, & T. S. Steenhuis (2012) Dissecting the variable source area concept–Subsurface flow pathways and water mixing processes in a hillslope, J. Hydrol., 420, 125–141, doi:10.1016/j.jhydrol.2011.11.052.

Detty, J.M., & McGuire, K.J. (2010) Topographic Controls on Shallow Groundwater Dynamics: Implications of Hydrologic Connectivity between Hillslopes and Riparian Zones in a till Mantled Catchment. Hydrol. Process. 24, 2222–2236.

Du, E., Jackson C. R., Klaus, J., McDonnell, J. J., Griffiths, N. A., Williamson, M. F., Greco, J. L., and Bitew, M. (2016) Interflow dynamics on a low relief forested hillslope: Lots of fill, little spill, J. Hydrol., doi:10.1016/j.jhydrol.2016.01.039.

Dusek, J., Vogel, T., (2016). Hillslope-storage and rainfall-amount thresholds as controls of preferential stormflow. J. Hydrol. 534, 590–605.

Dykes A.P., & Thornes J.B. (2000) Hillslope hydrology in tropical rainforest steeplands in Brunei. Hydrol Proc 14:215-235. doi:10.1002/(SICI)1099-1085(20000215)14:2.

Elsenbeer, H. (2001) Hydrologic flowpaths in tropical rainforest soilscapes?a review. Hydrol. Process. 15 (10), 1751–1759. doi:10.1002/hyp.237.

Gannon, J. P., S. W. Bailey, & K. J. McGuire (2014) Organizing groundwater regimes and response thresholds by soils: A framework for understanding runoff generation in a headwater catchment, Water Resour. Res., 50, 8403–8419, doi:10.1002/2014WR015498.

Gardner, C. B., Litt, G. F., Lyons, W. B., & Ogden, F. L. (2017). Evidence for the activation of shallow preferential flowpaths in a tropical Panama watershed using germanium and silicon. Water Resources Research, 53, 8533. https://doi.org/10.1002/2017WR020429.

Ghimire, C.P., Bruijnzeel, L.A., Bonell, M., Coles, N., Lubczynski, M.W. & Gilmour, D.A. (2014) The effects of sustained forest use on hillslope soil hydraulic conductivity in the Middle Mountains of Central Nepal. Ecohydrol., 7: 478-495. https://doi.org/10.1002/eco.1367.

Gish, T.J., Prueger, J.H., Daughtry, C.S.T., Kustas, W.P., McKee, L.G., Russ, A.L., & Hatfield, J.L., (2011) Comparison of field-scale herbicide runoff and volatilization losses: an eight-year field investigation. J Environ Qual 40:1432-1442.

Graham, C. B., R. A. Woods, & J. J. McDonnell (2010) Hillslope threshold response to rainfall: (1) A field based forensic approach, J. Hydrol., 393, 65–76, doi:10.1016/j.jhydrol.2009.12.015.

Hardie, M. A., R. B. Doyle, W. E. Cotching, & S. Lisson (2012) Subsurface lateral flow in texture-contrast (duplex) soils and catchments with shallow bedrock, Appl. Environ. Soil Sci., 2012, 11–16, doi:10.1155/2012/861358.

Hopp, L., & McDonnell, J.J., (2009) Connectivity at the hillslope scale: identifying interactions between storm size, bedrock permeability, slope angle and soil depth. J. Hydrol. 376, 378–391. http://dx.doi.org/10.1016/j.jhydrol.2009.07.047.

Hosoda I., Tani M., (2016) Influence of moisture fluctuation in thick, weathered bedrock layer on rainfall–runoff response in a small, forested catchment underline by Paleozoic sedimentary rocks in Japan (in Japanese with English abstract). Trans Jap Geomorph Union 37:465-492.

Itokazu, T., Kosugi, K., Onda, Y., Kuraji, K., Tanaka, N., Gotoh, T., Ohta, T., Mizuyama, T., (2013) Predicting hydrographs for an extremely large storm event using tank models calibrated by ordinary storm events. J Japan Soc Hydrol Water Res 26:85-98 (in Japanese). doi: 10.3178/JJSHWR.26.85.

Jencso, K. G., McGlynn, B. L., Gooseff, M. N., Wondzell, S. M., Bencala, K. E. & Marshall, L. A. (2009) Hydrologic connectivity between landscapes and streams: Transferring reach- and plot-scale understanding to the catchment scale, Water Resour. Res., 45, 1–16, https://doi.org/10.1029/2008WR007225.

Jencso, K.G., & McGlynn, B.L. (2011) Hierarchical controls on runoff generation: Topographically driven hydrologic connectivity, geology, and vegetation. Water Resour. Res. 47, W11527

Joshi, L, Wibawa, G., Vincent, G., Boutin, D., Akiefnawati, R., Manurung, G., Van Noordwijk, M., Williams, S. (2002) Jungle rubber: A traditional agroforestry system under pressure. International Centre for Research in Agroforestry. ICRAF, Indonesia.

Katsuyama, M., Ohte, N., & Kabeya, N. (2005) Effects of bedrock permeability on hillslope and riparian groundwater dynamics in a weathered granite catchment. Water Resour Res 41:W01010.

Kosugi, K.I., Katsura, S.Y., Mizuyama, T., Okunaka, S., & Mizutani, T. (2008) Anomalous behavior of soil mantle groundwater demonstrates the major effects of bedrock groundwater on surface hydrological processes. Water Resour Res 44:W01407.

Kinner, D. A., & Stallard, R. F. (2004). Identifying storm flow pathways in a rainforest catchment using hydrological and geochemical modelling. Hydrological Processes, 18, 2851–2875.

Lin H.S., Kogelmann W., Walker C., & Bruns, M.A. (2006) Soil moisture patterns in a forested catchment: A hydropedological perspective. Geoderma 131:345-368.

Montgomery, D., Dietrich, W. (1988) Where do channels begin?. Nature 336, 232–234. https://doi.org/10.1038/336232a0

Nash, J.E., & Sutcliffe, J.V. (1970) River flow forecasting through conceptual models part I − A discussion of principles. J Hydrol 10: 282-290. doi: 10.1016/0022-1694(70)90255-6.

Negishi, J. N., S. Noguchi, R. C. Sidle, A. D. Ziegler, and A. R. Nik (2007), Stormflow generation involving pipe flow in a zero-order basin of Peninsular Malaysia, Hydrol. Processes, 21(6), 789–806, doi:10.1002/hyp.6271.

Noguchi, S., Nik, A.R., Kasran, B., Tani, M., Sammori, T., & Morisada, K. (1997a) Soil physical properties and preferential flow pathways in tropical rain forest, Bukit Tarek, Peninsular Malaysia. J For Res 2:115-120. doi:10.1007/BF02348479.

Noguchi, S., Nik, A.R., Yusop, Z., Tani, M., & Sammori, T. (1997b) Rainfall-runoff responses and roles of soil moisture variations to the response in tropical rain forest, Bukit Tarek, Peninsular Malaysia. J For Res 2:125-132. doi:10.1007/BF02348209.

Ogden, F. L., Crouch, T. D., & Stallard, R. F. (2013). Effect of land cover and use on dry season river runoff, runoff efficiency, and peak storm runoff in the seasonal tropics of central Panama. Water Resources Research, 49, 8443–8463. https://doi.org/10.1002/2013WR013956

Onda, Y., Komatsu, Y., Tsujimura, M., & Fujihara, J.I. (2001) The role of subsurface runoff through bedrock on storm flow generation. Hydrol Process 15:1693-1706.

Penna, D., Brocca, L., Borga, M., & Fontana, D.G. (2013) Soil moisture temporal stability at different depths on two alpine hillslopes during wet and dry periods. J Hydrol 477:55-71.

Pirastru, M., Vincenzo, B., Massimo, I., Roberto, M., Mirko, C., Filippo, G., & Marcello, N. (2017) Subsurface flow and large-scale lateral saturated soil hydraulic conductivity in a Mediterranean hillslope with contrasting land uses, Journal of Hydrology and Hydromechanics, vol.65, no.3, 2017, pp.297-306. https://doi.org/10.1515/johh-2017-0006

Pratama, H., Sutikno, S., Yusa, M. (2019) Modeling of groundwater level fluctuation in the tropical peatland area of Riau, Indonesia, *IOP Conf. Series: Materials Science and Engineering* 796 (2020) 012037, doi:10.1088/1757-899X/796/1/012037

Liang, W–L., & Uchida, T., (2014) Effects of topography and soil depth on saturated-zone dynamics in steep hillslopes explored using the three-dimensional Richards' equation, J Hydrol 510:124-136, https://doi.org/10.1016/j.jhydrol.2013.12.029.

Qiu, Y., Fu, B., Wang, J., & Chen, L. (2001) Soil moisture variation in relation to topography and land use in a hillslope catchment of the Loess Plateau, China. J Hydrol 240:243-263.

Röll, A., Niu, F., Meijide, A., Hardanto A., Hendrayanto, A., Knohl, A., & Hölscher, D. (2015) Transpiration in an oil palm landscape: effects of palm age. Biogeosciences 12:5619-5633. doi:10.5194/bg-12-5619-2015.

Sayama, T., Araki, R., Yamamoto, K., & Apip (2021) Characteristics of soil and hillslope responses in humid tropical forests in Sumatra, Indonesia. Hydrol Res Lett 15:23-30.

Sela, S., Svoray, T., & Assouline, S. (2012) Soil water content variability at the hillslope scale: impact of surface sealing. Water Resour Res 48:W03522. doi:10.1029/2011WR011297.

Sidle, R. C., Tsuboyama, Y., Noguchi, S., Hosoda, I., Fujieda, M., & Shimizu, T. (2010) Stormflow generation in steep forested headwaters: A linked hydrogeomorphic paradigm, Hydrol. Process., 14, 369–385, https://doi.org/10.1002/(SICI)1099-1085(20000228)14:3<369:AID-

HYP943>3.0.CO;2-P.

Sugawara, Y., & Sayama, T. (2021) Development of a storage discharge relationship to reflect water retention curve, and its application to a distributed runoff model. J Jap Soc Civil Eng Ser. B1 (Hydraul Eng) 77:124-135 (In Japanese with English abstract).

St Clair, J., S. Moon, W. S. Holbrook, J. T. Perron, C. S. Riebe, S. J. Martel, B. Carr, C. Harman, K. Singha, & D. D. Richter (2015) Geophysical imaging reveals topographic stress control of bedrock weathering, Science, 350, 534–538, doi:10.1126/science.aab2210.

Tetzlaff, D., Birkel, C., Dick, J., Geris, J., & Soulsby, C. (2014) Storage dynamics in hydropedological units control hillslope connectivity, runoff generation, and the evolution of catchment transit time distributions, Water Resour. Res., 50, 969–985, doi: 10.1002/2013WR014147.

Tromp-van Meerveld, H. J., & J. J. McDonnell (2006) Threshold relations in subsurface stormflow: 1. A 147 storm analysis of the Panola hillslope, Water Resour. Res., 42, W02410, doi:10.1029/2004WR003778

van Verseveld, W. J., J. J. McDonnell, & K. Lajtha (2008) A mechanistic assessment of nutrient flushing at the catchment scale, J. Hydrol., 358, 268–287, doi:10.1016/j.jhydrol.2008.06.009.

Wilson, C.J., Dietrich, W.E. (1987) The contribution of bedrock groundwater flow to storm runoff and high pore pressure development in hollows, IAHS Publ 165:49-59.

Zimmer, M. A. & McGlynn, B. L. (2017) Ephemeral and intermittent runoff generation processes in a low relief, highly weathered catchment, Water Resour. Res., 53, 7055–7077, doi:10.1002/2016WR019742.

Chapter 4 Assessing Land Use Change Impacts on Water Balance and Groundwater Dynamics

4.1. Introduction

Land use change (LUC), particularly the conversion of forested areas to oil palm (OP) plantations, is a prevalent phenomenon in many humid tropical regions (Hansen et al. 2013; Gibbs et al. 2010; Margono et al. 2014). Approximately three billion people depend on palm oil as a regular dietary component, with it being a fundamental cooking oil in the food preparation of Africa and Asia. With the growing global population, the demand for palm oil is expected to increase further (Murphy et al. 2021). Indonesia is now the world's largest producer of palm oil, making almost half of the global supply. This has led to a rapid expansion of palm oil plantations in the country in recent decades (Shigetomi et al. 2020). The LUC often cause the increasing of deforestation (Austin et al. 2019), water abstraction (Merten et al. 2016), disruption of ecohydrological functions (Bruijnzeel 2004; Bradshaw et al. 2007; Ellison et al. 2017; Wilcove et al. 2010) and it has been recognized as a significant issue posing a threat to water reservoirs and river basin management (e.g., Woldemichael et al. 2012; Yigzaw & Hossain 2016).

Others LUC impacts are the changing on evapotranspiration and rainfall partitioning that would trigger the changes on hydrological responses. The rainfall partitioning divided into throughfall (T_F), stemflow (S_F) and interception (I_C).

Rainfall interception refers to the segment of incoming rainfall that is retained by above ground structures within an ecosystem (i.e., vegetation and litter layers) and subsequently released back into the atmosphere through evaporation, without reaching the soil surface (Savenije 2004). Interception can contribute to as much as 50% of total precipitation, depending on meteorological conditions and canopy characteristics (Gerrits et al. 2007, 2010; Roth et al. 2007; Sadeghi et al. 2018; Siegert et al. 2017b) then later be a critical component for precise calculation of the water budget (David et al. 2006).

Planting transpiration dominated terrestrial water fluxes from land surface to the atmosphere (Jasechko et al. 2013; Good et al. 2015), which in turn is strongly affected by a land canopy. LUC involving the conversion of forests to agricultural systems typically results in a significant decrease in evapotranspiration (Sampaio et al. 2007; Ellison et al. 2012; Silvério et al. 2015). The decreasing of evapotranspiration was linked to an increase of land surface temperature (Alkama & Cescatti 2016; Ellison et al. 2017; Sabajo et al. 2017). Recent research also suggested that the expansion, productivity and intensification of cropland could impact climate by enhancing evapotranspiration (Betts et al. 2013; Mueller et al. 2017).

Hydrological models are crucial tools for quantitatively comprehending hydrological processes and estimating their reactions to changing environments (Mirchi et al., 2010; Prasad et al., 2020). This enhancement renders them more robust in addressing intricate challenges and resolving issues related to water resources (Ciarapica & Todini 2002; Mu et al. 2023; Singh & Woolhiser, 2002). Some models have been utilized to examine hydrological aspects in watersheds, including Tank models (Ou et al., 2017), HEC-HMS (Meenu et al., 2013), HEC-RAS (Thakur et al., 2017), Artificial Neural Networks (ANN) (Saefulloh et al., 2018), and SWAT (e.g., Ridwansyah et al., 2012; Kundu et al., 2017). Among these models, the SWAT model is commonly employed to simulate hydrological processes in watersheds, considering diverse soils, land use, and various management strategies, particularly in humid tropical regions (eg. Khoi & Suetsugi 2014; Setyorini et al., 2017; Tarigan & Faqih 2019; Eva et al, 2020).

In SWAT model, the runoff calculation can be done by the soil conservation Service (SCS) curve number (CN) canopy interception method or by Green and Ampt infiltration equation. When we use the SCS-CN, the data was collected from temperate region which has a different environment characteristic with humid tropic region. Meanwhile by using the Green Ampt for calculating the infiltration in the model, the interception should be calculated separately.

Eva et al. (2022) and Yamamoto, K. et al. (2019) used potential evapotranspiration (PET) for simulating soil storage in Batanghari river basin. Even though the results were agreed with the observational data, however the results indicate there was no water or limited water available in some areas during dry season which contrary with the reality. Using PET on a hydrology simulation in this region will impact to overestimate of evapotranspiration. In humid tropical regions where sunlight and water are consistently abundant, evapotranspiration is often limited by plant factors rather than soil water availability. Therefore, calculating evapotranspiration based on physiological characteristics of plants is crucial in this region.

In order to encompass the complicated impacts of LUC in a humid tropical hillslope, this study integrated some hydrological modeling techniques to quantify potential evapotranspiration (PET) variations, rainfall partitioning between jungle rubber (JR) and oil palm (OP) plantations that two dominant LUC in the area, and Rainfall-Runoff-Inundation (RRI) model to estimate the GW dynamics and water balance changing. However, original RRI model uses PET as the input instead of actual evapotranspiration (AET). It is necessary to improve the RRI model ability to account the actual evapotranspiration for better application in humid tropic environment. Therefore, the objective of this research was to evaluate the impact of LUC to actual evapotranspiration and canopy interception, to clarified the effects of LUC on GW dynamics and water balance by using the modified RRI model and to elucidate the effects of varying rainfall and evapotranspiration inputs to a hydrological model (including gross rainfall, net rainfall, potential evapotranspiration, and actual evapotranspiration) in the LUC assessment.

4.2. Methods

4.2.1 Field Monitoring of Rainfall and GW in Hillslope

The monitoring period presented here is from December 2019 to December 2020. Ten-minute rainfall data were gauged with a tipping bucket (CPK-RAIN-1, Climatec; Phoenix, AZ, USA) to measure the rainfall rate. The rainfall gauged was located about 100 m from the hillslope and installed in an open area with 2 m above the ground that can protect from any obstruction.

We used a barometric (DAIKI, DIK-615A-B1) for gauging GWs level in the boreholes. The GWs level were recorded every 10 minutes from the three observation boreholes (named SK1, SK2, and SK3) installed along the JR hillslope. Then, these data were compensated with temperature and pressure data (TD-Diver DI800, Van Essen; Delft, Netherlands). The pressure head was measured by tensiometers (Uizin) that installed at 30, 60 and 90 cm near each borehole.

4.2.2 Hourly Potential Evapotranspiration

For calculating the PET, this study uses ERA5-Land dataset for meteorological variables indicated in **Table 4-1**. ERA5-Land provides a continuous perspective on changes in land variables over multiple decades with increased resolution (Muñoz-Sabater, 2019, 2021, and 2021). This dataset, created by replicating the land component of the ERA5 climate reanalysis, furnishes data at an hourly frequency. While no additional data assimilation was carried out in ERA5-Land, it is generated at 0.1° spatial resolution, making it has a higher resolution than

ERA5. As a result, ERA5-Land is more suitable for analyzing land surface processes compared to ERA5 (Li et al. 2022).

Table 4-1 Meteorological data required for P-M equation

Meteorological Variables	Symbols	Units	Spatial Resolution	Temporal Resolution	Datasets
2 m temperature	T_a	K	0.1° x 0.1°	Hourly	ERA5-Land
2 m dewpoint temperature	T_d	K	0.1° x 0.1°	Hourly	ERA5-Land
10 m u-component of wind	u	$m\ s^{-1}$	0.1° x 0.1°	Hourly	ERA5-Land
11 m v-component of wind	v	$m\ s^{-1}$	0.1° x 0.1°	Hourly	ERA5-Land
Surface pressure	P_a	P_a	0.1° x 0.1°	Hourly	ERA5-Land
Surface net solar radiation	R_s	$J\ m^{-2}$	0.1° x 0.1°	Hourly	ERA5-Land
Surface net thermal radiation	R_t	$J\ m^{-2}$	0.1° x 0.1°	Hourly	ERA5-Land

Table 4-2 Trees parameters required for P-M equation

Plant Variables	Symbols	Units	Values/ calculation method	References
Constant crop height	h	m	Jungle rubber = 20 Oil Palm = 13	Tania, et al., 2018
Zero plane displacement height	d	m^2	2/3 x h	Allen, R.G., et al.
Leaf area index active	LAI_{active}	m	Jungle rubber = 1.65 Oil Palm = 1.49	Bejo, et al. 2015
Roughness length governing momentum transfer	Z_{om}	m	Jungle rubber = 1.23 Oil Palm = 0.4	Tania, et al., 2018
Roughness length governing transfer of heat and vapor	Z_{oh}	m	$Z_{oh} = 0.1 \times Z_{om}$	Allen, R.G., et al.
Height of wind measurements	Z_m	m	Jungle rubber = 22 Oil Palm = 15	Assumption
Height of humidity measurements	Z_h	m	Jungle rubber = 22 Oil Palm = 15	Assumption

Following the Penman–Monteith (P–M) model parameter calculation method, seven meteorological variables from ERA5-Land were chosen, for more details of all selected variables are listed in **Table 4-1**. For other variables that were not provided by the ERA5–Land dataset (roughness length governing momentum transfer, zero plane displacement, and LAI) were collected from previous researches conducted in the same region with the similar plant characteristics (**Table 4-2**).

Some researchers got satisfying results on calculating PET through P–M model used to ERA5-Land data set. In Qinghai–Tibet Plateau, Li (2022) used ERA5-Land and ERA5 reanalysis to get the latent heat flux based on the P–M model, the result was agreed compared with an observed data by Eddy Covariance. Another PET resulting from ERA5-Land analysis was created by Singer et al (2021). They successfully mapping the PET for global land surface. To verify the results accuracy, we compared it with observation data collected by the Eddy Covariance from other resources.

The P-M method is consisting of two the components: the thermal term on the left and the dynamic term on the right (Huang et al. 1997; Penman 1948) with the following equation:

$$\lambda E = \frac{\Delta(R_n - G_0)}{\Delta + \gamma} + \frac{\rho_a C_p (e_s - e_a)/r_a}{\Delta + \gamma}$$

where λE (W m^{-2}) is the latent heat flux, Δ (kPa °C) is the slope of the saturation vapor pressure curve, R_n (W m^{-2}) is the net radiation flux, G_0 (W m^{-2}) is the surface soil heat flux, ρ_a (kg m^{-3}) is the air density, C_p (J kg^{-1} °C^{-1}) is the specific heat of air at constant pressure where the value of 1013 J kg^{-1} °C^{-1} is used. e_s (kPa) is the saturated vapor pressure, e_a (kPa) is the actual vapor pressure, r_a (m s^{-1}) is the aerodynamic resistance of vapor transport, and γ (kPa °C^{-1}) is the psychrometric constant. All the model parameters are on the hourly timescale. By calculating the hourly PET in JR and OP, we can estimate the different PET values among the two land cover conditions then apply it to an interception model. The parameters for the P–M model, along with their calculation methods, are comprehensively listed in **Table 4-3**.

Table 4-3 Parameters for the P-M model and their calculation method

Model Parameters	Symbols	Units	Calculation Methods	References
Slope of saturation vapor pressure curve	Δ	kPa °C^{-1}	$\Delta = \frac{4098.e_s}{(237.3+T_a)^2}$	Murray, F.W., 1967; Allen, R., 2005
Net radiation	R_n	W m^{-2}	$R_n = R_s + R_t$	Allen, R.G., et al., 1998; Brunt, D., 1952
Surface soil heat flux	G_0	W m^{-2}	$G_0 = 0.1 \,.\, R_n$ (for hourly period calculations)	Allen, R.G., et al., 1998
Air density	ρ_a	kg m^{-3}	$\rho_a = 1.293 \frac{P_a}{P_{atm}} \frac{273.15}{273.15+T_a}$	Xiaoqing, L., 2021; Jiumin, Y., et al., 2011
Specific heat of air at constant pressure	C_p	J kg^{-1} °C^{-1}	1013	Allen, R.G., et al., 1998
Saturated vapor pressure	e_s	kPa	$e_s = 0.6108 \,.\, \exp\left(\frac{17.27.T_a}{237.3+.T_a}\right)$	Murray, F.W., 1967; Tetens, O., 1930
Actual vapor pressure	e_a	kPa	$e_a = 0.6108 \,.\, \exp\left(\frac{17.27.T_d}{237.3+.T_d}\right)$	Murray, F.W., 1967; Tetens, O., 1930
Aerodynamic resistance of vapor transport	r_a	m s^{-1}	$r_a = \frac{ln\left[\frac{z_m-d}{z_{om}}\right] ln\left[\frac{z_h-d}{z_{oh}}\right]}{k^2 u_z}$	Allen, R.G., et al., 1998
Bulk surface resistance	r_s	m s^{-1}	$r_s = \frac{r_l}{LAI_{active}}$	Allen, R.G., et al., 1998
Psychrometric constant	γ	kPa °C^{-1}	$\gamma = \begin{cases} 0.665\ x\ 10^{-3} P_a T_d > 0 \\ 0.558\ x\ 10^{-3} P_a T_d \leq 0 \end{cases}$	Allen, R.G., et al., 1998; Brunt, D., 1952

4.2.3 Changing of Rainfall partitioning from Jungle rubber to Oil palm plantation

Precipitation above canopy is partitioned into three parts: throughfall, stemflow, and interception loss (Carlyle-Moses, 2004; Carlyle-Moses and Gash, 2011). Thus, these three processes show how the redistribution of rainfall within the vegetation when it reaches the canopy (Llorens and Domingo, 2007).

Throughfall and stemflow are water flows to the ground after approach or not with the vegetation, while interception loss is water that temporarily stored in the canopy and eventually evaporates (Llorens and Domingo, 2007; Sadeghi et al., 2016; Zheng et al., 2018). Throughfall is playing a crucial role in the water and chemical cycles of ecosystems, showing significant changes temporally and spatially (Levia & Frost, 2006). Stemflow, as a small part of the gross rainfall, is flowing down through branches and stems to enter deeper soil layers, providing water directly to the plant roots (Brasil et al., 2017; Zhang et al., 2015; Zheng et al., 2018).

To understand the changing of rainfall partitioning due to LUC, this study employed Suzuki interception model (Suzuki et al., 1979). In the model, the interception loss was predicted by using empirically-derived relationships with gross rainfall. The model represents the interception process by a water balance of rainfall input, storage and output in the form of P_n and evaporation. The steps of Suzuki interception model can be seen by the **Figure 4-1**. First, gross rainfall (P_G) reached the canopy then the water was store in the Tank A (b_t) and evaporated (E_C). Meanwhile the excess water, after evaporation, is falling down to the soil surface as throughfall (T_F) at the a_t rate and another water filled the Tank B as a stem/ trunk storage (b_s) at the a_s rate. Then again, water in the Tank B will be evaporated (E_T) before reaching the soil surface as a stemflow (S_F). Finally, together T_F and S_F were known as effective rainfall (P_n).

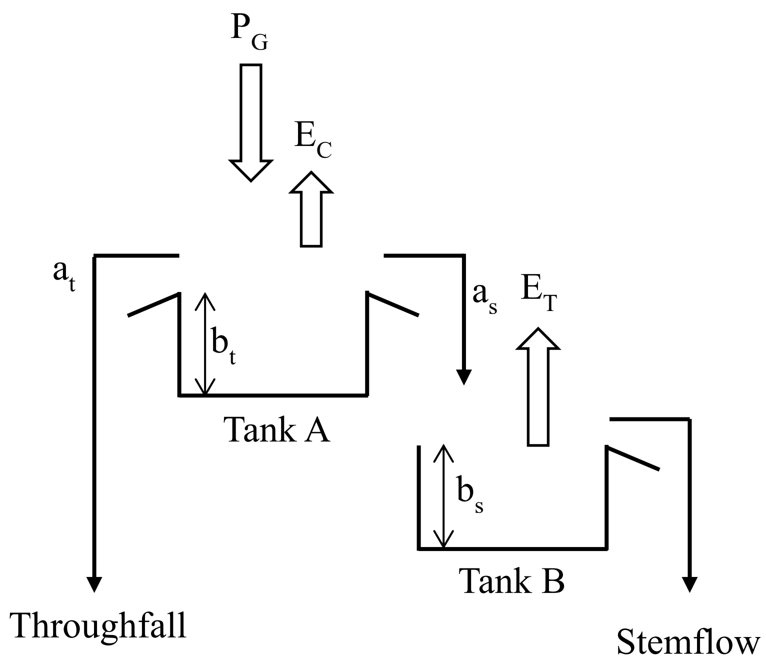

Figure 4-1 Interception calculative model (Suzuki et al., 1979)

For the evaporation rate in this model (E_C and E_T) is depend on the available water on tank A (canopy), B (stem) and PET. When water on tank A is less or equal than 0 then there is no evaporation at canopy and stem. Meanwhile, in case water in canopy storage is larger than 0, it would be two possibility. In condition where PET is less than water in canopy, evapotranspiration equal to PET. On the other way, when PET is larger or same as water on tank A, evapotranspiration rate is same as water in tank A. Then in case there is remaining PET available and water in tank B less than remaining PET, evapotranspiration from tank B is equal to water in tank B. However, if remaining PET less than water in tank B, evapotranspiration in tank b same as amount of the rest PET. For more detail regarding evapotranspiration in the Suzuki model is showed by **Figure 4-2.**

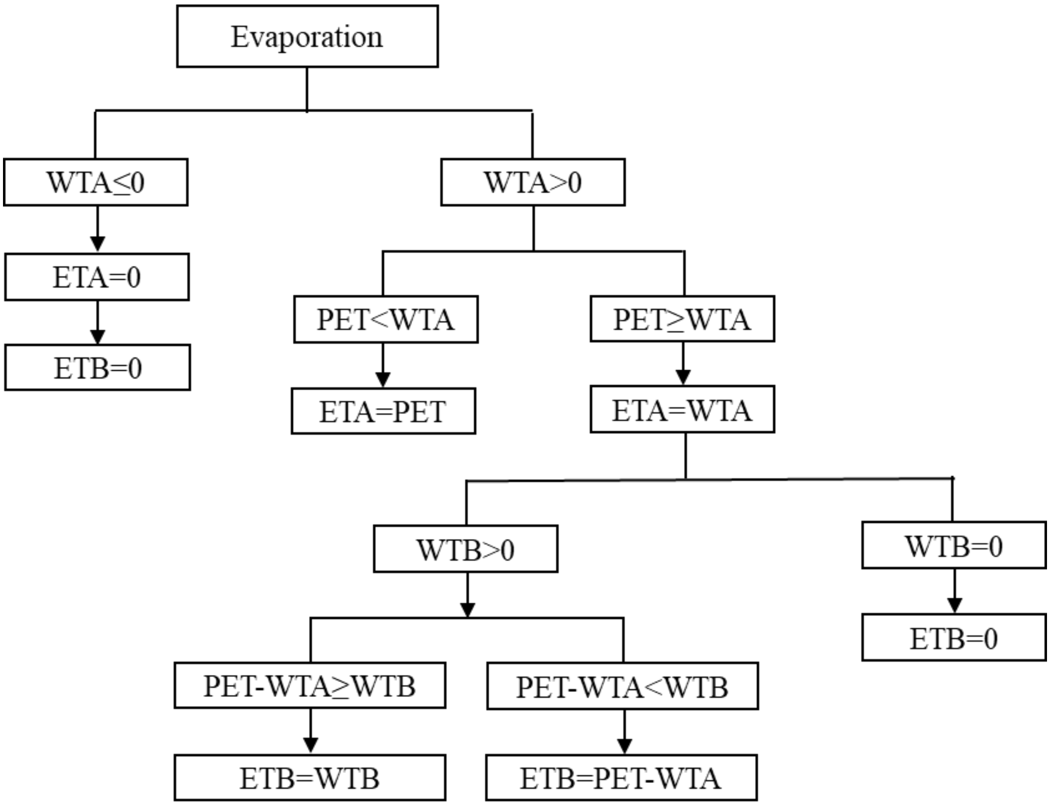

PET	=	Potential evapotranspiration
WTA	=	water in tank A (canopy)
WTB	=	water in tank B (stem)
ETA	=	Evapotranspiration in tank A
ETB	=	Evapotranspiration in tank B

Figure 4-2 Diagram of evapotranspiration in the Suzuki model

This research used T_F and S_F data from other research that conducted in the same province (Jambi) and has similarity trees types. In Jambi, Bejo et al. (2015) measured the T_F and S_F every rainy–day during November 2012 to March 2013. The tool for measuring the stemflow was used a zinc plate which is inserted into the trees and given silicon to prevent a leakage. After the plate was properly attached to the trunk, it was connected to a container. While for collecting the T_F, an ombrometer with area of 154 cm^2 was used. The placement of T_F gauges in OP was installed according to the distance between the plants. The spacing for oil palm plantations was 9 m x 9 m. In the oil palm, the placement of the T_F meters follows the distance from the bark's tree, which 1, 2, 3, 4 and 4.5 m. Meanwhile, the placement in the JR did not follow a certain distance from the barks because the distance between plants is irregular. The total six T_F gauges installed in the jungle rubber and 32 in the oil palm plantation.

In the land use scenario, we assumed the hillslope was changed from JR to OP, and as a reference of oil palm trees characteristics, we looked to the nearest oil palm plantation located approximately 900 meters away from our study site. Consequently, despite observing similarities in factors such as tree age, average trunk length, and the overall arrangement of mature oil palm trees at our site compared to theirs, we identified a slight distinction: the spacing between individual oil palm trees at our location was approximately 1 meter wider than that observed at their site.

Bejo et al (2015) made the regression by assuming the all site was covered by the canopy, while in our site there was an open space among trees (uncovered canopy) about 21.85m2 for each tree's square area (see Figure 4–3). Therefore, we accommodated the uncovered canopy space by adjusting the regressions. We assumed that the rainfall falls to the uncovered areas as a direct rainfall that increased the throughfall coefficient (aT) and reduced the maximum storage capacity of canopy (bT). On the other hand, no stemflow below uncovered canopy, consequently it reduced the maximum storage capacity of stems/ trunks (b_s) and the stemflow coefficient (a_s).

The gross rainfall (P_G) was measured in the forested hillslope (JR hillslope) from December 2019 to December 2020. The localities for the measurements of P_G was within a 100 m range from the foot hill. The gauge was placed at a height of 200 cm in open area where no trees or other taller objects can distract. The collector was a tipping bucket (CPK-RAIN-1, Climatec; Phoenix, AZ, USA) that gauge every ten-minute.

We calculate the effective rainfall based on the following equation with the estimated T_F and S_F by the model:

$$P_n = P_g - I_C = T_F + S_F$$

By summarizing the hourly values, we got the number of I_C, T_F, S_F, and effective rainfall during time period from both land covers.

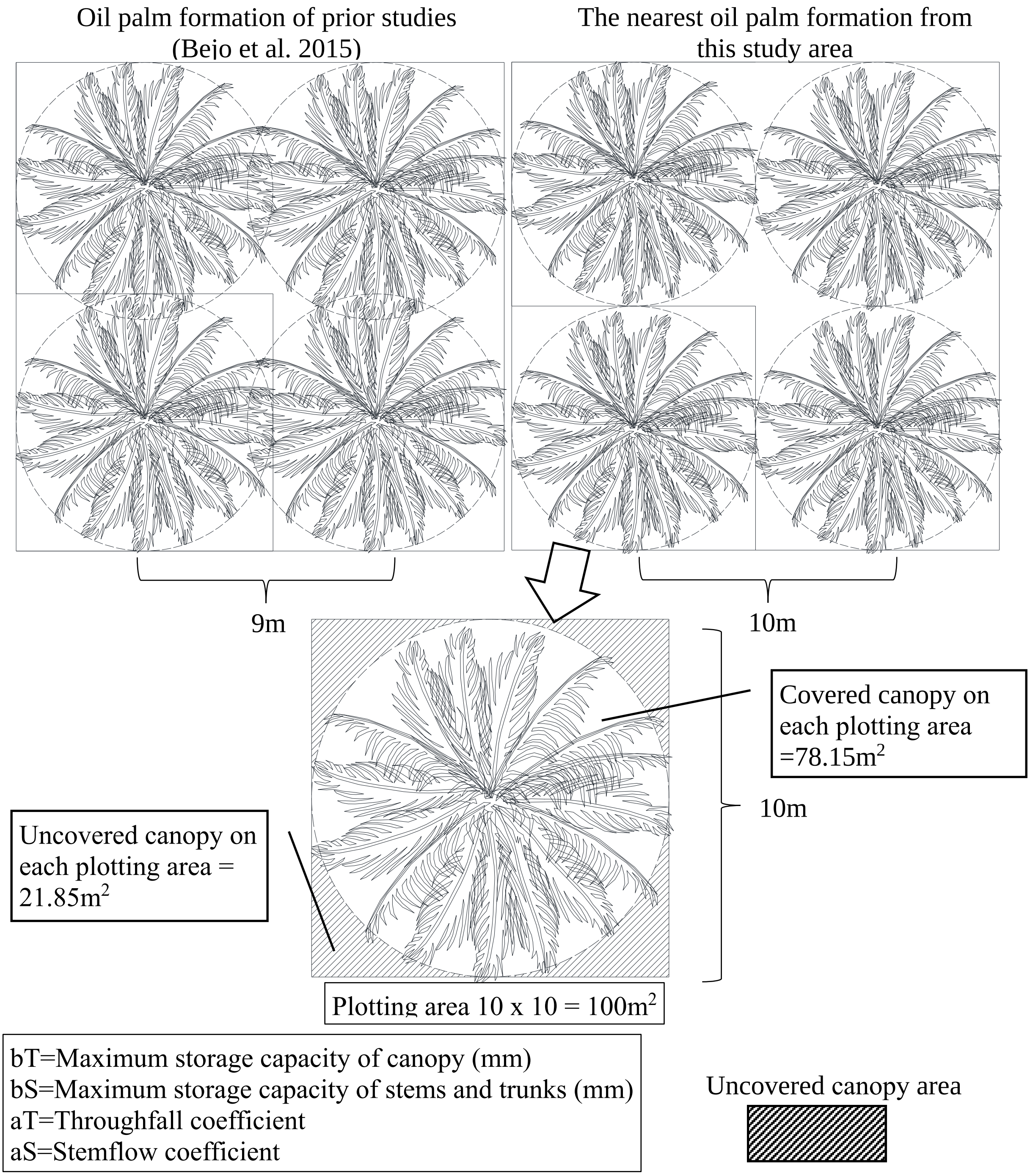

Figure 4-3 Oil palm configuration of this research and Bejo et al., (2015)'s research

4.2.4 Hillslope hydrologic modeling

The hillslope hydrologic model that used in this research is the rainfall–runoff–inundation (RRI) model that has a hillslope element to incorporate bedrock groundwater (Sayama et al. 2012, Sayama et al. 2015a, Sayama et al. 2015b). Unlike conventional kinematic wave–based distributed rainfall–runoff models that determining flow directions at each grid cell based on surface topography, the RRI model, utilizing a two–dimensional diffusive wave approach, dynamically accounts for flow direction alterations based on water levels. In a steep mountainous catchment, the RRI model effectively replicates both lateral subsurface and surface flow patterns.

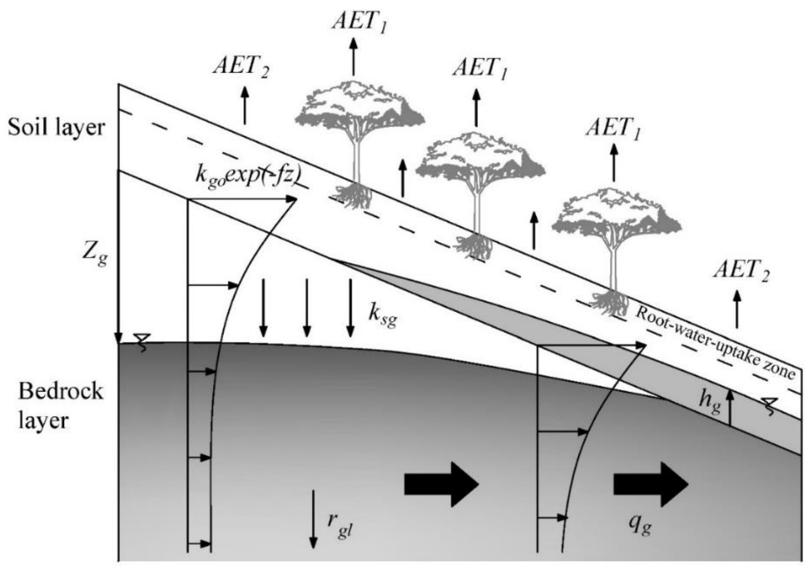

Figure 4-4 RRI–GW conceptual model (adopted from Sayama et al., 2015)

The model represents the interaction between bedrock groundwater and flow in the soil layer explained by **Figure 4–3**. The model utilizes the state variable "Z_g," which represents the distance from the soil and bedrock boundary to the groundwater table within the bedrock. Variables are allocated to each grid-cell and change over time due to lateral groundwater flow, coupled with recharge or seepage. Vertically, the model combines groundwater using the Dupuit–Forchheimer principle, assuming no explicit separation into three-dimensional layers. The model presumes that hydraulic conductivity declines exponentially in the vertical dimension. Consequently, by not requiring the specification of the lower groundwater boundary, the model can compute the finite flux of lateral groundwater movement.

In case the bedrock is not fully saturated with groundwater ($Z_g > 0$) and the upper soil layer contains water ($hs > 0$), water infiltrates the bedrock at a constant rate, referred to as *rsg*. The model disregards the impact of unsaturated bedrock portions. Thus, water that infiltrates from the soil layer promptly reaches the groundwater table without any time delay. In situations where the bedrock fully saturates, it can seep into the soil layer up to depths equivalent to $r_{gs} = -z_g \gamma_z$ and the groundwater depth " Z_g" is set to zero, where γ_z signifies the effective porosity of the bedrock. In this framework, groundwater discharge to the stream is solely feasible via the adjacent soil layer.

Based on the above assumptions, the model is realized by combination of the continuity equation and Darcy's law.

$$-\gamma_g \frac{\partial z_g}{\partial t} + \frac{\partial q_g}{\partial x} = r_{sg} - r_{gs} - r_{gl} \tag{1}$$

$$q_g = -\int_{z_g}^{\infty} k_{go} exp\left(-f_g z\right) I_g dz = -\frac{k_{g0}}{f_g} I_g exp\left(-f_g z_g\right) \tag{2}$$

$$r_{sg} = \begin{cases} k_{sg} \cdots \left(h_s > 0, z_g > 0\right) \\ \quad 0 \cdots (h_s = 0) \end{cases} \tag{3}$$

where q_g is the discharge of ground water flow per unit width, k_{sg} is the vertical saturated hydraulic conductivity, k_{g0} is the lateral saturated hydraulic conductivity, fg is a parameter controlling the vertical exponential decay in saturated hydraulic conductivity. I_g is the hydraulic gradient of the ground water, r_{gl} represents the discharge flowing from the ground water to outside the target watershed.

For the unsaturated flow component, the model enables to use measured water retention curve parameters that determined by experimental and observational data. To estimate the water retention curves and unsaturated hydraulic conductivities, the model employs the Brooks–Corey and Mualem model. RRI model assumed an equilibrium water distribution along vertical infiltration throughout the hillslope and hydraulic gradient equivalent to the surface topography (Sugawara and Sayama 2021). The model presumed immediate equilibrium conditions for the vertical water distribution within the soil profile.

The observed soil parameter data, such as hydraulic conductivity (*Ks*) and soil water retention characteristics (SWRCs) were used as initial parameters values to run the model. Then, if the simulation was not satisfactory, the parameter value and/or boundary conditions were adjusted within reasonable ranges until the simulated model results closely matched the observed data. For measuring the rate of satisfaction, the model results were measured by the Nash–Sutcliffe efficiency (NSE) index (Nash & Sutcliffe 1970).

On the original RRI model, actual evapotranspiration is calculated by deducting surface water and additional water from a cumulative infiltration amount, as estimated by the Green–Ampt model, until it reaches potential evapotranspiration. When the value approaches zero, there is no water to evaporate and actual evapotranspiration being lower than the potential evapotranspiration. However, in the humid tropical region where soil is always moisture during years (Sayama et al. 2021) the model would reach its potential evapotranspiration. In this research we eliminate the model to take water from the soil storage based on root characteristics (root depth and suction head).

This research admits two evapotranspiration from two different steps. The first evapotranspiration (*AET1*) is done by the Suzuki model in the interception process which represent evapotranspiration from canopy and stem (**Figure 4-2**). However, this *AET1* was used just for drying the water in the canopy and stem storage and will not be included to the water balance analysis. The water balance analysis in this research was done by RRI model. The second *AET* (*AET2*) is evapotranspiration from the soil column and calculated by the RRI model.

In the RRI-model, the constant evapotranspiration rate was given based on the capacity of the suction root and the model takes water from surface to the certain level based on root characteristics. From the literature review we got the root depth of the Rubber is 1.1m and 0.6m for oil palm. The suction capacity of the root is not same at all root depth accordingly we decide to set the optimum suction of the root at a half of the root depth, which comprise 0.55m for jungle rubber and 0.30m for oil palm (**Figure 4-5**). When the suction at optimum suction zone is less than Rψ (root suction capacity) then evaporation is stop. In contrary when the suction at optimum suction zone is larger than Rψ, evapotranspiration work as Figure 4-5.

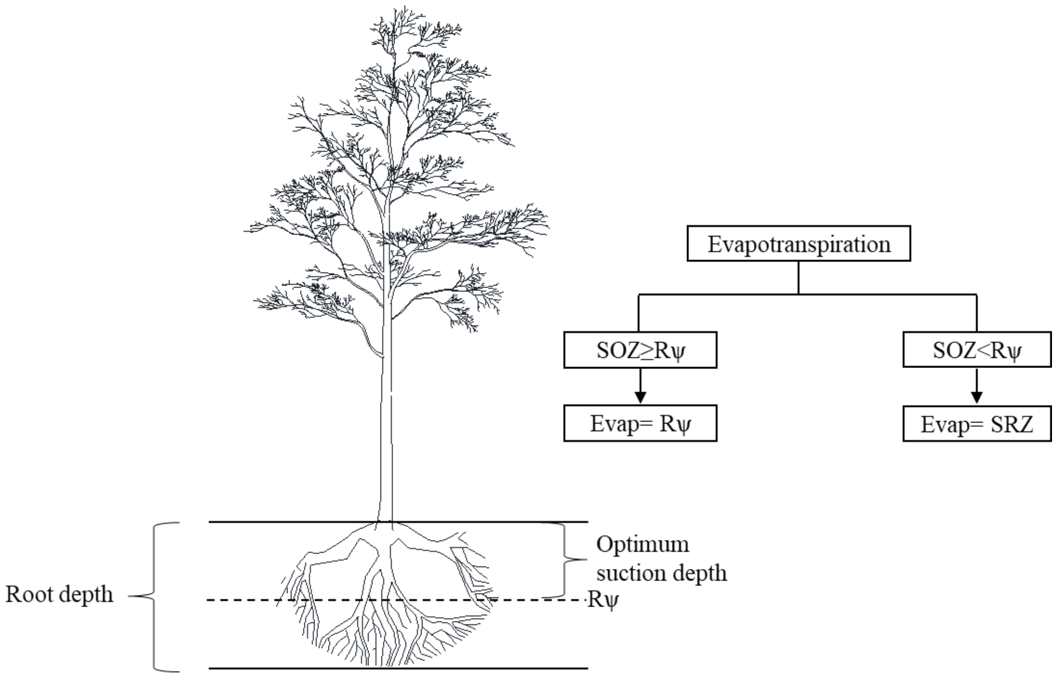

Evap = Evapotranspiration

Rψ = Root suction capacity

SOZ = Storage at the optimum suction zone

Figure 4-5 Evapotranspiration from the soil (AET2)

4.2.5 Model experiment settings

To understand the GW and water balance changed due to land cover change, we conducted a numerical experiment by the RRI model. The model produced GW fluctuation and water balance of a hillslope that covered by rubber forest and oil palm. Then, to understand how the model can improve the results, we set six simulations called simulation A, B, C, D, E, and D, with different parameters and model settings (**Table 4-4**).

The simulations A, C, and E were set as JR canopy, while simulation B, D, and F were OP canopy. Simulation A and B used P_G and simulation C-F employed P_n that results from the Suzuki model. For PET, P-M model was used to get the differences values from JR and OP. To differentiate evapotranspiration from the soil, we assumed the root depth of mature oil palm as 0.3m (Safitri et al. 2018) and 0.55m for rubber root depth (Yang et al. 2020). In term of suction head of the root, after manual calibration process, we decided that rubber has -1m and -2.5 for OP. It means, the model was taken water for evapotranspiration based on the root depth and suction set of each land cover.

Table 4-4 Model simulation settings

	Land cover	Rainfall (mm)	Root-water-uptake and suction
Simulation "A"	JR	Gross rainfall	No
Simulation "B"	OP	Gross rainfall	No
Simulation "C"	JR	Net rainfall	No
Simulation "D"	OP	Net rainfall	No

Simulation "E"	JR	Net rainfall	Yes
Simulation "F"	OP	Net rainfall	Yes

4.3. Results and Discussions

4.3.1 The changing of PET to land use changes

This research calculated PET using the obtained meteorological data and P–M equation. Then, hourly values of each land cover by year were accumulated to obtain the dynamic changes of monthly PET for the both land covers from December 2019 to December 2020. Even though we used the same meteorological data since we assume that the land use change occurs in the same hillslope but with different tree characteristics. The height of rubber trees in our site is 20 m on average while 13 m for mature oil palm. For the leaf area index of rubber as represent JR and oil palm we used the same data from Bejo et al (2018). By direct measurements, they got LAI data from rubber and oil palm in Jambi.

The total annual PET during period in JR was 1422 mm and 1059 mm in OP. The higher PET in JR is associated to the height of plants, LAI and roughness lengths (Allen et al. 1998). The monthly mean PET in JR was 118 mm while that in OP was about a half (88 mm). In August during a dry season, the PET become peaks in both JR and OP, which are 152 mm in JR and 103 mm in OP. Meanwhile for the lowest monthly PET, both land cover was not sharing the same month. With 103 mm, JR was facing the lowest value of PET in April and OP had 80 mm in June.

4.3.2 Attribution of changes in rainfall partitioning to land use change

The P_n distributes to the soil surface through T_F and S_F. The main contribution of the P_n is T_F. As T_F increases, the P_n will also increase, leading to a reduction of I_C. Contribution of the S_F is less than 1% of the P_G, due to that, S_F is often disregarded in water balance calculations (Park & Cameron 2008; Bahmani et al. 2012; Molina & Campo 2012). Utilizing throughfall variability provides a valuable approach for assessing rainfall interception variability within specific land covers.

To get rainfall partitioning, we used Suzuki model. This model was derived from the measurements of T_F and S_F in Jambi by Bejo et al. (2015). We also adjusted the regression on OP based on our OP site characteristics. The original and adjacent regression can be seen by **Table 4-5**. Then, we applied the new regressions to our own P_G. As a physical based model, applying Suzuki model for over monthly or longer time periods where cumulative interception was the objective, have generally provided good agreement with observed I_C (Moses & Gash 2011; Anna & Courtney 2020). Therefore, even though our time period and the previous research was different, the regressions were still appropriate to get an interception since our simulation was one-year period. Additionally, regarding the climatology condition, both researches shared similar condition.

Table 4-5 Throughfall and stemflow regression in OP

	Bejo et al., (2015)'s regression	New regression
Throughfall	Y = 0.8121x-0.031	Y = 0.8532x-0.0242
Stemflow	Y = 0.0023x – 0.0091	Y = 0.0018x – 0.0071

Hourly rainfall data from one–year study period was calculated to get interception, throughfall and stemflow. Total rainfall between 12 December 2019 to 12 December 2020 was 3343 mm with March being the wettest month, recorded 513 mm or 15.3% of the total P_G. Throughfall in JR comprises 70% of the P_G or 2328 mm. Only very small fraction of the rainwater appeared as stemflow that was 7 mm of the P_g. Interception loss, calculated as the difference between the sum of throughfall and stemflow from the total P_G was 1008 mm or about 30%. Differently compare to the OP canopy, the T_F in this land cover was 85% of P_G or 2840 mm during a year calculation. Meanwhile the stemflow was 3 mm with about a half of I_C percentage in the JR which recorded 15% (500 mm).

To discuss these results, we compared with previous researches in the humid tropic regions that conducted by direct measurements. The T_F, S_F and I_C of JR were similar with the Bejo et al. (2015) results that recorded 71.67%, 0.29%, and 28.04% respectively for JR. Dietz et al. (2006) found 70% of the rainfall in Sulawesi natural forest being accounted for throughfall, while proportion for interception and stemflow were 30% and <1%. Our rainfall partition in OP was compared by the original research from Bejo et al (2015). Our stemflow was under estimation (0.1%) likely due to the trees distance in our site was differ from their site.

Meanwhile, for the throughfall and interception were corresponding to their research that reported 81.7% and 14.8%. The proportion of throughfall, stemflow, and interception generally very differ depend on the tree's characteristics (age and LAI) and the rainfall intensity (Yusop et al. 2003). As reported by Farmanta et al. (2021), the percentage of the throughfall in OP was about 58 to 92%, stemflow ranging from 0.7 to 2.4% and interception was recorded 5.4-41%.

4.3.3 Seasonal observed and modeling GW results of some different settings

Figure 4-5 shows the observed GW patterns at JR hillslope. During study period, the GW table remained at a depth of ~300 cm from the soil surface in the early dry season (June), and decreased to 415 cm during the driest period (August–September). However, the persistent GW was observed even in the driest period.

We replicated the observed GW by RRI model and to improve model performance, particularly with reproducing GW depths, model parameters of hydraulic conductivity (*Ks*), air entry pressure (*psie*) and pore size distribution index (λ) were adjusted via manual calibrations as we can see in the **Table 4-6**. Since we did not take the soil samples from bedrock layer, in this simulation we assumed the hydraulic conductivity in bedrock layer (k_{gv}) is 1.18×10^{-6} (0.1 times of the measured *ks*) and the lateral hydraulic conductivity in bedrock is 1.18×10^{-8} (0.001 times of the measured k_s).

We simulated three GW simulation by RRI model with different settings to get the most appropriate GW that can reflect the land use change effects. Each land cover was simulated by using "Gross rainfall and PET", "Net rainfall and PET", and "Net rainfall and AET". More detail about the model settings were summarized by **Table 4-4** in the model simulation settings.

Table 4-6 Measured and calibrated parameters

Unsaturated Soil Parameters	Measured	Calibrated
λ	0.0904	0.05
psie (m)	-0.0716	-0.045
K_s ($m \cdot s^{-1}$)	1.1783×10^{-5}	8.5×10^{-6}

Bedrock Parameters	
kgv	1.1783×10^{-6}
tg	1.1783×10^{-8}
gamma	0.05
fpg	0.1

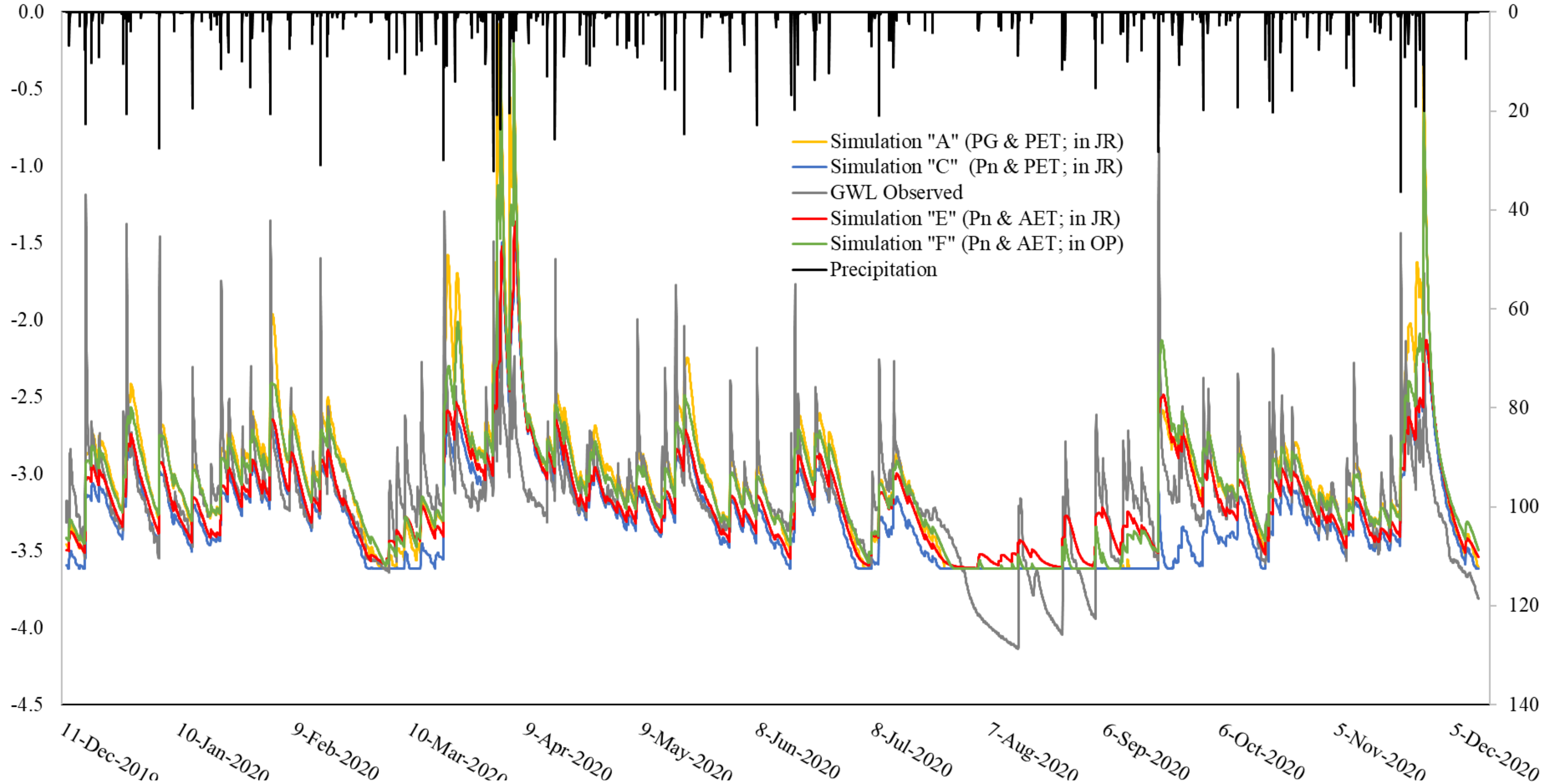

Figure 4-6 Comparison of the observed and simulated GWL from various simulation settings.

To get most appropriate GW results, we measured the Nash–Sutcliffe efficiency (NSE) values of GW in JR (simulation “A”, “C” and “E”). The simulation “A” had 0.1 NSE value. Simulation “C” got 0.2 and the “E” simulation can accelerate the NSE to be 0.43. Without interception step, the simulation “A” which used P_G as input data, in rainy season its GW was rose more than observation data and reached near the surface which the GW observation was not experience. Since the simulation “A” was not limiting the transpiration in the certain depth (assuming transpiration occur in all soil layer levels), in the driest season (July to September), no GW existed in the soil column.

With smaller rainfall input, simulation “C” had the deepest GW level. In the days with no rainfall as in the early of March and 4 to 7 July (**Figure 4-5**), its GW was no longer exist. This condition was worst in the driest period (July-September). In simulation “E” and “F”, we used P_n and restricted the evapotranspiration that worked based on trees characteristics. The optimum root suction zone of the JR (simulation ”E”) was set to 0.55m, it was deeper than that of OP (0.3m in simulation ”F”), while the evapotranspiration limits were set to be higher soil moisture level at JR (-2.5H2Om) and lower at OP (-1H2Om).

This evapotranspiration setting could reduce the GW sink in the dry season as simulation “C”, otherwise the GW still existed and fluctuated similar as a GW from observation. The persistence of GW even in the driest season indicated that the model can reflect the humid tropical environment which characterized by wet conditions, where the total evapotranspiration largely depend on atmospheric energy supply (Wohl et al. 2012), and the soil is always moist as reflected by the persistence of GW throughout the year.

Simulation E and F indicate that the LUC is prominent to impact the groundwater recharge (**Figure 4-5**). This result is in line with the published LUC studies that concluded the land use/cover has been found to be the second most important determinant for groundwater recharge following the precipitation (Kim and Jackson, 2012; Petheram et al., 2002). However, this research was contrary with groundwater research conducted in Australia. Allison et al (1990) summarized that clearing natural forests for agricultural purposes could potentially lead to a significant increase in groundwater recharge, possibly ranging from 1 to 2 orders of magnitude. But it could be understood since they compared GW from land covered by natural forest to Pasteur which had less evapotranspiration.

Groundwater recharge was linked to different evapotranspiration rates among different canopy covers. These differences arise from changes in solar radiation interception caused by canopy covers and disparities in water access due to differences of rooting characteristics (Zhang et al. 2001). As reported by Eva et al (2020), lower evapotranspiration would increase GW flow. The smaller evapotranspiration on the JR hillslope seems one of the reasons the GW in this scenario was maintained in the soil column rather than on JR hillslope.

4.3.4 Annual and monthly water budget

Based on GW simulation results above, with the highest NSE values, simulation E in JR and F in OP were the most suitable simulations to reflect the real LUC impacts. Accordingly, based on these settings we analyzed the water budget and runoff of both land cover. **Figure 4-6** shows the annual rainfall, PET, AET and discharge in JR and OP. The results show that PET in JR is higher than the one in OP, which is in line with the existing literatures (Röll et al., 2019; McJannet et al., 2007). The annual PET in JR is about 1422 mm while that in OP is 1059 mm. The higher PET in JR is associated to the height of plants, LAI and roughness lengths (Allen et al. 1998).

However, the AET in OP is estimated to be higher than the one in JR. The monthly patterns of the AET shows that they do not follow the PET monthly patterns especially during the dry season. The AET during the dry season is decreased due to the limited water availability. The reduction of AET is more significant in JR. Accordingly, the AET in OP was 32 % larger than that in JR which is equivalent to 600 mm/year.

Based on the field observations, the soil moisture at the two sites never dropped to the wilting points. Because of the abundant PET and limited water during the dry season, our numerical experiment suggested that unless we consider the “evapotranspiration limit” factor in our hydrologic model, the soil moisture becomes much lower than the reality. In this study we demonstrated the applications of root zone and evapotranspiration limit factors in the model to regulate plant water intake.

According to the previous studies in humid tropics (Bejo et al., 2015; Tania, et al., 2018), we estimated their parameters in JR and OP. The root zone of the JR was set to be deeper than that of OP, while the evapotranspiration limits were set to be higher soil moisture level at JR and lower at OP. The fact that the AET and water requirement are higher in OP has been reported by some previous studies (eg. Bejo et al. 2015; Carlson et al 2014; Dislich et al 2016; Fan et al. 2019; Manoli et al 2018; McJannet et al., 2007; Merten et al 2016; Röll et al., 2019) and consistent to our simulation results.

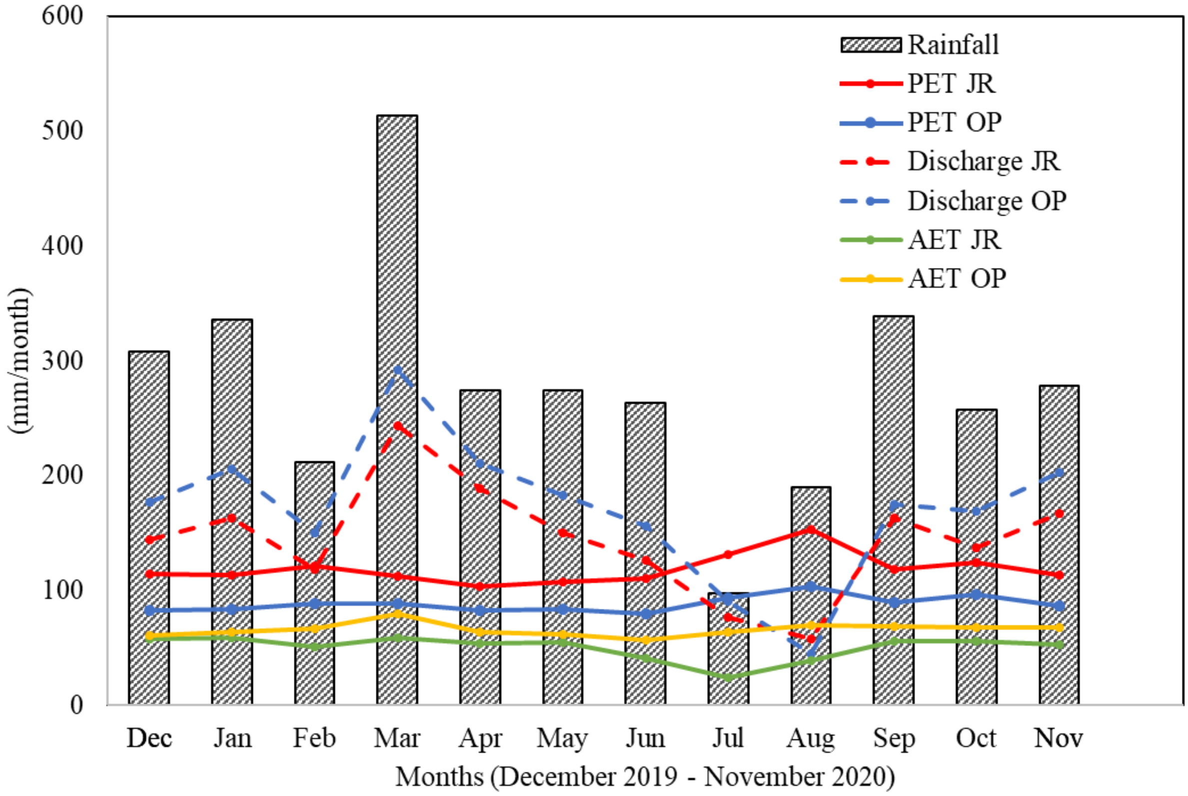

Figure 4-7 Change of PET, AET, and Discharge from JR to OP

These research findings are consistent with several studies suggesting that changes in land use from forest to other land uses (such as built-up, agricultural, or bare land) may lead to increases in runoff, frequency of flooding, and peak discharge (Bronstert et al., 2002; Xiaoming et al., 2007; Wang et al., 2008). Other studies also mentioned that deforestation can modify rainfall patterns because of vegetation atmosphere interactions at various spatial scales (Lawrence & Vandecar 2015, Spracklen et al. 2018). However, this might be different in the case of forest conversion to oil palm plantations in which evapotranspiration remains relatively high (Merten et al., 2020; Röll et al. 2019)

4.3.5 Impacts on runoff

To reflect the actual condition, we set evapotranspiration of the trees based on its root characteristics. This setting could reduce the discharge comparing with previous simulations. The JR hillslope (Simulation E) had 1736mm of discharge during a year while OP hillslope (Simulation F) recorded 2058mm, suggesting that the conversion from JR to OP may increase the annual runoff by 18 percent. Such increase in annual runoff by LUC has been reported by the previous studies (e.g. Bejo et al. 2015; Eva et al., 2020; Merten et al., 2020).

However, it could not simply assuming that this increasing of discharge was just related to the changing on interception rate and AET. If we see the percentage of the discharge, the Simulation F had a smaller discharge's percentage. It supposed the rising discharge in "Simulation F" was impact of the larger rainfall input. Regarding the AET, OP created about 200mm more even though we input potential evapotranspiration in the model setting almost 400mm less than JR. The higher of P_n, deeper root zone, and smaller suction capacity of the root were able to accelerate the actual evapotranspiration in OP.

The *AET* of this research was agreed with field observation by sap flux measurements and eddy covariance method from previous researches in Sumatra. Röll et al (2019) compared evapotranspiration of several land cover in Sumatra including Jungle rubber and Oil palm and conclude that land–cover change and land–use intensification substantially alter transpiration in lowland Sumatra. They found that oil palm leads to high transpiration (827 ± 77mm yr^{-1}) significantly surpassing rates at the jungle rubber sites (521 ± 80mm yr^{-1}). However, our *AET* estimated for secondary jungle rubber (JR) seems relatively lower than in undisturbed, old growth tropical lowland rainforests in Amazonia and South East Asia (1108mm yr−1, mean of 13 sites, Bruijnzeel 1990; Kume et al. 2011; Kumagai et al. 2004; Kunert et al. 2017; Lion et al. 2017). These results were confirmed that changing the land–cover from natural forest to agricultural forest (such as JR) as our mentioned in the introduction, would decreases evapotranspiration which was associated with increases in land surface temperature (Alkama & Cescatti 2016; Ellison et al., 2017; Sabajo et al., 2017).

Such impacts on the runoff can be also confirmed by the Flow Duration Curve (FDC) on the daily basis (**Figure 4-6**). In the extreme high (Q5), OP flood discharge was larger than JR. The higher discharge was induced by higher net rainfall, mainly associated to the lower interception. Moreover, the low flow (Q90-Q95) becomes lower in OP.

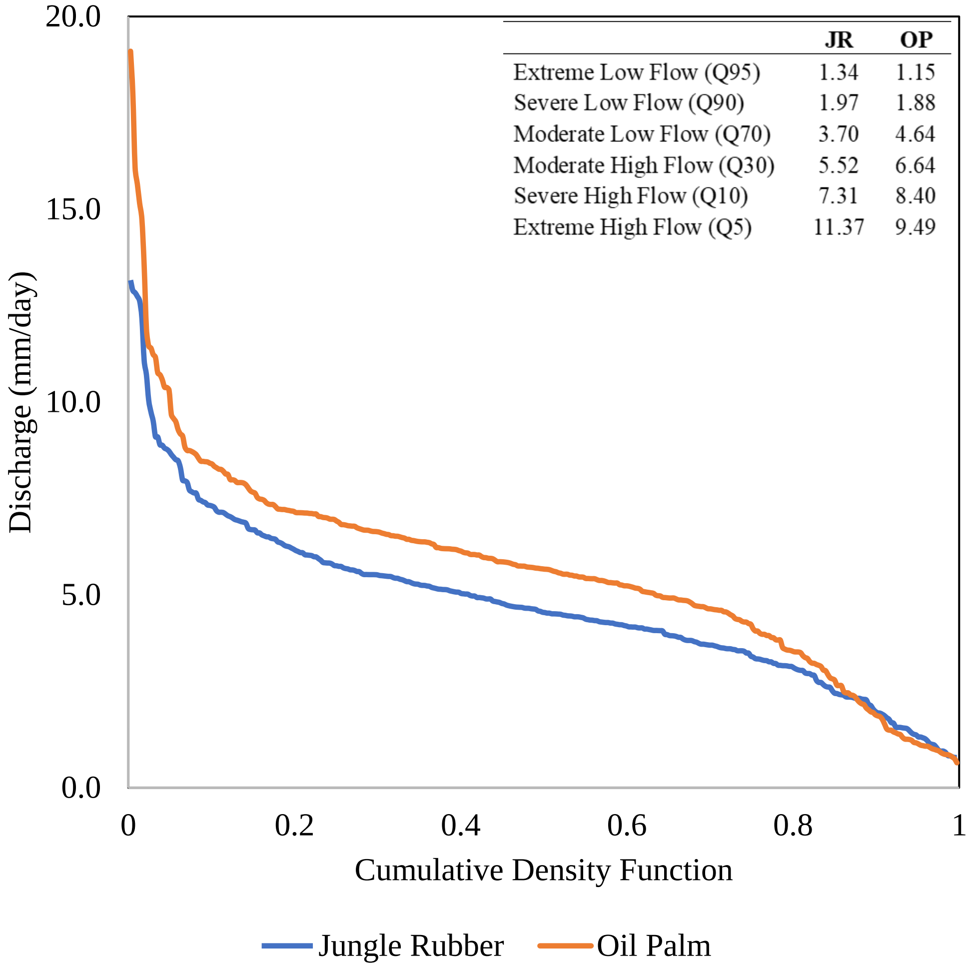

	JR	OP
Extreme Low Flow (Q95)	1.34	1.15
Severe Low Flow (Q90)	1.97	1.88
Moderate Low Flow (Q70)	3.70	4.64
Moderate High Flow (Q30)	5.52	6.64
Severe High Flow (Q10)	7.31	8.40
Extreme High Flow (Q5)	11.37	9.49

Figure 4-8 Flow Duration Curve (FDC) of daily discharge of JR and OP

On value (mm)

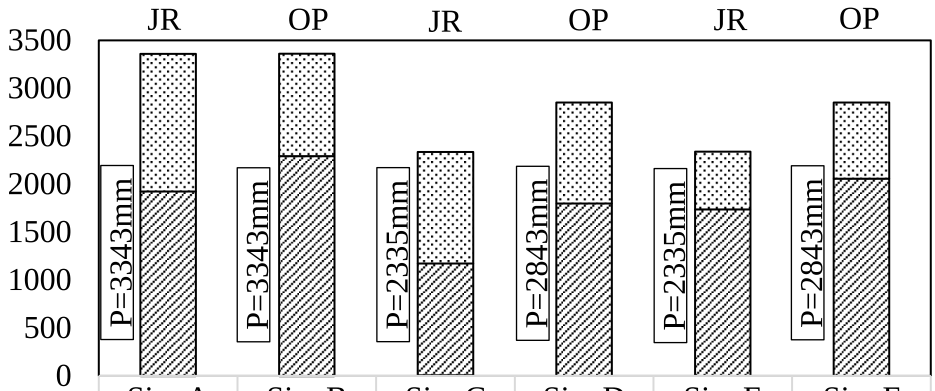

	Sim A	Sim B	Sim C	Sim D	Sim E	Sim F
AET	1434	1068	1162	1054	603	794
Discharge	1925	2292	1165	1798	1736	2058
dStorage	-16	-17	8	-9	-4	-9

On percentage from rainfall input

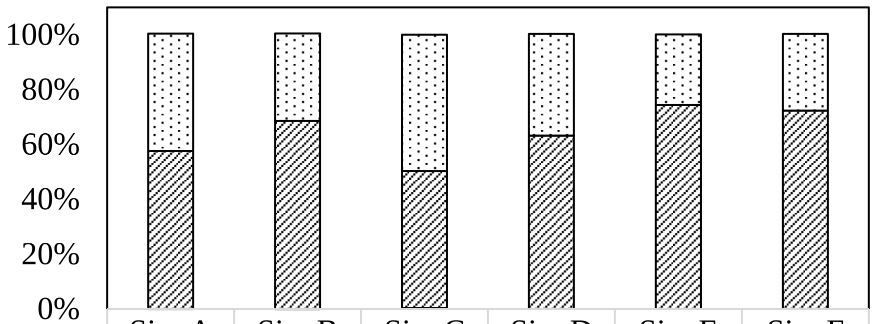

	Sim A	Sim B	Sim C	Sim D	Sim E	Sim F
AET	42.9%	32.0%	49.8%	37.1%	25.8%	27.9%
Discharge	57.6%	68.6%	49.9%	63.3%	74.4%	72.4%
dStorage	-0.5%	-0.5%	0.3%	-0.3%	-0.2%	-0.3%

P = Rainfall input
AET = Actual evapotranspiration from the soil
dStorage = Difference of water come and water out in the soil column, (-) means water out more than come, (+) means water come more than out or can be interpreted some water stayed on the soil column as a soil moisture.

Figure 4-9 Water balance of model simulations

4.3.6 Impacts of simulation conditions on the assessment

Earlier published researches on the impact of land use change (LUC) has employed different variables related to rainfall and evapotranspiration, including the use of "P_G" rather than "P_n" and "PET" instead of "AET". In regions characterized by humid tropical catchments, where subsurface flow plays a vital role in storm runoff processes, the outcomes of LUC may significantly depend on the chosen variables. To understand the influenced of these variables on LUC assessment. We simulated three model simulations by differences input model which is using "P_G and PET", "P_n and PET", and "P_n and AET".

The most common LUC studies were using P_G and PET. In our research, this setting was producing 1925mm/ year of discharge in JR and 2292mm/year in OP. It means the model showed that the LUC potentially increased the discharge by 19%. Since the model used PET as an AET and same rainfall input, the higher discharge in OP was due to JR had a higher PET input. Employing gross rainfall directly in the model clearly results in an overestimation of runoff, particularly during the rainy seasons.

In the second simulation, we employed P_n and PET. Both land cover had a smaller rainfall input than previous scenario because some rainfalls were intercepted by the canopy. Even though in this setting we did not limit the evapotranspiration based on the tree characteristics, however the model produced smaller AET because smaller water in the soil storage. With smaller rainfall input and higher AET in JR, the model resulted tremendous different discharge among JR and OP. Changing the land cover from JR to OP would increase the runoff from 1165mm/yr to 1798mm/yr or elevate to 54%.

The last model setting is using P_n and AET. AET in this simulation was limited based on the root deep and suction capability. This setting was still resulting the higher runoff in OP than in JR, however the difference in a year was just 18% which is relatively modest compared to previous studies in this area. For instance, Ridwansyah et al (2023) simulated the LUC in Batanghari and showed an increasing of surface runoff from 218mm/yr to 413mm/yr. Another study also mentioned an increasing of mean annual surface runoff and lateral flow for almost twofold (Marhaento et al., 2018). The increasing of the runoff in earlier studies were compensated of the decreasing of the evapotranspiration (eg. Ridwansyah et al 2023; Tarigan & Faqih, 2019; Marhaento, et al. 2018; Setyorini et al. 2017) which contrary from this research that LUC from JR to OP resulting an increasing the actual evapotranspiration.

This simulation setting was still using same rainfall input as previous second simulation which higher rainfall input in OP. However, OP was also facing higher AET than JR. This has been made the effect of LUC from JR to OP was not as much as significant as second simulation and earlier studies.

Conclusion

This research provides valuable insights into the hydrological consequences of LUC in humid tropical regions and how couples of hydrological models could reflect this phenomenon. in term rainfall partitioning, JR hillslope had a higher interception rather than OP, it comprised 70% of P_G while OP had 15%. It means changing the land cover from Jungle forest to Oil Palm plantation would trigger the increasing $P_{n.}$ from 2335 mm to be 2843 mm during a year of study period.

As atmospheric temperature and wind speed became smaller due to land use change from JR to OP, PET may also decreased from 1422.45mm/yr to 1058.93mm/yr. However, the AET in OP is estimated to be higher than the one in JR. The monthly patterns of the AET shows that they do not follow the PET monthly patterns especially during the dry season. The AET during the dry season is decreased due to the limited water availability. The reduction of AET is more significant in JR. Accordingly, the AET in OP was 32 % larger than that in JR which is equivalent to 600 mm/year.

Based on the field observations, the soil moisture at the two sites never dropped to the wilting points. Because of the abundant PET and limited water during the dry season, our numerical experiment suggested that unless we consider the "evapotranspiration limit" factor in our hydrologic model, the soil moisture becomes much lower than the reality. In this study we demonstrated the applications of root zone and evapotranspiration limit factors in the model to regulate plant water intake.

According to the previous studies in humid tropics (Bejo et al. 2015; Tania, et al. 2018), we estimated their parameters for JR and OP. The root zone of the JR was set to be deeper than that of OP, while the evapotranspiration limits were set to be higher soil moisture level at JR and lower at OP. The fact that the AET and water requirement are higher in OP has been reported by some previous studies (eg. Bejo et al. 2015; Carlson et al. 2014; Dislich et al. 2017; Fan et al. 2019; Manoli et al. 2018; McJannet et al. 2007; Merten et al. 2016; Röll et al. 2019) and consistent to our simulation results.

The annual runoff in JR is 1736mm and 2058mm in OP, suggesting that the conversion from JR to OP may increase the annual runoff by 18 percent. Such increase in annual runoff by LUC has been reported by the previous studies (e.g. Bejo et al. 2015; Eva et al., 2020; Merten et al. 2020). However, for the monthly basis, the runoff in the dry season in OP becomes lower than JR. In August, the JR limits AET and maintain stable runoff.

Such impacts on the runoff can be also confirmed by the Flow Duration Curve (FDC) on the daily basis. In the extreme high (Q5), OP flood discharge was larger than JR. The higher discharge was induced by higher net rainfall, mainly associated to the lower interception. Moreover, the low flow (Q90-Q95) becomes lower in OP.

Previous studies on the LUC impact use different variables of rainfall and evapotranspiration. Some use "P_G" instead of "P_n" or "PET" instead of "AET". In humid tropical catchments, where subsurface flow is the dominant storm runoff processes, the results by the LUC may be highly influenced depending on their choices. To clarify the effects, this study conducted a numerical experiment by switching from "P_n" to "P_G" and from "AET" to "PET" based on the above simulation with "P_n" and "AET" as discussed above. The summarized of the simulation results can be explained as below:

- P_G and PET

  One of the typical and simple way to assess the LUC impact is to use P_G and PET. This results in higher discharge in OP site because lower PET in OP, which is in line with the general perspective of deforestation. However, the direct use of P_G instead of P_n obviously overestimates the amount of runoff especially in the rainy seasons.

- P_n and PET

  The use of net rainfall requires additional information and the modeling, but it is essential to represent the role of canopy. However, the combination of net rainfall and PET may exaggerate the impact of the LUC, i.e. the difference of annual runoff may be overestimated. It is because the OP has higher P_n with smaller interception and smaller PET. The total runoff in OP becomes much lower than the reality.

- P_n and AET

The use of AET instead of PET together with P_n can represent what have been reported by previous studies. In summary, the LUC increases annual runoff and high flow during the wet season while low flow becomes lower during a dry season.

From these simulation results, it can be concluded that applying P_n and AET for LUC assessment is essential. This study proposed the integrated model based on the RRI model and the Suzuki model to estimate the interception and root zone suction processes. The model can successfully reproduce the reported signals in the runoff after the LUC, especially the increase of the annual runoff due to the LUC (Bejo et al. 2015; Eva et al. 202; Merten et al. 2020). Nevertheless, the estimated increasing rate by this study was 18%, which is relatively less significant compared to some previous studies. For examples, by using reference evapotranspiration, Marhaento et al. (2018) reported that the annual runoff increases almost twofold. Another erlier LUC study in the area also mentioned the increasing of the runoff from 218mm/yr to 413mm/yr (Ridwansyah et al. 2023). The increasing of the runoff in earlier studies were compensated by the decreasing of the evapotranspiration (eg. Ridwansyah et al. 2023; Tarigan & Faqih, 2019; Marhaento et al. 2018; Setyorini et al. 2017) which contrary from this research that LUC from JR to OP resulting an increasing the actual evapotranspiration.

As described above, our results indicated that the reduction of the interception and the increase of AET somewhat compensate each other, so that the estimated impacts become relatively smaller. We confirmed that the use of net rainfall and AET can increase the model performance of representing the GW pattern. Although the proposed model is demonstrated at the hillslope scale, the model can be extended to the river basins scale for assessing the LUC impact on hydrology at the larger scale.

References

Alkama, R., Cescatti, A. (2016) Biophysical climate impacts of recent changes in global forest cover.Science, 351,600-604.DOI:10.1126/science.aac8083

Allen, R. Penman-Monteith equation. In Encyclopedia of Soils in the Environment; Elsevier: Oxford, UK, 2005; pp. 180–188.

Allen, R. G., Pereira, L. S., Raes, D. & Smith, M. (1998) Crop evapotranspiration-Guidelines for computing crop water requirements-FAO Irrigation and drainage paper 56. Fao, Rome 300, D05109.

Allison, G.B., Cook, P.G., Barnett, S.R., Walker, G.R., Jolly, I.D., Hughes, M.W., (1990). Land clearance and river salinisation in the western Murray Basin, Australia. J. Hydrol. 119:1–20. doi:10.1016/0022-1694(90)90030-2

Anna C. L., and Courtney M. S. (2020). Calibration reveals limitations in modeling rainfall interception at the storm scale. Journal of Hydrology, volume 584, 2020, 124624, ISSN 0022-1694, https://doi.org/10.1016/j.jhydrol.2020.124624

Arnold, J.G. and Fohrer, N. (2005), SWAT2000: current capabilities and research opportunities in applied watershed modelling. Hydrol. Process., 19: 563-572. https://doi.org/10.1002/hyp.5611

Austin, K. G., Schwantes, A., Gu, Y. & Kasibhatla, P. S. (2019) What causes deforestation in Indonesia?. Environ. Res. Lett. 14, 024007.

Bahmani, S.M.H.G., Attarod, P., Bayramzadeh, V., Ahmadi, M.T., Radmehr, A., (2012). Throughfall, stemflow, and rainfall interception in a natural pure forest of chestnut-leaved Oak (Quercus castaneifolia C.A. Mey.) in the Caspian Forest of Iran. Ann. For. Res. 55(2): 197-206, 2012.

Bejo, S., (2015) Interception and Surface Runoff in the Transformation of the Jambi Lowland Tropical Rain Forest (In Bahasa with English abstract). Doctoral Dissertation, Sekolah Pascasarjana-Institut Pertanian Bogor, Indonesia

Betts, A. K., Desjardins, R., Worth, D., and Cerkowniak, D. (2013), Impact of land use change on the diurnal cycle climate of the Canadian Prairies, J. Geophys. Res. Atmos., 118, 11,996–12,011, doi:10.1002/2013JD020717.

Bieger, Katrin, Arnold, Jeffrey G., Rathjens, Hendrik, White, Michael J., Bosch, David D., Allen, Peter M., Volk, Martin, and Srinivasan, Raghavan (2017). Introduction to SWAT+, a Completely Restructured Version of the Soil and Water Assessment Tool. Journal of the American Water Resources Association (JAWRA) 53(1): 115–130. DOI: 10.1111/1752-1688.12482

Bosch, D.D., J.G. Arnold, M. Volk, and P.M. Allen, (2010). Simulation of a Low-Gradient Coastal Plain Watershed Using the SWAT Landscape Model. Transactions of the ASABE 53(5): 1445-1456, DOI: 10.13031/2013.34899

Bradshaw, C. J. A., N. S. Sodhi, K. S.-H. Peh, and B. W. Brook. (2007). Global evidence that deforestation amplifies flood risk and severity in the developing world. Global Change Biology 13 (11):2379-2395. https://doi.org/10.1111/j.1365-2486.2007.01446.x

Brasil, J.B., Palácio, H.A., de, Q., Araújo Neto, J.R.de, Ribeiro Filho, J.C., Andrade, E.M.de, 2017. Características das chuvas e interceptação vegetal no bioma caatinga. Irriga 22, 560–574.

Bruijnzeel, L. A. (2004). Hydrological functions of tropical forests: not seeing the soil for the trees? Agriculture, Ecosystems and Environment 104(1):185-228. https://doi.org/10.1016/j.agee.2004.01.015

Bruijnzeel, L. A. (1990) Hydrology of moist tropical forests and effects of conversion: a state of knowledge review. pp.vi +224 pp. ref.40.

Brunt, D. Physical and Dynamical Meteorology, 2nd ed; Cambridge University Press: Cambridge, UK, 1952; 428p.

Carlson, K., Curran, L., Asner, G. et al. (2013) Carbon emissions from forest conversion by Kalimantan oil palm plantations. Nature Clim. Change 3, 283–287. https://doi.org/10.1038/nclimate1702

Carlyle-Moses, D.E. (2004). Throughfall, stemflow, and canopy interception loss fluxes in a semi-arid Sierra Madre Oriental matorral community. J. Arid Environ. 58(2). 181-202. https://doi.org/10.1016/S0140-1963(03)00125-3

Carlyle-Moses, D.E., Gash, J.H.C. (2011). Rainfall Interception Loss by Forest Canopies. In: Levia, D., Carlyle-Moses, D., Tanaka, T. (eds) Forest Hydrology and Biogeochemistry. Ecological Studies, vol 216. Springer, Dordrecht. https://doi.org/10.1007/978-94-007-1363-5_20

Ciarapica, L., & Todini, E. (2002). TOPKAPI: A model for the representation of the rainfall-runoff process at different scales. Hydrological Processes, 16(2), 207–229. https://doi.org/10.1002/hyp.342

David, T. S., Gash, J. H. C., Valente, F., Pereira, J. S., Ferreira, M. I., & David, J. S. (2006). Rainfall interception by an isolated evergreen oak tree in a Mediterranean savannah. Hydrological Processes, 20(13), 2713–2726. Retrieved from https://doi.org/10.1002/hyp.6062.

Dislich, C., Keyel, A.C., Salecker, J., Kisel, Y., Meyer, K.M., Auliya, M., Barnes, A.D.,Corre, M.D., Darras, K., Faust, H., Hess, B., Klasen, S., Knohl, A., Kreft, H., Meijide,A., Nurdiansyah, F., Otten, F., Pe'er, G., Steinebach, S., Tarigan, S., Tölle, M.H.,Tscharntke, T., Wiegand, K., (2016) A review of the ecosystem functions in oilpalm plantations, using forests as a reference system. Biol. Rev. 49, http://dx.doi.org/10.1111/brv.12295

Ellison, D.N., Morris, C. E., Locatelli, B., Sheil, D., Cohen, J., Murdiyarso, D., Gutierrez, V., vanNoordwijk, M., Creed, I. F., Pokorny, J., Gaveau, D., Spracklen, D. V., Tobella, A. B., Ilstedt, U., Teuling, A. J., Gebrehiwot, S. G., Sands, D. C., Muys, B., Verbist, B., Springgay, E., Sugandi, Y., Sullivan., C. A. (2017). Trees, forests and water: cool insights for a hot world. Global Environmental Change 43(51):51-61. https://doi.org/10.1016/j.gloenvcha.2017.01.002

Ellison, D.N., Futter, M., Bishop, K., (2012). On the forest cover–water yield debate: from demand- to supply-side thinking. Glob. Change Biol. 18, 806–820. doi: http://dx.doi.org/10.1111/j.1365-2486..02589.x

Farmanta, Y., Sung, C.T.B., Giap, S.E.G., Paing, T.N., Handoko, Impron, (2021) Net Rainfall Components under Various Ages of the Oil Palm. Malaysian Journal of Soil Science Vol. 25 : 159-169.

Fan, Y., Meijide, A., Lawrence, D. M., Roupsard, O., Carlson, K. M., Chen, H.Y., (2019). Reconciling canopy interception parameterization and rainfall forcing frequency in the Community Land Model for simulating evapotranspiration of rainforests and oil palm plantations in Indonesia. Journal of Advances in Modeling Earth Systems, 11, 732–751. https://doi.org/10.1029/2018MS001490

Gerrits, A. M. J., Pfister, L., & Savenije, H. H. G. (2010). Spatial and temporal variability of canopy and forest floor interception in a beech forest. Hydrological Processes, 24(21), 3011–3025

Gerrits, A. M. J., Savenije, H. H. G., Hoffmann, L., & Pfister, L. (2007). New technique to measure forest floor interception? An application in a beech forest in Luxembourg. Hydrology and Earth System Sciences, 11, 695–701.

Gassman, P.W., M.R. Reyes, C.H. Green, and J.G. Arnold, 2007. The Soil and

Water Assessment Tool: Historical Development, Applications, and Future Research Directions. Transactions of the ASABE 50(4): 1211-1250, DOI: 10.13031/2013.23637.

Gibbs, H. K., Ruesch, A. S., Achard, F., Clayton, M. K., Holmgren, P., Ramankutty, N., and Foley, J. A. (2010). Tropical forests were the primary sources of new agricultural land in the 1980s and 1990s, P. Natl. Acad. Sci. USA, 107, 16732–16737

Good, S. P., D. Noone, and G. Bowen (2015), Hydrologic connectivity constrains partitioning of global terrestrial water fluxes, Science, 349(6244), 175–177

Hansen, M. C., Potapov, P. V., Moore, R., Hancher, M., Turubanova, S. A., Tyukavina, A., Thau, D., Stehman, S. V., Goetz, S. J., Loveland, T. R., Kommareddy, A., Egorov, A., Chini, L., Justice, C. O., and Townshend, J. R. G. (2013). High-Resolution Global Maps of 21st-Century Forest Cover Change, Science, 342, 850–853, https://doi.org/10.1126/science.1244693

Huang, H. Principle and Simulation of Soil-Vegetation-Atmosphere Interaction; China Meteorological Press: Beijing, China, 1997; pp. 66–72.

Jasechko, S., Sharp, Z., Gibson, J. et al. (2013). Terrestrial water fluxes dominated by transpiration. Nature 496, 347–350 https://doi.org/10.1038/nature11983

Jiumin, Y.; Lili,W.; Haibin, K.; Yuhua, Z.; Jinzhong, L.; Lili, Z. Improvement of air density and gas universal constant measurement experiment. Phys. Exp. 2011, 31, 24–26.

Khoi, D.N., Tadashi Suetsugi, T. (2014) Impact of climate and land-use changes on hydrological processes and sediment yield—a case study of the Be River catchment, Vietnam, Hydrological Sciences Journal, 59:5, 1095-1108, DOI:10.1080/02626667.2013.819433

Kim, J.H., Jackson, R.B. (2012) A Global Analysis of Groundwater Recharge for Vegetation, Climate, and Soils. Vadose Zone Journal; 11 (1): vzj2011.0021RA. doi: https://doi.org/10.2136/vzj2011.0021RA

Kundu S, Khare D, Mondal A (2017) Individual and combined impacts of future climate and land use changes on the water balance. Ecol Eng 105:42–57.

Lawrence, D., Vandecar, K. Effects of tropical deforestation on climate and agriculture. Nature Clim Change 5, 27–36 (2015). https://doi.org/10.1038/nclimate2430

Levia, D.F., Frost, E.E., (2006). Variability of throughfall volume and solute inputs in wooded ecosystems. Prog. Phys. Geogr. 30, 605–632. doi: 10.1177/0309133306071145

Li, H.; Chen, R.; Han, C.; Yang, Y. (2022) Evaluation of the Spatial and Temporal Variations of Condensation and Desublimation over the Qinghai–Tibet Plateau Based on Penman Model Using Hourly ERA5-Land and ERA5 Reanalysis Datasets. Remote Sens. 14, 5815. https://doi.org/10.3390/rs14225815

Llorens, P., Domingo, F., (2007) Rainfall partitioning by vegetation under Mediterranean conditions. A review of studies in Europe. J. Hydrol. 335,37-54. DOI：10.1016/j.jhydrol.2006.10.032

Manoli, G., Meijide, A., Huth, N., Knohl, A., Kosugi, Y., Burlando, P., et al. (2018). Ecohydrological changes after tropical forest conversion to oil palm. Environmental Research Letters, 13(6). https://doi.org/10.1088/17489326/aac54e

Margono, B. A., P. V. Potapov, S. Turubanova, F. Stolle, and M. C. Hansen. (2014). Primary forest cover loss in Indonesia over 2000-2012. Nature Climate Change 4:730-735. https://doi.org/10.1038/nclimate2277

Marhaento, H., Booij, M.J., Hoekstra, A.Y. (2018) Hydrological response to future land-use change and climate change in a tropical catchment, Hydrological Sciences Journal, 63:9, 1368-1385, DOI: 10.1080/02626667.2018.1511054

McJannet, D., Fitch, P., Disher, M. and Wallace, J. (2007), Measurements of transpiration in four tropical rainforest types of north Queensland, Australia. Hydrol. Process., 21: 3549-3564. https://doi.org/10.1002/hyp.6576

Meenu R, Rehana S, Mujumdar P (2013) Assessment of hydrologic impacts of climate change in Tunga-Bhadra river basin, India with HEC-HMS and SDSM. Hydrol Process 27(11):1572–1589

Merten, J., Röll, A., Guillaume, T., Meijide, A., Tarigan, S., Agusta, H., Dislich, C., Dittrich, C., Faust, H., Gunawan, D., Hein, J., Hendrayanto, Knohl, A., Kuzyakov, Y., Wiegand, K., Hölscher, D. (2016) Water scarcity and oil palm expansion: social views and environmental processes. Ecology and Society 21(2):5. http://dx.doi.org/10.5751/ES-08214-210205

Merten, J.A., Stiegler, C. N., Hennings, E. S., Purnama, Röll, A., Agusta, H., Dippold, M. A., Fehrmann, L., Gunawan, D., Hölscher, D., Knohl, A., Kückes, J., Otten, F., Zemp, D. C., Faust., H. (2020) Flooding and land use change in Jambi Province, Sumatra: integrating local knowledge and scientific inquiry. Ecology and Society 25(3):14. https://doi.org/10.5751/ES-11678-250314

Mirchi, A., Watkins, D., Jr., & Madani, K. (2010). Chapter 6: Modeling for watershed planning, management, and decision making. In J. C. Vaughn (Ed.), Watersheds: Management, restoration and environmental impact. Nova Science Publishers, Hauppauge.

Molina, A.J., del Campo, A.D., (2012). The effects of experimental thinning on throughfall and stemflow: A contribution towards hydrology-oriented silviculture in Aleppo pine plantations. For. Ecol. Manage. 269, 206–213. https://doi.org/10.1016/j.foreco.2011.12.037

Mu, D., Xun, Y., Gao, Y., Ren, D., Sun, C., Ma, X., Huang, G., & Xu, X. (2023). A modified SWAT model for mechanistic simulation of soil water-salt transport and the interactions with shallow groundwater. Hydrological Processes, 37(9), e14980. https://doi.org/10.1002/hyp.14980

Mueller, N. D., A. Rhines, E. E. Butler, D. K. Ray, S. Siebert, N. M. Holbrook, and P. Huybers, 2017: Global Relationships between Cropland Intensification and Summer Temperature Extremes over the Last 50 Years. J. Climate, 30, 7505–7528, https://doi.org/10.1175/JCLI-D-17-0096.1

Muñoz-Sabater, J. (2021) ERA5-Land Hourly Data from 1950 to 1980—Copernicus Climate Change Service (C3S) Climate Data Store (CDS). Available online: https://cds.climate.copernicus.eu/cdsapp#!/dataset/reanalysis-era5-land?tab=overview/ (accessed on 10 March 2022).

Muñoz-Sabater, J. ERA5-Land Hourly Data from 1981 to Present—Copernicus Climate Change Service (C3S) Climate Data Store (CDS). 2019. Available online: https://cds.climate.copernicus.eu/cdsapp#!/dataset/reanalysis-era5-land?tab=overview/ (accessed on 10 March 2022).

Muñoz-Sabater, J.; Dutra, E.; Agustí-Panareda, A.; Albergel, C.; Arduini, G.; Balsamo, G.; Boussetta, S.; Choulga, M.; Harrigan, S.; Hersbach, H.; et al. ERA5-Land: A state-of-the-art global reanalysis dataset for land applications. Earth Syst. Sci. Data 2021, 13, 4349–4383.

Murray, F.W. On the Computation of Saturation Vapor Pressure. J. Appl. Meteorol. Climatol. (1967) 6, 203–204.

Murphy, D.J., Goggin, K. & Paterson, R.R.M. (2021) Oil palm in the 2020s and beyond: challenges and solutions. CABI Agric Biosci 2, 39. https://doi.org/10.1186/s43170-021-00058-3

Nash, J.E., & Sutcliffe, J.V. (1970) River flow forecasting through conceptual models part I − A discussion of principles. J Hydrol 10: 282-290. doi: 10.1016/0022-1694(70)90255-6.

Ou X, Gharabaghi B, McBean E, Doherty C (2017) Investigation of the tank model for urban storm water management. J Water Manag Model. https ://doi.org/10.14796 /JWMM.C421

Park, A., Cameron, J.L., (2008). The influence of canopy traits on throughfall and stemflow in five tropical trees growing in a Panamanian plantation. For. Ecol. Manage. 255 (5–6), 1915–1925. https://doi.org/10.1016/j.foreco.2007.12.025.

Penman, H.L. Natural Evaporation from Open Water, Bare Soil and Grass. Proc. R. Soc. Lond. Ser. A Math. Phys. 1948, 193, 120–145.

Petheram, C., Walker, G., Grayson, R., Thierfelder, T., Zhang, L. (2002). Towards a framework for predicting impacts of land-use on recharge: 1. A review of recharge studies in Australia.Aust. J. Soil Res. 40:397–417. doi:10.1071/SR00057

Prasad, V., Yousuf, A., & Sharma, N. (2020). Hydrological modeling for watershed management. Journal of Natural Resource Conservation and Management, 1(1), 29–34. https://doi.org/10.51396/anrcm.1.1.2020.29-34

Kumagai, T., Saitoh, T.M., Sato, Y., Morooka, T., Manfroi, O.J., Kuraji, K., Suzuki, M. (2004) Transpiration, canopy conductance and the decoupling coefficient of a lowland mixed dipterocarp forest in Sarawak, Borneo: dry spell effects. Journal of Hydrology 287 (1–4), 237–251.

Kume, T., Tanaka, N., Kuraji, K., Komatsu, H., Yoshifuji, N., Saitoh, T.M., Suzuki, M., Kumagai, T., 2011. Ten-year evapotranspiration estimates in a Bornean tropical rainforest. Agric. For. Meteorol. 151 (9), 1183–1192.

Kunert, N., Aparecido, L.M.T., Wolff, S., Higuchi, N., Santos, J., dos, Araujo, de, A.C., Trumbore, S., 2017. A revised hydrological model for the Central Amazon: The importance of emergent canopy trees in the forest water budget. Agric. For. Meteorol. 239, 47–57. https://doi.org/10.1016/j.agrformet.2017.03.002.

Lion, M., Kosugi, Y., Takanashi, S., Noguchi, S., Itoh, M., Katsuyama, M., Matsuo, N., Shamsuddin, S.A., 2017. Evapotranspiration and water source of a tropical rainforest in peninsular Malaysia. Hydrol. Process. 31 (24), 4338–4353. https://doi.org/10. 1002/hyp.11360

Refsgaard, J. C., Hjberg, A. L., Møjller, I., Hansen, M., & Søndergaard, V. (2010). Groundwater modeling in integrated water resources management–Visions for 2020. Groundwater, 48(5), 633–648.

Ren, D. Y., Xu, X., Hao, Y. Y., & Huang, G. H. (2016). Modeling and assessing field irrigation water use in a canal system of Hetao, upper Yellow River basin: Application to maize, sunflower and watermelon. J. Hydrol., 532, 122–139. https://doi.org/10.1016/j.jhydrol.2015.11.040

Ridwansyah, I., Apip, A., Wibowo, H., Rahmadya, A., Susiwidiyaliza, S., Handoko, U., Setiawan, F., Utami, N. (2023) The Impact of Land-Use and Climate Change on Water and Sediment Yields in Batanghari Watershed, Sumatra, Indonesia. Sains Malaysiana 52(3)(2023): 705-721. http://doi.org/10.17576/jsm-2023-5203-03

Ridwansyah I, Sapei A, Raimadona M (2012) Applying SWAT to predict impact of landuse change on hydrological response in upper Cimanuk catchment area.

In: The 5th international remote sensing and GIS workshop series on demography, land use-land cover and disaster.

Roth BE, Slatton KC, Cohen MJ (2007) On the potential for high-resolution lidar to improve rainfall interception estimates in forest ecosystems. Front Ecol Environ 5:421–428

Röll, A., Niu, F., Meijide, A., Ahongshangbam, J., Ehbrecht, M., Guillaume, T., Gunawan, D., Hardanto, A., Hendrayanto, Hertel, D., Kotowska, M.M., Kreft, H., Kuzyakov, Y., Leuschner, C., Nomura, M., Polle, A., Rembold, K., Sahner, J., Seidel, D., Zemp, D.C., Knohl, A., Hölscher, D. (2019) Transpiration on the rebound in lowland Sumatra. Agric. For. Meteorol. 274, 160–171. https://doi.org/10.1016/j.agrformet.2019.04.017

Sabajo, C. R., le Maire, G., June, T., Meijide, A., Roupsard, O., and Knohl, A. (2017) Expansion of oil palm and other cash crops causes an increase of the land surface temperature in the Jambi province in Indonesia, Biogeosciences, 14, 4619–4635, https://doi.org/10.5194/bg-14-4619-2017

Sadeghi, S.M.M., Attarod P., VanStan J.T., Pypker, T.G. (2016) The importance of considering rainfall partitioning in afforestation initiatives in semiarid climates: a comparison of common planted tree species in Tehran, Iran. Sci Tot Environ 568:845–855. https://doi.org/10.1016/j.scitotenv.2016.06.048

Sadeghi, S.M.M., Van Stan, J.T., Pypker, T.G., Tamjidi, J., Friesen, J., Farahnaklangroudi, M., (2018). Importance of transitional leaf states in canopy rainfall partitioning dynamics. Eur. J. For. Res. 137, 121–130. https://doi.org/10.1007/s10342-017-1098-4

Saefulloh DF, Hadihardaja IK, Harlan D (2018) Modeling of triangular unit hydrographs using an artificial neural network in a tropical river basin. Int J Geo 15(51):69–76

Safitri, L., Suryanti, S., Kautsar, V., Kurniawan, A., Santiabudi, F. (2018) IOP Conf. Ser.: Earth Environ. Sci. 141 012031

Savenije, H. H. G. (2004). The importance of interception and why we should delete the term evapotranspiration from our vocabulary. Hydrological Processes, 18(8), 1507–1511. https://doi.org/10.1002/hyp.5563.

Setyorini, A., Khare, D. & Pingale, S.M. Simulating the impact of land use/land cover change and climate variability on watershed hydrology in the Upper Brantas basin, Indonesia. Appl Geomat 9, 191–204 (2017). https://doi.org/10.1007/s12518-017-0193-z

Shigetomi, Y., Ishimura, Y. & Yamamoto, Y. (2020) Trends in global dependency on the Indonesian palm oil and resultant environmental impacts. Sci Rep 10, 20624. https://doi.org/10.1038/s41598-020-77458-4

Siegert, C.M., Levia, D.F., Leathers, D.J. (2017) Do storm synoptic patterns affect biogeochemical fluxes from temperate deciduous forest canopies?. Biogeochemistry 132, 273–292. https://doi.org/10.1007/s10533-017-0300-6

Silve´rio, D. V., Brando, P. M., Macedo, M. N., Beck, P. S. A., Bustamante, M., & Coe, M. T. (2015). Agricultural expansion dominates climate changes in southeastern Amazonia: The overlooked non-GHG forcing. Environmental Research Letters, 10,1–8.

Singer, M.B., Asfaw, D.T., Rosolem, R. et al. Hourly potential evapotranspiration at 0.1° resolution for the global land surface from 1981-present. Sci Data 8, 224 (2021). https://doi.org/10.1038/s41597-021-01003-9

Singh, V. P., & Woolhiser, D. A. (2002). Mathematical modeling of watershed hydrology. Journal of Hydrologic Engineering, 7, 270–292. https://doi.org/10.1061/(ASCE)1084-0699(2002)7:4(270)

Spracklen, D.V., Baker, J.C.A., Garcia-Carreras, L., Marsham, J.H. (2018) The Effects of Tropical Vegetation on Rainfall. Annual Review of Environment and Resources 2018 43:1, 193-218

Sugawara, Y., & Sayama, T. (2021) Development of a storage discharge relationship to reflect water retention curve, and its application to a distributed runoff model. J Jap Soc Civil Eng Ser. B1 (Hydraul Eng) 77:124-135 (In Japanese with English abstract).

Suzuki, M., Kato, H., Tani, M., Fukushima, Y., (1979). Throughfall, stemflow and rainfall interception in Kiryu Experimental Catchment. I. Throughfall and stemflow. J. Jpn. For. Soc. 61, 202–210 in Japanese with English abstract.

Tania J., Meijide, A., Christian Stiegler, C., Kusuma, A.P., Knohl, A., (2018) IOP Conf. Ser.: Earth Environ. Sci. 149 012048 DOI 10.1088/1755-1315/149/1/012048

Tarigan, S. and Faqih, A. (2019) “IMPACT OF CHANGES IN CLIMATE AND LAND USE ON THE FUTURE STREAMFLOW FLUCTUATION”, Jurnal Pengelolaan Sumberdaya Alam dan Lingkungan (Journal of Natural Resources and Environmental Management). Bogor, ID, 9(1), pp. 181-189. doi: 10.29244/jpsl.9.1.181-189.

Tetens, O. Uber einige meteorologische Begriffe. Z. (1930) Geophys. 6, 297–309.

Thakur B, Parajuli R, Kalra A, Ahmad S, Gupta R (2017) Coupling HEC-RAS and HEC-HMS in precipitation runoff modelling and evaluating flood plain inundation map. World Environ Water Resour Congress 2017:240–251. https ://doi.org/10.1061/9780784480 625.022

Wilcove, D. S. & Koh, L. P. (2010) Addressing the threats to biodiversity from oil-palm agriculture. Biodivers. Conserv. 19, 999–1007

Woldemichael, A. T., Hossain, F., Pielke, R., and Beltrán-Przekurat, A. (2012). Understanding the impact of dam-triggered land use/land cover change on the modification of extreme precipitation, Water Resour. Res., 48, W09547. doi:10.1029/2011WR011684

Xiaoqing, L. Design and improvement of the experiment for determining air density. Exp. Teach. Appar. 2021, 38, 25–26.

Xiong, L. Y., Xu, X., Ren, D. Y., Huang, Q. Z., & Huang, G. H. (2019). Enhancing the capability of hydrological models to simulate the regional agro-hydrological processes in watersheds with shallow groundwater: Based on the SWAT framework. Journal of Hydrology, 572, 1–16. https://doi.org/10.1016/j.jhydrol.2019.02.043

Wohl, E., Barros, A., Brunsell, N. et al. The hydrology of the humid tropics. Nature Clim Change 2, 655–662 (2012). https://doi.org/10.1038/nclimate1556

Yamamoto, E.M.S., Sayama, T., Yamamoto, K., Apip, Comparison of runoff generation methods for land use impact assessment using the SWAT model in humid tropics, Hydrological Research Letters, 2020, Volume 14, Issue 2, Pages 81-88, Released on J-STAGE June 10, 2020, Online ISSN 1882-3416, https://doi.org/10.3178/hrl.14.81.

Yang, B., Meng, X., Singh, A.K., Wang, P., Song, L., Zakari, S., Liu, W., 2020. Intercrops improve surface water availability in rubber-based agroforestry systems. Agric. Ecosyst. Environ. 298, 106937 https://doi.org/10.1016/j.agee.2020.106937.

Yigzaw, W. & Hossain F., (2016). Land Use and Land Cover Impact on Probable Maximum Flood and Sedimentation for Artificial Reservoirs: Case Study in the Western United States. J. Hydrol. Eng. 21:501-502. doi: 10.1061/(ASCE)HE.1943-5584.0001287

Yusop, Z., Yen, C.S., Hui, C.J., (2003) Throughfall, Stemflow, and Interception Loss of Old Rubber Trees. Jurnal Kejuruteraan Awam 15(1): 24-33.

Zhang, Y.feng, Wang, X.ping, Hu, R., Pan, Y.xia, Paradeloc, M., (2015) Rainfall partitioning into throughfall, stemflow and interception loss by two xerophytic shrubs within a rain-fed re-vegetated desert ecosystem, northwestern China. J. Hydrol. 527, 1084–1095. doi: 10.1016/j.jhydrol.2015.05.060 .

Zheng, J., Fan, J., Zhang, F., Yan, S., Xiang, Y., 2018. Rainfall partitioning into throughfall, stemflow and interception loss by maize canopy on the semi-arid Loess Plateau of China. Agric. Water Manag. 195, 25–36. doi: 10.1016/j.agwat.2017.09.013

Chapter 5 Concluding Remarks

5.1 Conclusion

Hydrological processes in humid tropical hillslopes are unique and distinct from global locations. Soils in this region are characterized by depth of several meters and higher clay content. The clayey soils typically exhibit lower permeability and impeding the rain water infiltrate into deeper soil. However, some previous studies reported that subsurface flow may be a dominant storm runoff process because of high hydraulic conductivity and water retention capacity. Such soil characteristics facilitate fast and deep percolation that result in dynamic and fast GW response during storm events.

This study observed GW at the two adjacent hillslopes with contrasting soil depth, land cover and soil properties to understand the GW dynamics and the main triggering factor of its high response. This dissertation was also evaluating the impact of LUC to rainfall partitioning, evapotranspiration, and GW characteristics. Moreover, we clarify the effects of LUC from different variables of rainfall and evapotranspiration input to the RRI model.

In chapter 3, the study investigates two GW from JR and OP hillslopes by measuring the GW level from three observation boreholes installed along each hillslope. We monitored the GW fluctuation from August 2017 to December 2020 in JR and from November 2018 to December 2020 in OP. As a result, the slower groundwater response observed in the OP hillslope, which has a thicker soil depth of approximately 8 meters. During storm events, we found that the GW response was much smaller and slower. This pattern differed significantly from the rapid groundwater response observed in the foot of the forested hillslope (JR hillslope). Even though the soil depth was 5 meters thick at the foot of the forested hillslope, the surface soil depth in the mid–to–upper slope was only about 1.5 meters. Below this soil layer, we discovered a weathered bedrock layer where GW remains relatively stable throughout the year. Based on GW and soil moisture observations, the rapid GW dynamics at the foot of the slope are influenced by direct infiltration and subsurface water from the upper part of the slope.

Regarding the main factors influencing groundwater dynamics, through numerical experiments involving the exchange of model parameters such as hydraulic conductivities, soil water retention curves, and soil depths, we observed that the GW dynamics in the forested slope became slightly smaller than those in the OP slope, contrary to the observed pattern. However, even if all these parameters were swapped, the GW patterns did not completely change. This indicates that factors besides soil depth and hydraulic conductivity, topography and the position of GW monitoring points played crucial roles. At the foothill position with long and steep hillslope, even with thicker soil depth in the uphill and smaller hydraulic conductivity than the actual case, the GW dynamics remained faster than those observed in the OP site. Conversely, if the soil depth became relatively shallower (around 5 meters) with higher hydraulic conductivity, the GW dynamics still remained slower than those observed at the foot of the forested site.

Chapter 4 offers valuable insights into the hydrological impacts of LUC in humid tropical regions and explores how pairs of hydrological models can effectively capture this phenomenon. In terms of rainfall partitioning, JR hillslope had a higher interception rate than OP. It was estimated to be 30% while that of OP was estimated to be 15%. It means changing the land cover from Jungle rubber forest to Oil Palm plantation would trigger the increase of net rainfall (from 2335 mm to 2843 mm) during our study period for one year.

Due to the LUC from forest to oil palm, the PET is also decreased from 1422 mm/yr to 1059 mm/yr. On the other hand, the estimated AET in OP is higher than that in JR. The monthly AET patterns was different from the PET patterns, particularly during the dry season, where AET decreases due to limited water availability. The reduction in AET is more pronounced in JR. Consequently, AET in OP is 32% larger than in JR, equivalent to 600 mm/year.

The yearly runoff is 1736 mm in JR and 2058 mm in OP, indicating an 18 percent increase in annual runoff following the transition from JR to OP. However, on a monthly basis, OP exhibits lower runoff than JR during the dry season. In August, JR restricts AET, maintaining stable runoff. The impact on runoff is further evident in the Flow Duration Curve (FDC) on a daily basis. The high flow (Q5) at the OP is suppressed compared to the one at JR. This higher discharge is attributed to increased net rainfall, mainly associated to the reduced interception. Additionally, low flow (Q90-Q95) decreases in OP.

Employing net rainfall and AET for land use change (LUC) assessment is crucial. This study introduces an integrated model based on the RRI model and the Suzuki model, effectively estimating interception and root zone suction processes. The model successfully replicates observed changes in runoff post a LUC, particularly the increase in annual runoff. However, the estimated increase in this study, at 18%, is relatively modest compared to some earlier research.

As discussed earlier, our results indicate that the reduction in interception and rising in AET to each other, resulting in a relatively smaller estimated impact of LUC from JR to OP. The use of net rainfall and AET improves the model's ability to represent groundwater patterns. Although the model is demonstrated at the hillslope scale, its applicability can be extended to river basin scales for a broader assessment of LUC impact on hydrology.

5.2 Assumptions

This study assessed the main factors influencing groundwater dynamics in humid tropical hillslopes. Through numerical experiments, we finally agreed that topography (including surface and bedrock) and the position of GW monitoring points have a crucial role. In the model simulation, there are some assumptions that need to be considered.

First, as we mentioned above the bedrock topography is one of the prominent factors to alter the GW dynamic. However, due to limitation of the used cone penetration stick and mobilization in the hillslopes, we just measured five points to represent the soil depths or bedrock topography for the forested hillslope which has 80 m of length. Meanwhile in oil palm hillslope we measured only two points which in the ridge and the top hill and we assumed the foothill has same soil depth as the ridge and uphill.

Second, the soil properties were collected from 5, 30, 60, 90cm of each bore holes, therefore bedrock soil properties were unknown. Then, for the unsaturated zone we used the soil properties values such as hydraulic conductivity and water retention curve by averaging all soil samples of each hillslopes. This step was used due to limitation of the model. Then, for the soil properties in the bedrock layer, the model assumed hydraulic conductivity was 10% of the averaged observed *Ks* value then decreased exponentially following the soil bedrock depths. Therefore, the soil properties that we used in the model could not represent precisely the value distributed spatially and vertically as in the field.

Regarding the RRI model that we used in this research is presumed immediate equilibrium water distribution along vertical infiltration throughout the hillslope and recognizing single soil column. However, in humid tropical hillslopes, which often have several-meter depths, there are some questioning of the result's validity.

Lastly, due to error of our discharge sensors, we could not get a discharge data from the hillslope outlets. Observation discharge data was needed for validation and calibration the model results. Instead of using the observation discharge data, this research was used observation GW data for getting model accuracy on simulating the LUC impacts.